

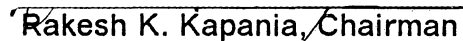
**Delamination Buckling, Postbuckling, and Growth
in Axially Loaded Beam-Plates**

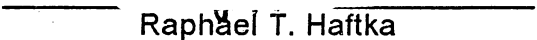
by

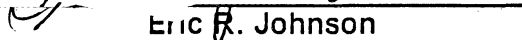
David R. Wolfe

Thesis submitted to the Faculty of the
Virginia Polytechnic Institute and State University
in partial fulfillment of the requirements for the degree of
Master of Science
in
Aerospace Engineering

APPROVED:


Rakesh K. Kapania, Chairman


Raphael T. Haftka


Eric R. Johnson

June 1987

Blacksburg, Virginia

**Delamination Buckling, Postbuckling, and Growth
in Axially Loaded Beam-Plates**

by

David R. Wolfe

Rakesh K. Kapania, Chairman

Aerospace Engineering

(ABSTRACT)

The purpose of this study is to develop a simple one-dimensional model to analyze axially loaded beam-plates containing cracks which extend through the thickness of the beam-plates. Although the material analyzed is isotropic, these cracks will be referred to as delaminations. Buckling, postbuckling, and growth of delaminations in these beam-plates will be analyzed. A finite element method in which all of the terms of the stiffness matrices are obtained by exact integration is employed to determine the linear buckling load and postbuckling solution. The energy release rate is then determined using the postbuckling solution. Curves are provided to show the effect of delamination length and location on buckling loads, energy release rates, and strengths of the beam-plates. The problem of buckling and postbuckling of beams with multiple delaminations is also considered. A method of calculating the energy release rate for beams with multiple delaminations using numerical differentiation is introduced.

Acknowledgements

I am greatly indebted to Dr. Rakesh K. Kapania and Dr. Eric R. Johnson for the help they have given me throughout this work. I also wish to thank Dr. R.T. Haftka for serving on my committee.

This thesis is dedicated to my loving parents.

Table of Contents

| | |
|---|----|
| Chapter 1. Introduction | 1 |
| Chapter 2. Finite Element Formulation | 8 |
| 2.1: Overview | 8 |
| 2.2: Geometry of Problem | 8 |
| 2.3: Finite Element Modeling | 11 |
| 2.4: Equilibrium and Compatibility Conditions | 11 |
| Chapter 3. Buckling and Postbuckling Solution | 18 |
| 3.1: Overview | 18 |
| 3.2: Prebuckling Solution and Linear Stability Analysis | 19 |
| 3.3: Derivation of Nonlinear Stiffness Matrices | 19 |
| 3.4: Large Displacement Postbuckling Analysis | 28 |
| 3.5: Constant Mode Shape Postbuckling Analysis | 30 |

| | |
|--|----|
| 3.6: Energy Release Rate | 34 |
| Chapter 4. Linear Buckling Results | 38 |
| 4.1: Overview | 38 |
| 4.2: Symmetric Delaminations with Simple Boundary Conditions | 39 |
| 4.3: Symmetric Delaminations with Various Boundary Conditions | 42 |
| 4.4: Nonsymmetric Delaminations | 51 |
| 4.5: Multiple Delaminations | 55 |
| 4.6: Conclusions | 62 |
| Chapter 5. Postbuckling and Energy Release Rate Results | 64 |
| 5.1: Overview | 64 |
| 5.2: Incremental Method | 65 |
| 5.3: Comparison of Beams with and without Delaminations | 72 |
| 5.4: Constant Mode Shape Method | 77 |
| 5.5: Various Boundary Conditions | 82 |
| 5.6: Nonsymmetric Delaminations | 88 |
| 5.7: Conclusions | 90 |
| Chapter 6. Multiple Delaminations | 94 |
| 6.1: Overview | 94 |

| | |
|--|---------|
| 6.2: Numerical Differentiation | 95 |
| 6.3: Results Using Numerical Differentiation | 96 |
| 6.4: Conclusions | 109 |
| Chapter 7. Final Remarks and Recommendations | 111 |
| 7.1: Final Remarks | 111 |
| 7.2: Recommendations for Future Work | 112 |
| References | 114 |
| Appendix 1: Constant Mode Shape Program | 118 |
| Appendix 2: Incremental Program | 138 |
| Vita | 153 |

List of Figures

| | | |
|-----------|---|----|
| Fig. 1 - | Buckling of a typical delaminated beam-plate | 2 |
| Fig. 2 - | Schematic diagram of a beam-plate with delamination under axial load | 9 |
| Fig. 3 - | Beam-plate under uniform axial load | 10 |
| Fig. 4 - | Neutral axes of separate regions | 12 |
| Fig. 5 - | Generalized nodal forces and displacements (a) before and (b) after performing transformation | 13 |
| Fig. 6 - | Neutral axes of separate regions (a) before and (b) after buckling | 14 |
| Fig. 7 - | The three modes of cracking | 35 |
| Fig. 8 - | Dimensionless critical load vs. dimensionless delamination length for clamped-clamped beams | 40 |
| Fig. 9 - | Dimensionless critical load vs. dimensionless delamination length for pinned-pinned beams | 41 |
| Fig. 10 - | Dimensionless critical load vs. dimensionless delamination length for pinned-clamped beams | 43 |
| Fig. 11 - | Dimensionless critical load vs. dimensionless delamination length for clamped-free beams | 44 |
| Fig. 12 - | Dimensionless critical load vs. dimensionless delamination length for elastically-supported beams with $\frac{h}{t} = 0.3$ and $\alpha = 0.1$ | 46 |
| Fig. 13 - | Dimensionless critical load vs. dimensionless delamination length for elastically-supported beams with $\frac{h}{t} = 0.3$ and $\alpha = 1$ | 47 |
| Fig. 14 - | Dimensionless critical load vs. dimensionless delamination length for elastically-supported beams with $\frac{h}{t} = 0.3$ and $\alpha = 10$ | 48 |
| Fig. 15 - | Dimensionless critical load vs. dimensionless delamination length for elastically-supported beams with $\frac{h}{t} = 0.3$ and $\alpha = 100$ | 49 |

| | | |
|-----------|---|----|
| Fig. 16 - | Schematic diagram of beam-plate with two delaminations | 56 |
| Fig. 17 - | Dimensionless critical load vs. dimensionless delamination length for pinned-pinned beams with one and two delaminations and $\frac{a}{L} = 0.5$ | 58 |
| Fig. 18 - | Dimensionless critical load vs. dimensionless delamination length for clamped-clamped beams with one and two delaminations and $\frac{a}{L} = 0.5$ | 59 |
| Fig. 19 - | Dimensionless critical load vs. dimensionless delamination length for pinned-pinned beams with one and two delaminations and $\frac{a}{L} = 0.5$ | 60 |
| Fig. 20 - | Dimensionless critical load vs. dimensionless delamination length for clamped-clamped beams with one and two delaminations and $\frac{a}{L} = 0.5$ | 61 |
| Fig. 21 - | Diagram of applied loads used to find nonlinear postbuckling solution | 66 |
| Fig. 22 - | Dimensionless axial load vs. dimensionless energy release rate using incremental method for clamped-clamped beams with $\frac{h}{t} = 0.3$ and $\frac{a}{L} = 0.5$ | 68 |
| Fig. 23 - | Dimensionless axial load vs. dimensionless energy release rate using incremental method for clamped-clamped beams with $\frac{h}{t} = 0.1$ and $\frac{a}{L} = 0.5$ | 70 |
| Fig. 24 - | Dimensionless axial load vs. dimensionless energy release rate using incremental method for clamped-clamped beams with $\frac{h}{t} = 0.3$ | 71 |
| Fig. 25 - | Dimensionless axial load vs. dimensionless energy release rate using incremental method for clamped-clamped beams with $\frac{h}{t} = 0.1$ | 73 |
| Fig. 26 - | Load-deflection plot for undelaminated beam and beam with delamination at $\frac{h}{t} = 0.3$ | 75 |
| Fig. 27 - | Load-deflection plot for undelaminated beam and beam with delamination at $\frac{h}{t} = 0.1$ | 76 |
| Fig. 28 - | Load-end shortening plot for undelaminated beam and beams with delaminations | 78 |
| Fig. 29 - | Dimensionless axial load vs. dimensionless energy release rate using incremental and constant mode shape methods for clamped-clamped beams with $\frac{h}{t} = 0.3$ and $\frac{a}{L} = 0.5$ | 80 |
| Fig. 30 - | Dimensionless axial load vs. dimensionless energy release rate using incremental and constant mode shape methods for clamped-clamped beams with $\frac{h}{t} = 0.1$ and $\frac{a}{L} = 0.5$ | 81 |
| Fig. 31 - | Load-deflection plot for clamped-clamped beams with $\frac{a}{L} = 0.5$ | 83 |
| Fig. 32 - | Dimensionless axial load vs. dimensionless energy release rate using incremental and constant mode shape methods for pinned-pinned beams with $\frac{h}{t} = 0.1$ | 84 |

| | |
|--|-----|
| Fig. 33 - Dimensionless axial load vs. dimensionless energy release rate using incremental and constant mode shape methods for pinned-clamped beams with $\frac{h}{t} = 0.186$ | |
| Fig. 34 - Dimensionless axial load vs. dimensionless energy release rate using incremental and constant mode shape methods for elastically-supported beams with $\frac{h}{t} = 0.3, \alpha = 100, \beta = 10$ | 87 |
| Fig. 35 - Dimensionless axial load vs. dimensionless energy release rate using incremental and constant mode shape methods for clamped-clamped beams with nonsymmetric delaminations and $\frac{h}{t} = 0.3$ and $\frac{a}{L} = 0.5$ | 89 |
| Fig. 36 - Dimensionless axial load vs. dimensionless energy release rate using incremental and constant mode shape methods for clamped-clamped beams with nonsymmetric delaminations and $\frac{h}{t} = 0.1$ and $\frac{a}{L} = 0.5$ | 91 |
| Fig. 37 - Load-end shortening plot for clamped-clamped beams with $\frac{h}{t} = 0.3$ | 97 |
| Fig. 38 - Dimensionless axial load vs. dimensionless energy release rate using numerical differentiation for clamped-clamped beams with $\frac{h}{t} = 0.3$ | 99 |
| Fig. 39 - Load-end shortening plot for clamped-clamped beams with two delaminations at $\frac{h}{t} = 0.3$ and $\frac{H}{t} = 0.6$ | 101 |
| Fig. 40 - Dimensionless axial load vs. dimensionless energy release rate using numerical differentiation for clamped-clamped beams with $\frac{h}{t} = 0.3$ and $\frac{H}{t} = 0.6$ | 102 |
| Fig. 41 - Load-end shortening plot for pinned-pinned beams with two delaminations at $\frac{h}{t} = 0.3$ and $\frac{H}{t} = 0.6$ | 103 |
| Fig. 42 - Dimensionless axial load vs. dimensionless energy release rate using numerical differentiation for pinned-pinned beams with $\frac{h}{t} = 0.3$ and $\frac{H}{t} = 0.6$ | 104 |
| Fig. 43 - Load-end shortening plot for clamped-clamped beams with two delaminations at $\frac{h}{t} = 0.2$ and $\frac{H}{t} = 0.5$ | 106 |
| Fig. 44 - Dimensionless axial load vs. dimensionless energy release rate using numerical differentiation for clamped-clamped beams with $\frac{h}{t} = 0.2$ and $\frac{H}{t} = 0.5$ | 107 |
| Fig. 45 - Load-end shortening plot for clamped-clamped beams with two delaminations at $\frac{h}{t} = 0.1$ and $\frac{H}{t} = 0.4$ | 108 |
| Fig. 46 - Dimensionless axial load vs. dimensionless energy release rate using numerical differentiation for clamped-clamped beams with $\frac{h}{t} = 0.1$ and $\frac{H}{t} = 0.4$ | 110 |

List of Tables

| Table | Title | |
|-------|--|----|
| 1 | Critical buckling loads for elastically-supported beams without delaminations | 50 |
| 2 | Critical buckling loads for clamped-clamped beams with nonsymmetric delamination locations | 52 |
| 3 | Critical buckling loads for pinned-pinned beams with nonsymmetric delamination locations | 53 |

Nomenclature

| | |
|--------------|---|
| a | delamination length |
| A | area |
| b, c, d, e | constants in constant mode shape solution |
| b_1 | length of region after delamination |
| E | Young's Modulus |
| f_i | shape functions in cubic finite element equation |
| F_x | force in x-direction |
| F_y | force in y-direction |
| G | energy release rate |
| \bar{G} | dimensionless energy release rate |
| G_c | critical energy release rate |
| g_i | shape functions in linear finite element equation |
| h | delamination height from top of beam-plate |
| H | delamination height from bottom of beam-plate |
| $[K]$ | basic stiffness matrix |
| $[K_T]$ | tangent stiffness matrix |
| $[K_{tot}]$ | sum of linear and nonlinear stiffness matrices |

| | |
|---------------|---|
| $[K_{uu}]$ | partition of $[K]$ matrix |
| $[K_{ww}]$ | partition of $[K]$ matrix |
| $[K_o]$ | component of tangent stiffness matrix |
| l | length of region before delamination |
| L | total length of beam-plate |
| m | delamination height of middle region |
| M | bending moment |
| M^* | bending moment in energy release rate equation |
| $M_{m.s.}$ | bending moment about middle surface |
| $[N]$ | incremental stiffness matrix |
| $[N_1]$ | nonlinear stiffness matrix of first order |
| $[\bar{N}_1]$ | normalized nonlinear stiffness matrix of first order |
| $[N_2]$ | nonlinear stiffness matrix of second order |
| $[\bar{N}_2]$ | normalized nonlinear stiffness matrix of second order |
| $[N_{uv_1}]$ | partition of $[N_1]$ matrix |
| $[N_{vu_1}]$ | partition of $[N_1]$ matrix |
| $[N_{vv_1}]$ | partition of $[N_1]$ matrix |
| P | axial load |
| $\{P\}$ | force vector |
| \bar{P} | dimensionless axial force |
| P_{cr} | critical buckling load of delaminated beam |
| P_{cp} | critical buckling load of undelaminated beam |
| P_i | total load |
| $\{P_r\}$ | residual load vector |
| $\{P_2\}$ | second load vector found in incremental procedure |
| \hat{P} | vector containing zero's and a one at applied load |
| P^* | axial force in energy release rate equation |
| $\{P^*\}$ | load vector used in incremental procedure |

| | |
|------------------|---|
| $\{q\}$ | displacement vector |
| q_i | displacements |
| $\{q_1\}$ | beginning displacement vector |
| $\{q_2\}$ | second displacement vector in incremental procedure |
| $\{\Delta q\}$ | incremental displacement vector |
| $\{\Delta q^1\}$ | second incremental displacement vector |
| $\{q^*\}$ | sum of $\{q_1\}$ and $\{\Delta q\}$ |
| $\{q_n^*\}$ | sum of $\{q^*\}$ and $\{\Delta q^1\}$ |
| Q_B | transverse force applied to region 2 |
| Q_T | transverse force applied to region 3 |
| $\{Q_u\}$ | axial displacement vector |
| $\{Q_v\}$ | transverse displacement vector |
| $\{\bar{Q}_v\}$ | normalized transverse displacement vector |
| t | thickness of beam-plate |
| u | axial displacement |
| U | strain energy |
| \bar{u} | dimensionless axial displacement |
| u_1 | axial displacement at point of applied load |
| u_{ij} | axial displacement at node i of region j |
| v | transverse displacement |
| v_{ij} | transverse displacement at node i of region j |
| V | shear force |
| w | width of beam-plate |
| x | axial direction |
| y | transverse direction |
| α | extensional spring constant |
| β | rotational spring constant |
| δ | amplitude of mode shape |

| | |
|---------------|---|
| σ_c | critical stress of plate with crack length $2a$ |
| θ | rotation |
| θ_{ij} | rotation at node i of region j |

Chapter 1. Introduction

The use of composite materials has been greatly increasing because of their superior strength-to-weight and stiffness-to-weight ratios over conventional metals. These properties make composites very attractive especially for use in the aerospace industry. During the fabrication of these composites certain defects such as weakened fibers or cracked matrix materials can cause delaminations (debonding of adjacent layers) to occur. Studies conducted by Rhodes, Williams, and Starnes [1,2] showed that delaminations can also develop due to the low-velocity impact of foreign objects. These delaminations can greatly reduce the performance of a composite plate or shell; for example, the disbonded area may buckle under compressive loads and subsequently spread. The delamination can cause a decrease in the compressive load carrying capacity of the structure, thereby leading to loss of global plate stability. Figure 1 shows a typical buckling mode shape of a delaminated

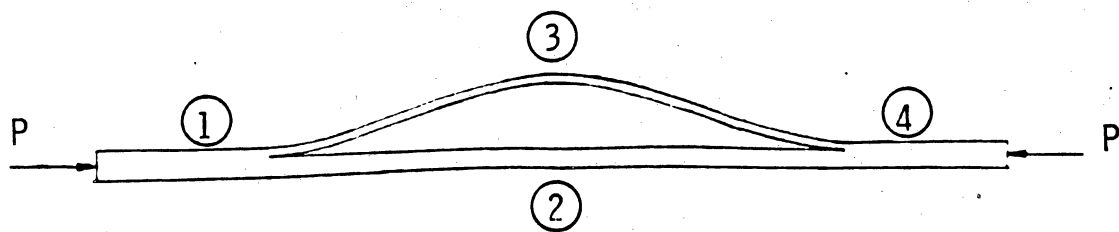


Figure 1: Buckling of a typical delaminated beam-plate

beam-plate. A review of various problems of delamination growth in composites was given by Wilkins et al [3].

Recently, a large number of investigators have studied the problem dealing with delamination buckling and growth in composite materials. Chai, Babcock, and Knauss [4] studied this phenomenon using a delaminating, one-dimensional beam-column wherein the local delamination, its growth, stability and arrest were governed by a fracture mechanics-based energy release rate. For the cases where region 3 in Figure 1 is much thinner than region 2, they presented a special model called the thin-film model.

Simites, Sallam, and Yin [5] also developed a one-dimensional model for predicting delamination buckling loads of simply-supported and clamped beams. The effects of delamination position, size, and thickness on the critical loads were studied in detail. In a subsequent paper Yin, Sallam, and Simites [6] presented results of an elastic buckling and postbuckling analysis of an axially loaded beam-plate with an across-the-width delamination symmetrically located at an arbitrary depth. The analysis was done for clamped-clamped beams only. They studied the process of delamination growth on the basis of a Griffith-type fracture criterion. They used an expression for the energy release rate derived by Yin and Wang [7] obtained using a path independent J-integral. It was shown that for certain geometries the buckling load can serve as a measure of the load carrying capacity of the delaminated configuration. In other cases, the buckling load was found to be

very small and delamination growth was found to be a strong possibility, depending upon the toughness of the material.

This is in comparison to Chai et al. [4] who computed the energy release rate associated with delamination growth by numerical differentiation. In the study by Yin and Wang [7] mentioned previously curves were provided that determined the possibility and the stability characteristics of delamination growth and provide a basis for determining the ultimate axial load capacity. Kardomateas and Schmueser [8] expanded the work of Simites et al. [5] to include the effects of transverse shear on buckling and postbuckling of beam-plates. They found that these shear effects enhance the possibility of crack growth because the extra energy from these transverse forces can be released when the load is applied.

Recently, Yin [9] also studied cylindrical buckling of delaminated plates using a one-dimensional model with general laminate structure (as opposed to the isotropic beam-plate assumed in References 5 and 6) to do an elastic postbuckling analysis. The path-independent J-integral was again used to find the energy release rate. The postbuckling analysis was done for cross-ply and angle-ply laminates. In another paper Yin [10] obtained the energy release rate for the uniform-expansion growth of a circular delamination in a compressively loaded laminate using the M-integral. Yin and Fei [11] examined circular plates being subjected to axisymmetric in-plane loads and analyzed the effect of concentric circular delaminations on the critical buckling

load. This was done only for simply-supported and clamped boundary conditions. They later presented results for elastic postbuckling of delaminated circular plates with clamped boundaries [12]. Certain results were found to be qualitatively similar to those of the axially loaded beam-plates with one-dimensional delaminations (Reference 7). In this study they also obtained an analytical expression for the energy release rate. Next, Yin [13] provided two approximate solutions for acceleration of crack growth for thin, buckled strip delaminations. In this study he used a global energy balance compatibility condition and found that crack growth speeds are comparable to flexural wave speeds. The strain energy release rates were again evaluated using the J-integral.

Bottega and Maewal [14] studied the axisymmetric delamination buckling and growth in a compressively loaded two layer circular plate. The influence of imperfections in the form of transverse loads was also examined. Finally, Whitney [15] employed a higher order plate theory to determine the mode II (explained later) strain energy release rate in an end notch flexure specimen. This theory was found to be more accurate than classical theory.

All the above studies employed analytical methods; therefore, these studies are restricted to simple boundary conditions. Furthermore, it is extremely difficult to employ the analytical methods if the loading is dynamic (causing delaminated plies to repeatedly impact each other) or if the beam dimensions are such that certain regions develop plastic zones. For these complicating

nonlinear effects, it is convenient to employ a finite element method. In fact, the finite element method was employed by Whitcomb [16] to perform a parametric study of postbuckled through-width delaminations in laminated coupons. However, the analysis was performed for a two-dimensional model by employing a four-node, isoparametric quadrilateral element. The second dimension thus makes the analysis quite complicated. Horban and Palazotto [17] also used a finite element model to study buckling of cylindrical composite panels. They used the STAGSC-1 code for the finite element analysis. Experimental results were also presented in this paper.

Seifert and Palazotto [18] presented experimental results for the buckling loads of eight-ply graphite epoxy cylindrical panels with midplane delaminations. The study included two different ply orientations, two different aspect ratios, two different delamination sizes, and one set of boundary conditions: clamped along the top and bottom edges and simply-supported along the vertical sides. The experimental test results were compared to the linear bifurcation load and nonlinear collapse load of panels with square cut-outs using the STAGSC-1 finite element program.

Williams, Stouffer, Ilic, and Jones [19] also used a one-dimensional model to study delaminations in laminate structures. They provided analytical, finite element, and experimental results which determined that delamination growth results from crack propagation that depends on the stress field at the crack tip produced by buckling of the delaminated section. Also, a study conducted by

Vizzini and Lagace [20] based on the strength of materials approach provided experimental and analytical results for the growth of delaminations in sandwich columns. They introduced the concept of the interply matrix layer acting as an elastic foundation. They related the growth point to a critical center deflection rather than to the applied load but did not perform a postbuckling analysis.

The objective of this study is to develop a simple one-dimensional model to study buckling and postbuckling of isotropic beam-plates with delaminations. In this study a simple 6 degree-of-freedom beam-column element is used to analyze delamination buckling and instability-related delamination growth in a one-dimensional model. The buckling loads for different values of crack length, crack location, and crack depth are obtained for beam-plates with various boundary conditions by this analysis. The present results are found to be in excellent agreement with those of Simiteses, Sallam, and Yin [5]. The postbuckling analysis is performed using two different methods: 1) the conventional large displacement incremental approach using the tangent stiffness matrix employed by Yang and Saigal [21], and 2) the displacement analysis formulations similar to those employed by Kapania and Yang [22]. For both these methods the energy release rate is computed using the expression given by Yin and Wang [7]. For beams with more than one delamination this expression cannot be used, hence a numerical differentiation method is introduced to handle this problem.

Chapter 2. Finite Element Formulation

2.1 OVERVIEW

This chapter describes the geometry of the problem, what happens during bending, the key assumptions, the finite element model, and the equilibrium and compatibility conditions.

2.2 GEOMETRY OF PROBLEM

In this study the beam-plate is assumed to be homogeneous and to demonstrate linear elastic material behavior. The dimensions of the model are shown in Figure 2 which is a front view of the plate. The sides of the plate are free. The plate is subjected to a uniform axial compressive force along the x-axis (see Figure 3). The delamination, which runs through the width, is located h units from the top (or H units from the bottom) and has a length of

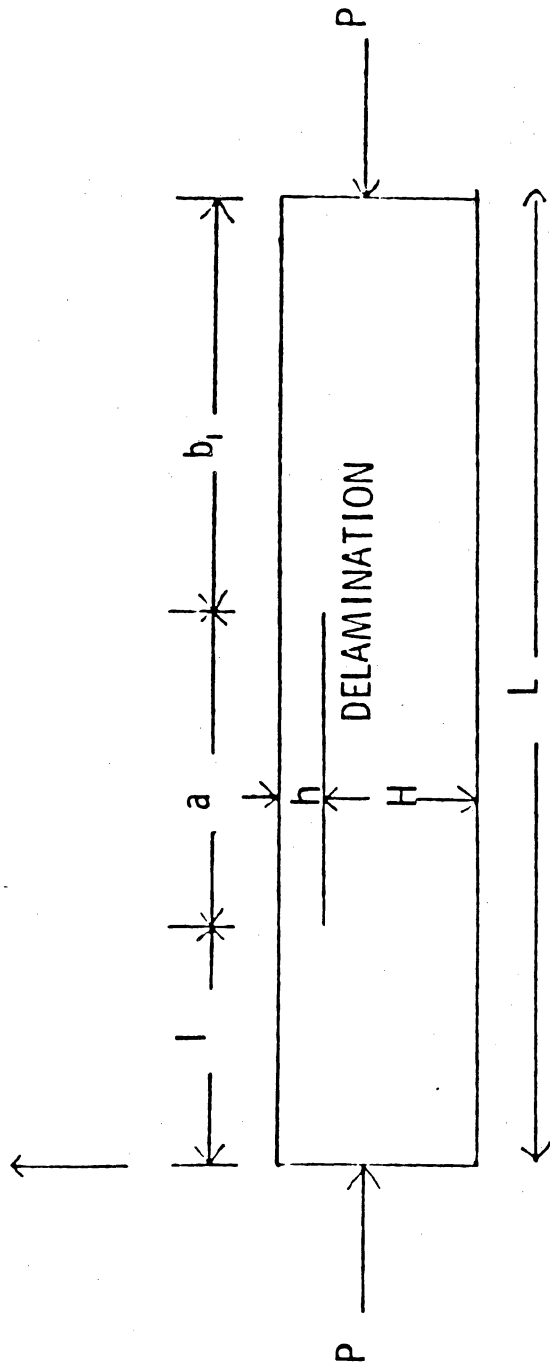


Figure 2: Schematic diagram of a beam-plate with delamination under axial load

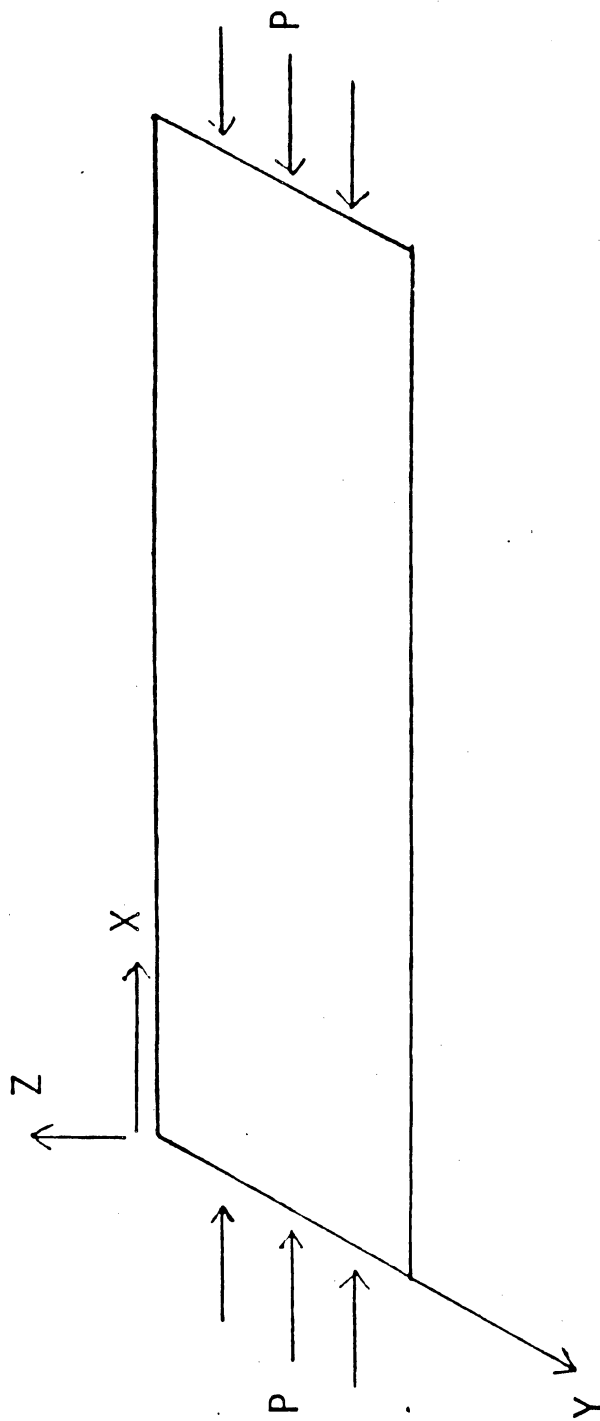


Figure 3: Beam-plate under uniform axial load

a units. The delamination divides the plate into four separate regions (Figure 4).

2.3 FINITE ELEMENT MODELING

The four separate regions are modeled by beam-column elements located along the neutral axes of each of these regions. A typical finite element modeling is shown in Figure 5. There are two separate sections between nodes 2 and 3 which represent the regions above and below the delamination. These regions can move up and down independently. Figure 6 shows conceptually what happens to the model during bending, and demonstrates the key assumption in this study, namely that plane sections remain plane. The thick bars represent *rigid connectors* which do not deform during bending. In the next section this assumption is used to develop equilibrium and compatibility conditions.

2.4 EQUILIBRIUM AND COMPATIBILITY CONDITIONS

The forces and displacements before assemblage, shown in Figure 5a, are now related to those in Figure 5b in order to develop the equilibrium and compatibility conditions. P_{ij} , V_{ij} , and M_{ij} represent axial forces, transverse forces, and bending moments, respectively, while u_{ij} , v_{ij} , and θ_{ij} are the corresponding displacements. The first subscript i denotes the local x-location in the region ($i=1$ is the beginning of the region and $i=2$ is the end of the

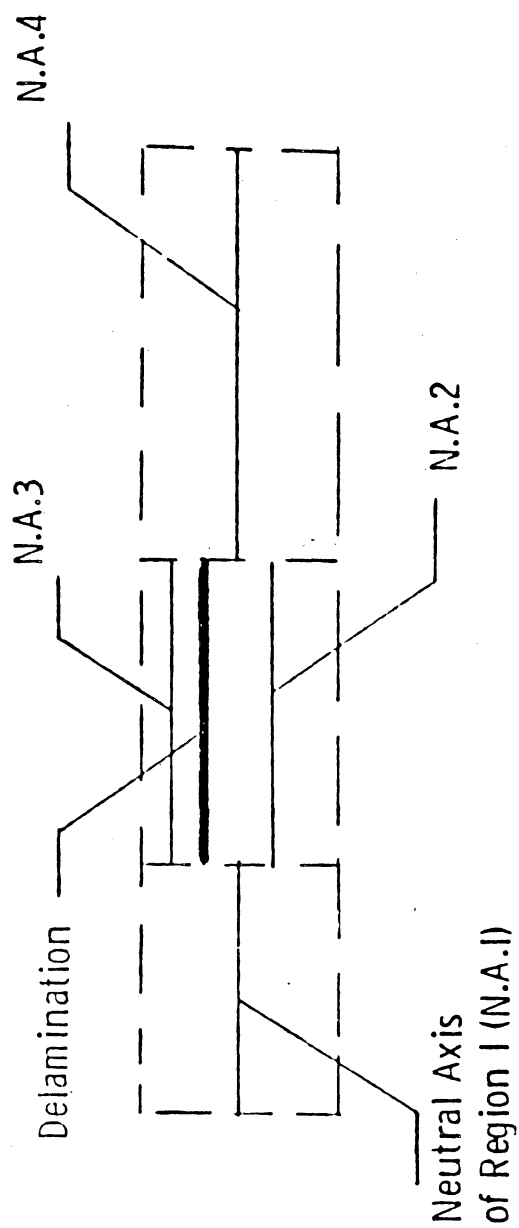


Figure 4: Neutral axes of separate regions

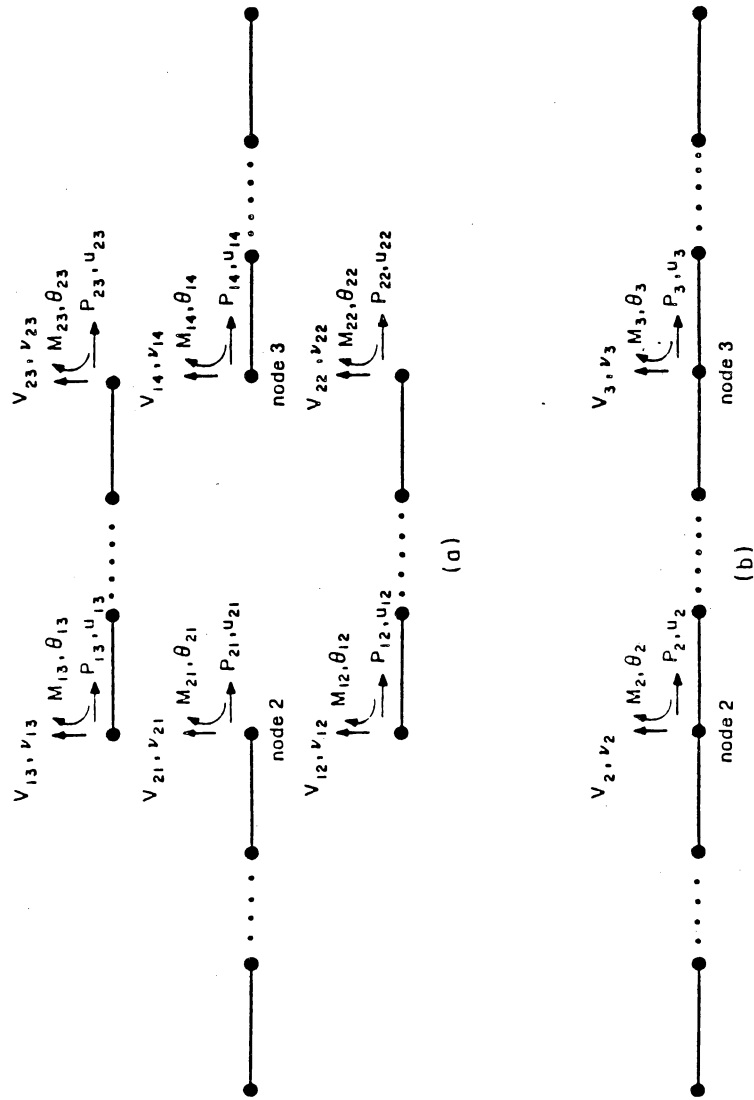


Figure 5: Generalized nodal forces and displacements (a) before and (b) after performing transformation

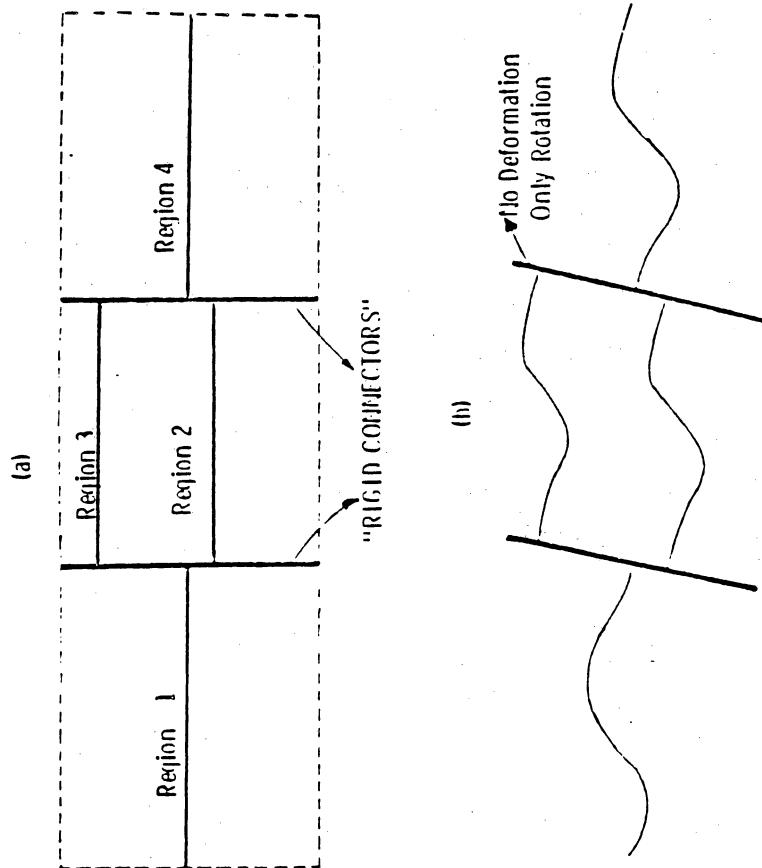


Figure 6: Neutral axes of separate regions (a) before and (b) after buckling

region), and the second subscript j denotes the region number. Summing the forces and then the moments about the middle surface of the beam-plate yields the equilibrium conditions. The equilibrium conditions at node 2 are:

$$\Sigma F_x = P_2 = P_{21} + P_{12} + P_{13} \quad (2.1)$$

$$\Sigma F_y = V_2 = V_{21} + V_{12} + V_{13} \quad (2.2)$$

$$\Sigma M_{m.s.} = M_2 = M_{21} + M_{12} + M_{13} + \frac{H}{2}P_{13} - \frac{h}{2}P_{12} \quad (2.3)$$

Similarly, at node 3:

$$\Sigma F_x = P_3 = P_{22} + P_{23} + P_{14} \quad (2.4)$$

$$\Sigma F_y = V_3 = V_{22} + V_{23} + V_{14} \quad (2.5)$$

$$\Sigma M_{m.s.} = M_3 = M_{22} + M_{23} + M_{14} + \frac{H}{2}P_{23} - \frac{h}{2}P_{22} \quad (2.6)$$

Now making use of the rigid connector idea (plane sections remain plane), all vertical displacements and all rotations are equal at the same value of x . Also, the u -displacements can be related to each other by the rotation angle and the vertical distance between the respective neutral axes. Making use of these ideas, the following compatibility conditions are obtained at node 2:

$$u_{21} = u_2 \quad (2.7a)$$

$$u_{12} = u_2 - \frac{h}{2}\theta_2 \quad (2.7b)$$

$$u_{13} = u_2 + \frac{H}{2}\theta_2 \quad (2.7c)$$

$$v_2 = v_{21} = v_{12} = v_{13} \quad (2.8)$$

$$\theta_2 = \theta_{21} = \theta_{12} = \theta_{13} \quad (2.9)$$

Similar conditions are obtained at node 3:

$$u_{14} = u_3 \quad (2.10a)$$

$$u_{22} = u_3 - \frac{h}{2}\theta_3 \quad (2.10b)$$

$$u_{23} = u_3 + \frac{H}{2}\theta_3 \quad (2.10c)$$

$$v_3 = v_{22} = v_{23} = v_{14} \quad (2.11)$$

$$\theta_3 = \theta_{22} = \theta_{23} = \theta_{14} \quad (2.12)$$

These conditions are used to develop a transformation matrix to transform from the untransformed model in Figure 5a to the transformed model in Figure 5b. The linear stiffness, incremental stiffness, and geometrical nonlinear stiffness finite element matrices are assembled using the first model and then transformed to the second model using the transformation matrix. This

transformation matrix can easily be obtained for beam-plates with more than one delamination using the same principles.

Chapter 3. Buckling and Postbuckling Solution

3.1 OVERVIEW

In this chapter procedures are given to find the prebuckling state, the linear buckling load, and the postbuckling solution. The energy release rates are computed from the postbuckling solution. Two different methods are used for the postbuckling solution. The first method employs an incremental load procedure which allows for changing mode shape. The Newton-Raphson method is used to iterate and find the postbuckling solution. The second method is designed to reduce the high computer cost of the incremental procedure. This simple, economical method involves the assumption that the spatial variation of the mode shape does not change; consequently, the method is accurate for small displacements. The linear buckling results are presented in Chapter 4 after which the postbuckling and energy release rate results are given in Chapter 5.

3.2 PREBUCKLING SOLUTION AND LINEAR STABILITY ANALYSIS

The prebuckling solution is one of pure compression, the transverse displacement being identically equal to zero. Therefore, if the load is less than the critical value, no shear forces and bending moments are developed in the beam that can increase the length of the delamination. Hence, a linear stability analysis is first performed to determine the critical buckling load.

After assemblage and transformation, the governing equations for the linear buckling analysis are written as

$$[K]\{q\} - P_{cr}[N]\{q\} = \{0\} \quad (3.1)$$

where $[K]$ and $[N]$ are, respectively, the restrained stiffness and restrained incremental stiffness matrices; $\{q\}$ is the vector of generalized nodal displacements; and P_{cr} is the critical value of the inplane compressive load. An eigenvalue analysis of the above equations yields the lowest critical stability load.

3.3 DERIVATION OF NONLINEAR STIFFNESS MATRICES

The next step is to perform a postbuckling analysis. In order to do so, it is necessary to obtain the $[N_1]$ and $[N_2]$ nonlinear stiffness matrices. The tangent stiffness matrix, $[K_T]$, which is needed in the incremental postbuckling analysis, is also derived in this section. The first step in these derivations is

to write the finite element equations for the axial and transverse displacements. The simple linear approximation for u , the axial displacement, is used in this study so that all of the stiffness matrices may be obtained using exact integration. The linear equation is

$$u = (1 - \frac{x}{L})u_1 + \frac{x}{L}u_2 \quad (3.2)$$

where the u_i 's are the axial displacements at node i , and the shape functions are, obviously

$$g_1 = (1 - \frac{x}{L}) \quad g_2 = \frac{x}{L} \quad (3.3)$$

The cubic approximation is used for v , the transverse displacement, and here, the shape functions are numbered from three to six for clarity:

$$v = f_3v_1 + f_4\theta_1 + f_5v_2 + f_6\theta_2 \quad (3.4)$$

The v_i 's and the θ_i 's are the transverse displacements and rotations, respectively, at node i . The shape functions in Equation (3.4) are

$$f_3 = 1 - 3(\frac{x}{L})^2 + 2(\frac{x}{L})^3 \quad (3.5a)$$

$$f_4 = x - 2(\frac{x^2}{L}) + \frac{x^3}{L^2} \quad (3.5b)$$

$$f_5 = 3(\frac{x}{L})^2 - 2(\frac{x}{L})^3 \quad (3.5c)$$

$$f_6 = -\left(\frac{x^2}{L}\right) + \frac{x^3}{L^2} \quad (3.5d)$$

The matrices $[N_1]$ and $[N_2]$ are both obtained explicitly in this study starting with the following strain energy expression for a beam:

$$U = \frac{1}{2}EA \int_0^L \left[\left(\frac{\partial u}{\partial x} \right)^2 + \frac{1}{2} \left(\frac{\partial v}{\partial x} \right)^2 \right] dx \quad (3.6a)$$

Expanding this equation

$$U = \frac{1}{2}EA \int_0^L \left[\left(\frac{\partial u}{\partial x} \right)^2 + \frac{1}{4} \left(\frac{\partial v}{\partial x} \right)^4 + \left(\frac{\partial u}{\partial x} \right) \left(\frac{\partial v}{\partial x} \right)^2 \right] dx \quad (3.6b)$$

The nonlinear stiffness matrices are obtained by taking first derivatives of U with respect to the displacements. q_i will represent the displacement vector which contains six elements. The first two elements of q_i are the axial displacements, u_1 and u_2 , and the last four elements are the transverse displacements and rotations, v_1 , θ_1 , v_2 , and θ_2 . Also the g_i 's and the f_i 's are the shape functions given previously, and, for example, f_i' denotes the first derivative of f_i with respect to x . Taking the derivative of the second term of Equation (3.6b) with respect to the v -displacements yields:

$$\frac{\partial U}{\partial q_i} = \frac{1}{2}EA \int_0^L \left(\frac{\partial v}{\partial x} \right)^3 f_i' dx \quad (3.7a)$$

or, rearranging,

$$\frac{\partial U}{\partial q_i} = \sum_{j=3}^6 \frac{1}{2} EA \int_0^L \left(\frac{\partial v}{\partial x} \right)^2 f_i' f_j' q_j dx \quad (3.7b)$$

where i and j go from 3 to 6. Now taking derivatives of the third term of Equation (3.6b) with respect to the v -displacements:

$$\frac{\partial U}{\partial q_i} = \frac{1}{2} EA \int_0^L 2 \left(\frac{\partial v}{\partial x} \right) \left(\frac{\partial v}{\partial x} \right) f_i' dx \quad (3.8a)$$

or,

$$\frac{\partial U}{\partial q_i} = \sum_{j=1}^2 EA \int_0^L \frac{\partial v}{\partial x} f_i' g_j' q_j dx \quad (3.8b)$$

where i goes from 3 to 6 and j goes from 1 to 2. Finally, taking derivatives of the third term of Equation (3.6b) with respect to the u -displacements

$$\frac{\partial U}{\partial q_i} = \frac{1}{2} EA \int_0^L \left(\frac{\partial v}{\partial x} \right)^2 g_i' dx \quad (3.9a)$$

or,

$$\frac{\partial U}{\partial q_i} = \sum_{j=3}^6 \frac{1}{2} EA \int_0^L \frac{\partial v}{\partial x} g_i' f_j' q_j dx \quad (3.9b)$$

where i ranges from 1 to 2 and j from 3 to 6.

Equation (3.7b) forms a 4 x 4 matrix multiplied by the v -displacement vector. This matrix is called the $[N_2]$ nonlinear stiffness matrix. Similarly, Equations

(3.8b) and (3.9b) also form matrices which are multiplied by the u - and v -displacements respectively. The matrix in Equation (3.8b) is a 4×2 matrix called $[N_{vu_1}]$, and the matrix in Equation (3.9b) is a 2×4 matrix called $[N_{uv_1}]$. The sum of these two matrices forms the $[N_1]$ matrix. Note that $[N_1]$ is not symmetric.

Normally, the nonlinear matrices are obtained using numerical integration; however, in this study the components of $[N_1]$ and $[N_2]$ are found exactly by integrating term by term. The $[N_{uv_1}]$ matrix is obtained from (see Equation 3.9b)

$$\int_0^L g_i' f_j' \left(\frac{\partial v}{\partial x} \right) dx \quad (3.10)$$

where i goes from 1 to 2 and j goes from 3 to 6. The $[N_{vu_1}]$ matrix is obtained by multiplying the transpose of $[N_{uv_1}]$ by two. The g_i' 's are

$$g_1' = -\frac{1}{L} \quad g_2' = \frac{1}{L} \quad (3.11)$$

which do not depend on x . The first derivatives of the f_j' 's are

$$f_3' = \frac{6}{L} \left[-\frac{x}{L} + \left(\frac{x}{L} \right)^2 \right] \quad (3.12a)$$

$$f_4' = 1 - 4\frac{x}{L} + 3\left(\frac{x}{L}\right)^2 \quad (3.12b)$$

$$f_5' = \frac{6}{L} \left[\frac{x}{L} - \left(\frac{x}{L} \right)^2 \right] \quad (3.12c)$$

$$f_6' = -2 \frac{x}{L} + 3 \left(\frac{x}{L} \right)^2 \quad (3.12d)$$

Now, the integrals for $[N_1]$ are calculated:

$$\int_0^L f_3' \left(\frac{\partial v}{\partial x} \right) dx = \frac{6}{5L} v_1 + \frac{1}{10} \theta_1 - \frac{6}{5L} v_2 + \frac{1}{10} \theta_2 \quad (3.13a)$$

$$\int_0^L f_4' \left(\frac{\partial v}{\partial x} \right) dx = \frac{1}{10} v_1 + \frac{2}{15} L \theta_1 - \frac{1}{10} v_2 - \frac{1}{30} L \theta_2 \quad (3.13b)$$

$$\int_0^L f_5' \left(\frac{\partial v}{\partial x} \right) dx = -\frac{6}{5L} v_1 - \frac{1}{10} \theta_1 + \frac{6}{5L} v_2 - \frac{1}{10} \theta_2 \quad (3.13c)$$

$$\int_0^L f_6' \left(\frac{\partial v}{\partial x} \right) dx = \frac{1}{10} v_1 - \frac{1}{30} L \theta_1 - \frac{1}{10} v_2 + \frac{2}{15} L \theta_2 \quad (3.13d)$$

The integrals needed for the $[N_2]$ matrix (see Equation (3.7b)) are:

$$\int_0^L f_i' f_j' \left(\frac{\partial v}{\partial x} \right)^2 dx \quad (3.14)$$

where i and j both range from 3 to 6. Performing the integrations:

$$\begin{aligned} \int_0^L f_3'^2 \left(\frac{\partial v}{\partial x} \right)^2 dx = & \frac{1}{35} \left[\frac{72}{L^3} v_1^2 + \frac{18}{L^2} v_1 \theta_1 + \frac{3}{L} \theta_1^2 - \frac{144}{L^3} v_1 v_2 \right. \\ & \left. - \frac{18}{L^2} v_2 \theta_1 + \frac{18}{L^2} v_1 \theta_2 + \frac{72}{L^3} v_2^2 - \frac{18}{L^2} v_2 \theta_2 + \frac{3}{L} \theta_2^2 \right] \end{aligned} \quad (3.15a)$$

$$\int_0^L f_4'^2 \left(\frac{\partial v}{\partial x} \right)^2 dx = \frac{1}{210} \left[\frac{18}{L} v_1^2 - 3v_1\theta_1 + 12L\theta_1^2 - \frac{36}{L} v_1v_2 + 3v_2\theta_1 \right. \\ \left. + 3v_1\theta_2 + \frac{18}{L} v_2^2 - 3L\theta_1\theta_2 - 3v_2\theta_2 + L\theta_2^2 \right] \quad (3.15b)$$

$$\int_0^L f_6'^2 \left(\frac{\partial v}{\partial x} \right)^2 dx = \frac{1}{210} \left[\frac{18}{L} v_1^2 + 3v_1\theta_1 + L\theta_1^2 - \frac{36}{L} v_1v_2 - 3v_2\theta_1 \right. \\ \left. - 3v_1\theta_2 + \frac{18}{L} v_2^2 - 3L\theta_1\theta_2 + 3v_2\theta_2 + 12L\theta_2^2 \right] \quad (3.15c)$$

$$\int_0^L f_3'f_4' \left(\frac{\partial v}{\partial x} \right)^2 dx = \frac{1}{140} \left[\frac{36}{L^2} v_1^2 + \frac{24}{L} v_1\theta_1 - \theta_1^2 - \frac{72}{L^2} v_1v_2 \right. \\ \left. - \frac{24}{L} v_2\theta_1 + \frac{36}{L^2} v_2^2 + 2\theta_1\theta_2 + \theta_2^2 \right] \quad (3.15d)$$

$$\int_0^L f_3'f_6' \left(\frac{\partial v}{\partial x} \right)^2 dx = \frac{1}{140} \left[\frac{36}{L^2} v_1^2 + \theta_1^2 - \frac{72}{L^2} v_1v_2 + \frac{24}{L} v_1\theta_2 + \frac{36}{L^2} v_2^2 \right. \\ \left. + 2\theta_1\theta_2 - \frac{24}{L} v_2\theta_1 - \theta_2^2 \right] \quad (3.15e)$$

$$\int_0^L f_4'f_6' \left(\frac{\partial v}{\partial x} \right)^2 dx = \frac{1}{210} \left[3v_1\theta_1 + \frac{3}{2}L\theta_1^2 - 3v_2\theta_1 + 3v_1\theta_2 + 2L\theta_1\theta_2 \right. \\ \left. - 3v_2\theta_2 - \frac{3}{2}L\theta_2^2 \right] \quad (3.15f)$$

Note that $f_5' = -f_3'$ which avoids performing several of the integrations. It is noted that use of exact integral formulation considerably simplifies the analysis and is also more economical compared to using numerical integration.

The tangent stiffness matrix, which is used in the incremental postbuckling analysis, is now derived. This matrix is obtained from the expression

$$[K_T] = \frac{\partial^2 U}{\partial q_i \partial q_j} \quad (3.16)$$

where i and j range from 1 to 6; therefore, two derivatives of the strain energy must be taken. From the second term of the strain energy expression, taking the derivative with respect to the v -displacements twice (see Equation (3.7a) for first derivative)

$$\frac{\partial^2 U}{\partial q_i \partial q_j} = \frac{3}{2} EA \int_0^L \left(\frac{\partial v}{\partial x} \right)^2 f_i' f_j' dx \quad (3.17)$$

which equals three times the $[N_2]$ matrix derived previously. In Equation (3.17) i and j range from 3 to 6. Now, taking the u -derivative and then the v -derivative of the third term in Equation (3.6b)

$$\frac{\partial^2 U}{\partial q_i \partial q_j} = EA \int_0^L \left(\frac{\partial v}{\partial x} \right) g_i' f_j' dx \quad (3.18)$$

where i goes from 1 to 2 and j goes from 3 to 6 (see Equation (3.9a) for first derivative). This equation forms a matrix which is two times the $[N_{uv_1}]$ matrix derived previously. Next, from the same term, taking the v -derivative first, and then u

$$\frac{\partial^2 U}{\partial q_i \partial q_j} = EA \int_0^L \left(\frac{\partial v}{\partial x} \right) f_i' g_j' dx \quad (3.19)$$

which is equal to $[N_{vu_1}]$. In the previous equation i goes from 3 to 6 and j goes from 1 to 2. Finally, taking two derivatives with respect to v of the same term

$$\frac{\partial^2 U}{\partial q_i \partial q_j} = EA \int_0^L \left(\frac{\partial u}{\partial x} \right) f_i' f_j' dx \quad (3.20)$$

Here, when the i 's and j 's vary from 3 to 6 a matrix is formed which is called the $[K_\sigma]$ matrix. Therefore, the equation for the tangent stiffness matrix may be written:

$$[K_T] = [K] + [N_1] + 3[N_2] + [K_\sigma] \quad (3.21)$$

where $[N_1]$ is now symmetric because $[N_{uv_1}]$ is not multiplied by one half. The equation for the axial load is

$$P = EA \left[\frac{\partial u}{\partial x} + \frac{1}{2} \left(\frac{\partial v}{\partial x} \right)^2 \right] \quad (3.22)$$

Noting that $[N]$, the incremental stiffness matrix, comes from the first term of Equation (3.22) and that $[N_2]$ comes from the second term, $[K_T]$ may be rearranged and written as shown:

$$[K_T] = [K] + [N_1] + 2[N_2] + P[N] \quad (3.23)$$

3.4 LARGE DISPLACEMENT POSTBUCKLING ANALYSIS

The next step in this analysis is to find the relationship between the axial load and the displacement vector in the postbuckling range by performing a large displacement analysis. A large number of investigations have been performed on geometrically nonlinear structures and postbuckling of these structures (see, for example, References 21 and 22 for a review). In these studies an incremental/iteration approach (either of total Lagrangian or of updated Lagrangian type) is generally used employing the so-called tangent stiffness matrix in conjunction with the Newton-Raphson method. This incremental approach, which allows for changing mode shape, is described in this section.

The governing postbuckling equation is

$$[K]\{q\} + [N_1]\{q\} + [N_2]\{q\} = \{P\} \quad (3.24)$$

The first step is to find the tangent stiffness matrix using a beginning axial load and vector of displacements. Then, using a small incremental load, calculate

$$[K_T]^{-1}\{\Delta P\} = \{\Delta q\}. \quad (3.25)$$

$\{\Delta q\}$ is then added to the original displacement vector to form $\{q^*\}$:

$$\{q^*\} = \{q_1\} + \{\Delta q\}, \quad (3.26)$$

where $\{q^*\}$ is the current displacement vector. Now, define

$$[K_{tot}] = [K] + [N_1] + [N_2] \quad (3.27)$$

where $[N_1]$ and $[N_2]$ are the nonlinear stiffness matrices derived in Section 3.3.

$[K_{tot}]$ is then found using $\{q^*\}$, and $\{P^*\}$, the internal load vector, is calculated as

$$\{P^*\} = [K_{tot}]\{q^*\} \quad (3.28)$$

Then the residual load is found from

$$\{P_r\} = \{P_2\} - \{P^*\} \quad (3.29)$$

where $\{P_2\}$ is the sum of the first axial load and the incremental load. The next step is to find

$$\{\Delta q^1\} = [K_T]^{-1}\{P_r\} \quad (3.30)$$

Then, the new $\{q^*\}$ is calculated as

$$\{q_n^*\} = \{q^*\} + \{\Delta q^1\}. \quad (3.31)$$

The steps in Equations (3.27-31) are then repeated until the residual load is sufficiently small. The convergence criteria used is, from Reference 22:

$$\left[\frac{\left(\sum_{i=1}^N P_{r_i}^2 \right)}{\left(\sum_{i=1}^N P_i^2 \right)} \right]^{\frac{1}{2}} \leq .001 \quad (3.32)$$

where P_i is the total load vector, P_{r_i} is the residual load, and N is the total number of degrees of freedom. When Equation (3.32) is satisfied $\{q_n^*\}$ becomes $\{q_2\}$, and this vector, along with $\{P_2\}$ is the next point of the postbuckling solution. To proceed to the next point, the tangent stiffness matrix is recalculated using the current displacement vector, $\{q_2\}$, and the whole process is repeated starting with Equation (3.25). Thus the postbuckling solution is found using the incremental method.

3.5 CONSTANT MODE SHAPE POSTBUCKLING ANALYSIS

A somewhat simpler and much more economical approach to find the postbuckling solution is to assume the spatial distribution of the displacement to be the same as the linear buckling mode and to obtain the variation of the axial load with respect to the displacement vector by using the $[N_1]$ and $[N_2]$ nonlinear matrices as described subsequently. This constant mode shape assumption is consistent with Koiter's initial postbuckling analysis [23]. No iterations are involved in this procedure. It is noted that this approach is generally valid for small transverse displacements only. For large displacements in the postbuckling range, the incremental approach (though

very expensive) should be used since, for large displacements, the spatial variation of the displacement changes with applied axial load.

To find the constant mode shape solution, the governing postbuckling equation of (3.24) is partitioned as follows:

$$\begin{bmatrix} K_{uu} & | & 0 \\ - & - & - \\ 0 & | & K_{vv} \end{bmatrix} \begin{Bmatrix} Q_u \\ Q_v \end{Bmatrix} + \begin{bmatrix} 0 & | & N_{uv_1} \\ - & - & - \\ N_{vu_1} & | & 0 \end{bmatrix} \begin{Bmatrix} Q_u \\ Q_v \end{Bmatrix} + \begin{bmatrix} 0 & | & 0 \\ - & - & - \\ 0 & | & N_{vv_2} \end{bmatrix} \begin{Bmatrix} Q_u \\ Q_v \end{Bmatrix} = \begin{Bmatrix} P \\ 0 \end{Bmatrix} \quad (3.33)$$

Here, $\{Q_u\}$ is the axial displacement vector and $\{Q_v\}$ is the transverse displacement vector. Thus,

$$[K_{uu}]\{Q_u\} + [N_{uv_1}]\{Q_v\} = \{P\} \quad (3.34a)$$

$$[K_{vv}]\{Q_v\} + [N_{vu_1}]\{Q_u\} + [N_{vv_2}]\{Q_v\} = \{0\} \quad (3.34b)$$

Solving Equation (3.34a) for $\{Q_u\}$,

$$\{Q_u\} = [K_{uu}]^{-1}\{P\} - [K_{uu}]^{-1}[N_{uv_1}]\{Q_v\} \quad (3.35)$$

Substituting $\{Q_u\}$ into Equation (3.34b) yields

$$[K_{vv}]\{Q_v\} + [N_{vu_1}]\left[[K_{uu}]^{-1}\{P\} - [K_{uu}]^{-1}[N_{uv_1}]\{Q_v\}\right]$$

$$+ [N_{vv_2}]\{Q_v\} = \{0\} \quad (3.36)$$

Normalizing,

$$\{Q_v\} = \delta\{\bar{Q}_v\} \quad (3.37)$$

Here, $\{\bar{Q}_v\}$ is the normalized linear buckling mode with maximum transverse deflection equal to unity, and δ is the amplitude of the buckling mode shape.

Also, since $[N_1]$ is a linear function of δ and $[N_2]$ is a quadratic function of δ ,

$$\{N_1\} = \delta\{\bar{N}_1\} \quad (3.38a)$$

and

$$\{N_2\} = \delta^2\{\bar{N}_2\} \quad (3.38b)$$

The bar indicates that the respective matrix is computed using the buckling mode shape vector normalized with respect to unity. Substituting into Equation (3.36) we obtain,

$$\begin{aligned} & \delta[K_{vv}]\{\bar{Q}_v\} + P\delta[\bar{N}_{vu_1}][K_{uu}^{-1}]\{\hat{P}\} - \delta^3[\bar{N}_{vu_1}][K_{uu}^{-1}][\bar{N}_{uv_1}]\{\bar{Q}_v\}] \\ & + \delta^3[\bar{N}_{vv_2}]\{\bar{Q}_v\} = \{0\} \end{aligned} \quad (3.39)$$

$\{\hat{P}\}$ contains all zero's and a 1 where the load is being applied (at one end of the beam). Premultiplying Equation (3.39) by $\{\bar{Q}_v\}^T$ and dividing by δ , one obtains

$$b + Pe - c\delta^2 + d\delta^2 = 0 \quad (3.40a)$$

or, solving for P

$$P = \frac{-b}{e} + \frac{c-d}{e}\delta^2 \quad (3.40b)$$

where

$$b = \{\bar{Q}_v\}^T [K_{vv}] \{\bar{Q}_v\} \quad (3.41a)$$

$$c = \{\bar{Q}_v\}^T [\bar{N}_{vu_1}] [K_{uu}^{-1}] [\bar{N}_{uv_1}] \{\bar{Q}_v\} \quad (3.41b)$$

$$d = \{\bar{Q}_v\}^T [\bar{N}_{vv_2}] \{\bar{Q}_v\} \quad (3.41c)$$

$$e = \{\bar{Q}_v\}^T [\bar{N}_{vu_1}] [K_{uu}^{-1}] \{\hat{P}\} \quad (3.41d)$$

The variation of P with δ may now be found using Equation (3.40b) along with Equations (3.41a-d). Note that b , c , d , and e are constants and do not change as the loads and deflections increase; hence, they need be calculated only once for a given delaminated beam.

3.6 ENERGY RELEASE RATE

The final step is to calculate the energy release rate, G which is found in order to determine whether there exists a sufficient amount of energy for crack growth to occur. The energy release rate is very important because if crack growth begins, the beam-plate usually fails catastrophically. First, the three different cracking modes are discussed: the opening mode, the sliding mode, and the tearing mode. Figure 7, obtained from Reference 24, illustrates these three different modes of cracking. The opening mode occurs when the region above the crack is pulled upwards and the region below the crack is pulled downwards. The sliding mode is caused by in-plane shearing stress where the top region is pushed forward and the bottom region is pulled in the opposite direction. Consequently, the two regions try to slide across each other in the plane of the crack. The final type of cracking is the tearing mode which happens when the top region is pushed to one side and the bottom is pushed to the other side (out-of-plane shearing) [24].

The opening mode is the mode that occurs in a compressively loaded delaminated beam-plate, and the following discussion pertains to this first mode. The critical energy release rate for mode I cracking, G_c , is calculated from

$$G_c = \frac{\pi \sigma_c^2 a w}{E} \quad (3.42)$$

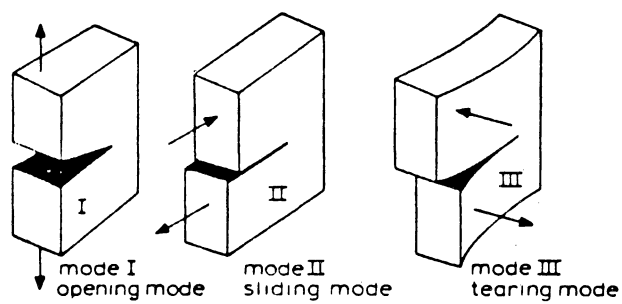


Figure 7: The three modes of cracking

where w is the width of the beam-plate (a unit width is used) and σ_c is the stress required to fracture a beam-plate with a delamination of length $2a$ units. When the energy release rate reaches this critical value, the delamination begins to grow [19]. Yin and Wang [7] derived an algebraic expression to determine the energy release rate for beams with one delamination:

$$G = \frac{1}{24EI} \left[\frac{(tP^*)^2}{\bar{h}(1-\bar{h})} + \frac{12(M^*)^2}{\bar{h}^3} + \frac{12(\frac{tP^*}{2} - M^*)^2}{(1-\bar{h})^3} \right] \quad (3.43)$$

where t is the thickness of the beam-plate. In this expression

$$\bar{h} = \frac{h}{t}, \quad (3.44)$$

$$P^* = \bar{h} \left[P_1 + 6(1-\bar{h}) \frac{M_1}{t} \right] - P_3, \quad (3.45)$$

$$M^* = M_3 - M_1 \bar{h}^3, \quad (3.46)$$

and the P_i 's and the M_i 's are the internal forces at the crack tip. Note that this expression cannot be used for beam-plates with more than one delamination. The problem of multiple delaminations is discussed in Chapter 6. The axial displacement vector $\{Q_u\}$ is found from

$$\{Q_u\} = [K_{uu}]^{-1} \{P\} - \delta^2 [K_{uu}]^{-1} [\bar{N}_{uv1}] \{\bar{Q}_v\} \quad (3.47)$$

In the incremental procedure this vector is already known. The required forces in Equation (3.43) can then be found by multiplying the appropriate element displacement vectors by the respective element stiffness matrices.

Chapter 4. Linear Buckling Results

4.1 OVERVIEW

The present developments were used to find critical loads for various types of delaminated, isotropic beam-plates. Linear buckling results are provided for beams with various boundary conditions and with symmetric, nonsymmetric, and multiple delaminations. The effects of delamination depth, location, and size are also examined. The results are compared to the analytical results of Simitises, Sallam, and Yin [5]; however, the analytical results were only provided for the simple cases of pinned-pinned and clamped-clamped beams. Finally, the case of beams with two delaminations is examined in Section 4.5.

4.2 SYMMETRIC DELAMINATIONS WITH SIMPLE BOUNDARY CONDITIONS

The two cases that are discussed in this section are pinned-pinned beams and clamped-clamped beams both with symmetric delaminations. If the delamination is centered along the length of the beam and the boundary conditions are the same on both sides, the problem is symmetric and only one half of the beam need be modeled. In these two cases regions 1, 2, and 3 (see Figure 1) are modeled by one element each. This results in a simple 5×5 eigenvalue problem for the case of the clamped-clamped beam and a 6×6 eigenvalue problem for the pinned-pinned case.

Figures 8 and 9 show the variation of the dimensionless critical load versus the dimensionless delamination length for four different delamination heights. The buckling loads, as they are throughout, are nondimensionalized by the buckling loads for beams with no delaminations, and the delamination lengths are nondimensionalized by the total beam lengths. For the purpose of comparison the results obtained by Simites et al. [5] are also shown.

The graphs show that the further the delamination is from the mid-height of the beams, the less stable the beams are in buckling. Beams with delaminations that are both thin (close to the top or bottom) and short are extremely sensitive to increasing delamination length as the buckling load drops off very quickly in this region. In general the dimensionless critical loads for the clamped-clamped beams decrease more quickly with increasing delamination

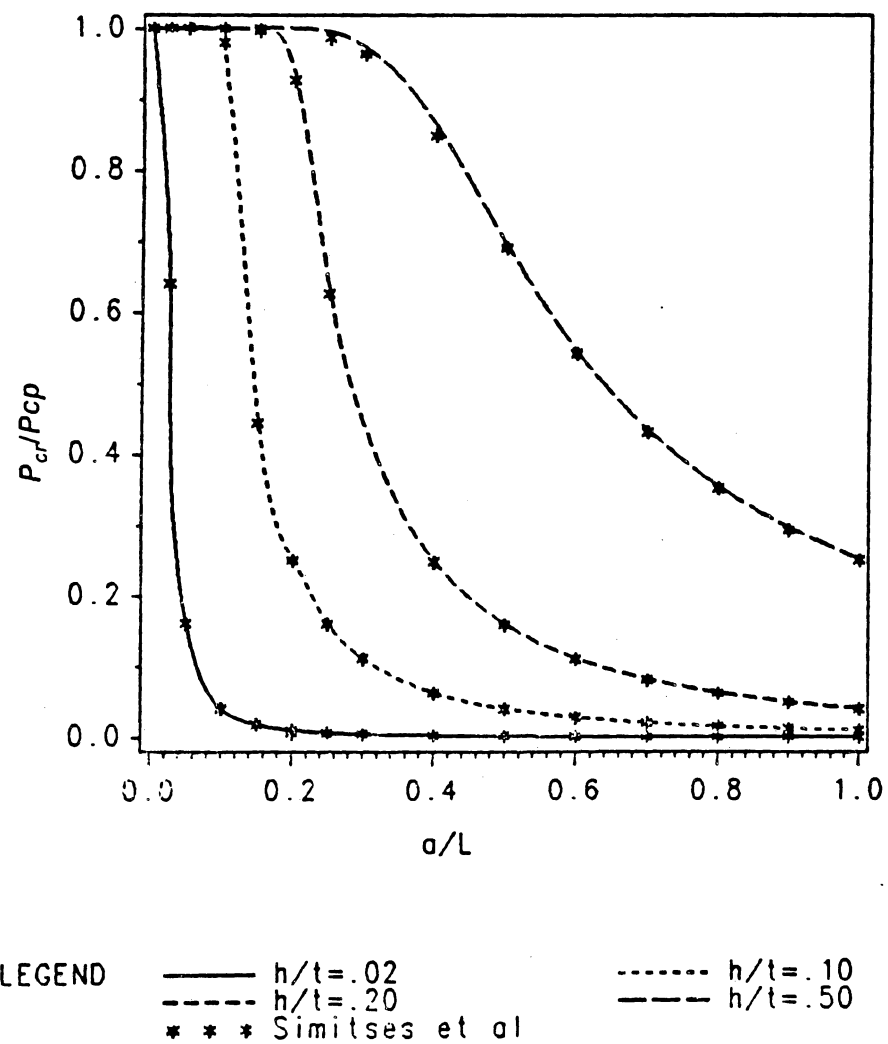
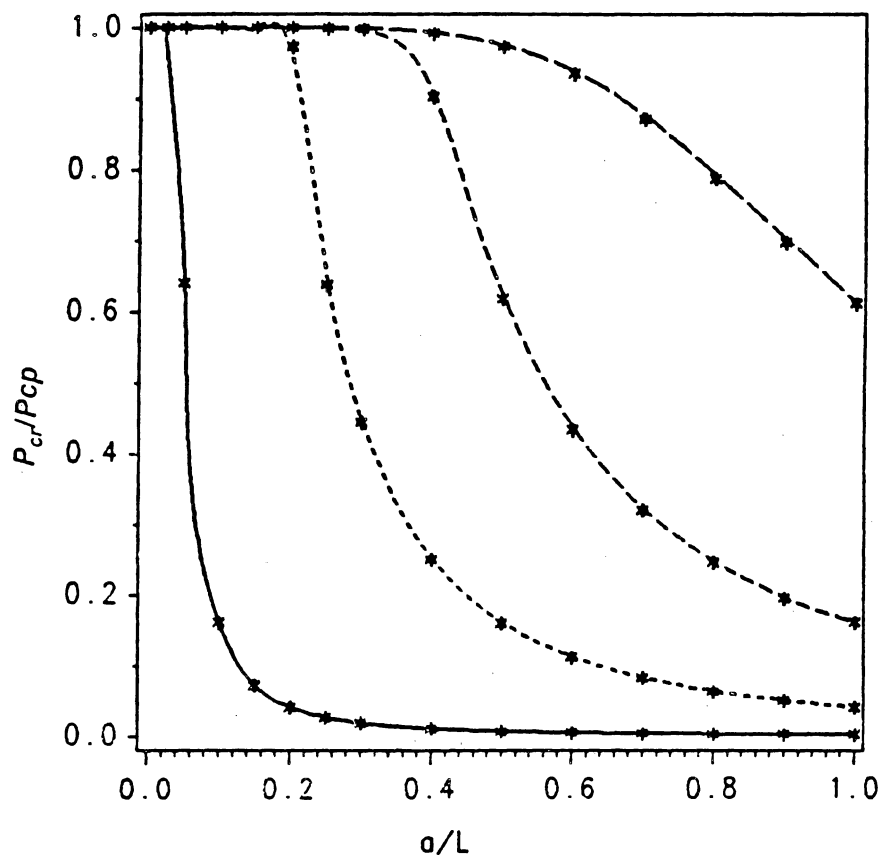


Figure 8: Dimensionless critical load vs. dimensionless delamination length for clamped-clamped beams



LEGEND

— $h/t = .02$

- - - $h/t = .20$

* * * Simiteses et al

..... $h/t = .10$

- . - $h/t = .50$

Figure 9: Dimensionless critical load vs. dimensionless delamination length for pinned-pinned beams

length than those for the pinned-pinned beams. After comparing the buckling load results with those of Simites et al. [5], it is seen that they agree almost exactly even though the minimum number of finite elements is used for these cases.

It is important to note that the buckling loads are calculated assuming the slopes at the crack tips are the same in the regions above and below the delamination. Therefore, even when $\frac{a}{L} = 1.0$ the beams still do not behave independently. For example, the dimensionless buckling load of the pinned-pinned beam with $\frac{h}{t} = 0.5$ was 0.61, whereas if the top and bottom portions behaved independently, a value of 0.25 would be expected (one half of the beam-plate would carry one half of the axial load and half the beam-plate has one eighth of the moment of inertia of whole beam).

4.3 SYMMETRIC DELAMINATIONS WITH VARIOUS BOUNDARY CONDITIONS

In this section beams with clamped-pinned and clamped-free boundary conditions and also beams with elastic boundary conditions are discussed. Since the boundary conditions are now nonsymmetric, the whole beam must be modeled. In this and the following section the results are obtained by modeling regions 1, 2, 3, and 4 (see Figure 1) by 1, 2, 2, and 1 or a total of 6 elements respectively. Figures 10 and 11 show the variation of critical load versus delamination length for clamped-pinned and clamped-free beams respectively. The same general trends are observed; however, in Figure 10

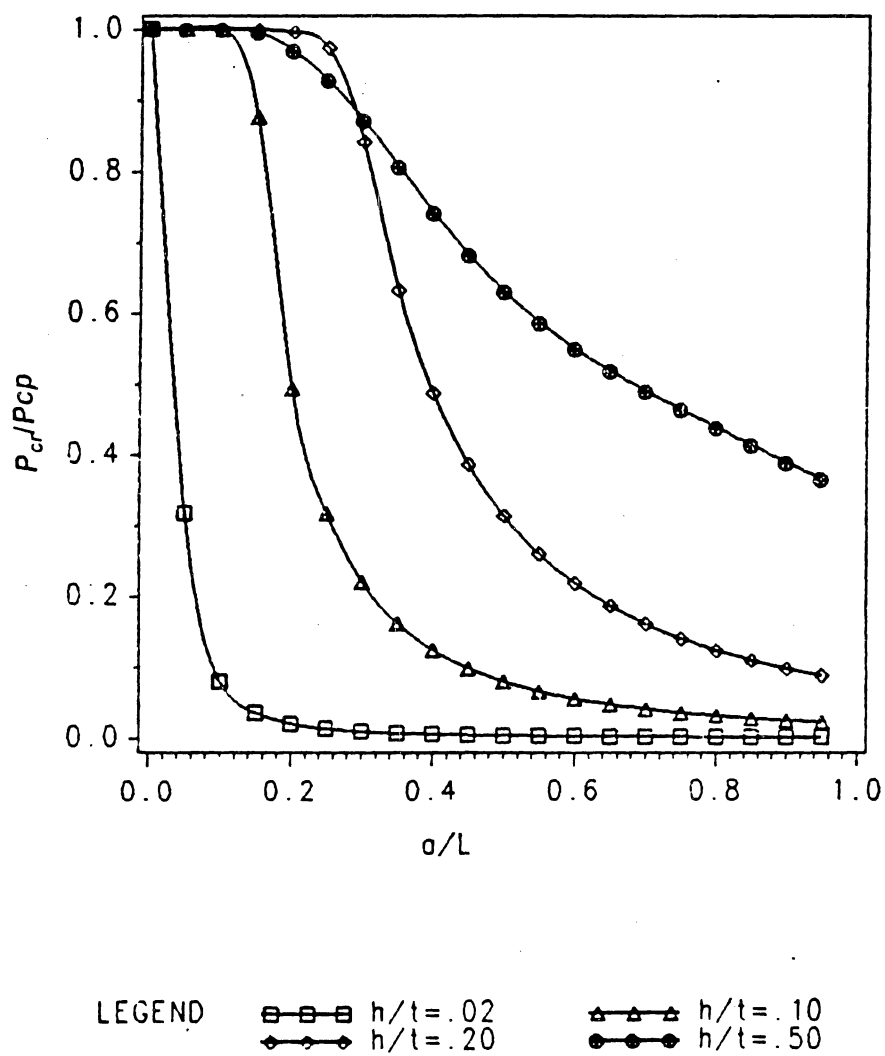


Figure 10: Dimensionless critical load vs. dimensionless delamination length for pinned-clamped beams

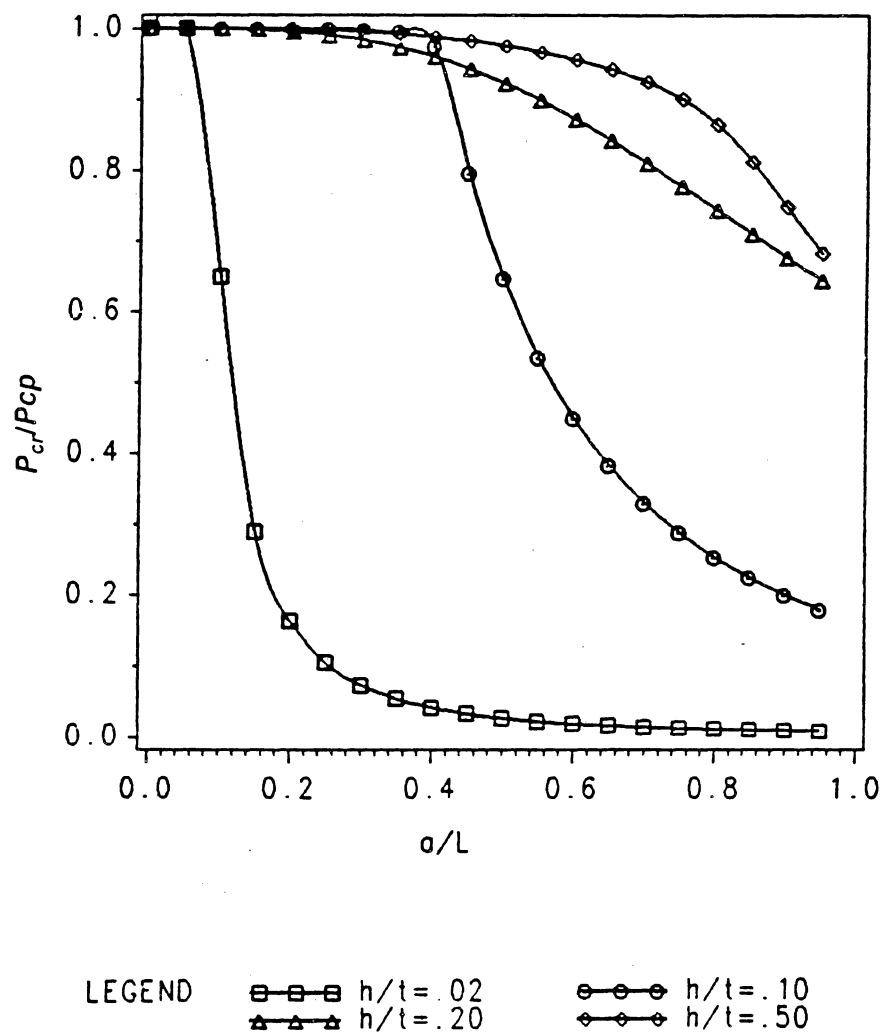
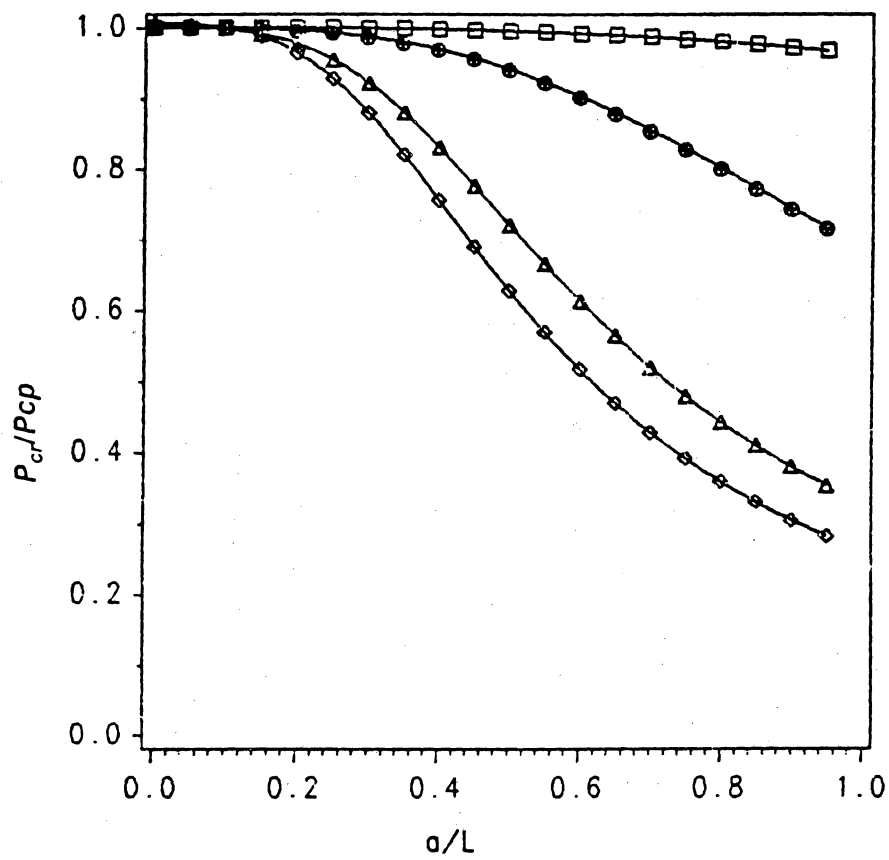


Figure 11: Dimensionless critical load vs. dimensionless delamination length for clamped-free beams

the curve for $\frac{h}{t} = 0.5$ drops below the curve for $\frac{h}{t} = 0.2$, whereas the curves did not cross in the previous cases. In Figure 10 it is observed that the clamped-free beams are less affected by the delaminations than all previous cases. In fact, for $\frac{h}{t} = 0.5$ and $\frac{h}{t} = 0.2$ even with a delamination extending along 95 percent of the beam, the buckling load is still approximately 65 percent of the buckling load for the same beam with no delaminations.

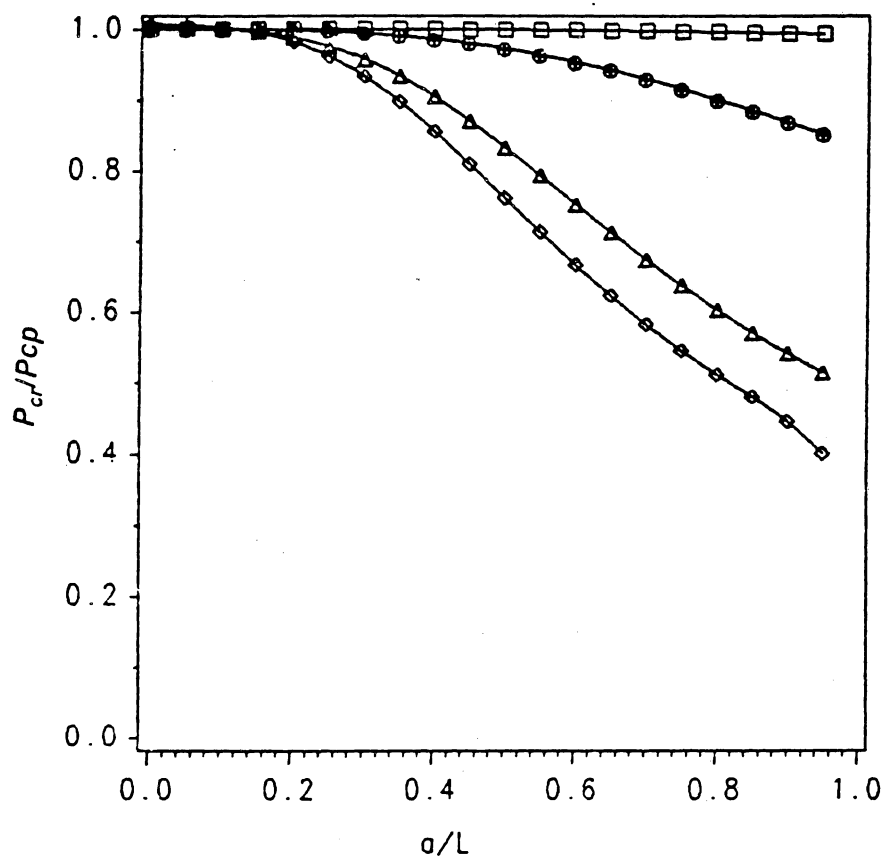
Next, dimensionless critical load versus dimensionless delamination length plots are shown in Figures 12 through 15 for beams with elastic supports. The elastic supports considered here are two extensional springs resisting the vertical motion at each end of the beam and two rotational springs resisting the rotation of the beam at each end. A representative case of $\frac{h}{t} = 0.3$ is chosen. The extensional spring constant is α which varies from $.1 \frac{EI}{L^3}$ to $100 \frac{EI}{L^3}$. The rotational spring constant is β , and it varies from $.1 \frac{EI}{L}$ to $100 \frac{EI}{L}$.

Each of Figures 12 through 15 show dimensionless critical load versus dimensionless delamination length for $\frac{h}{t} = 0.3$ for one value of α and four different values of β . The critical loads are normalized by the critical load of a perfect beam with no delamination and the same boundary conditions. In the figures α is multiplied by $\frac{L}{EI}$ and β by $\frac{L^3}{EI}$. Note that the critical load of an undelaminated beam changes when α and β change. Critical loads for beams without delaminations (used for nondimensionalization) having different α 's and β 's are provided in Table 1.



LEGEND $\square-\square-\square$ $\beta=0.1$ $\bullet-\bullet-\bullet$ $\beta=1$
 $\triangle-\triangle-\triangle$ $\beta=10$ $\diamond-\diamond-\diamond$ $\beta=100$

Figure 12: Dimensionless critical load vs. dimensionless delamination length for elastically-supported beams with $\frac{h}{t} = .3$ and $\alpha = .1$



LEGEND $\square-\square-\square$ $\beta=0.1$ $\bullet-\bullet-\bullet$ $\beta=1$
 $\triangle-\triangle-\triangle$ $\beta=10$ $\diamond-\diamond-\diamond$ $\beta=100$

Figure 13: Dimensionless critical load vs. dimensionless delamination length for elastically-supported beams with $\frac{h}{t} = .3$ and $\alpha=1$

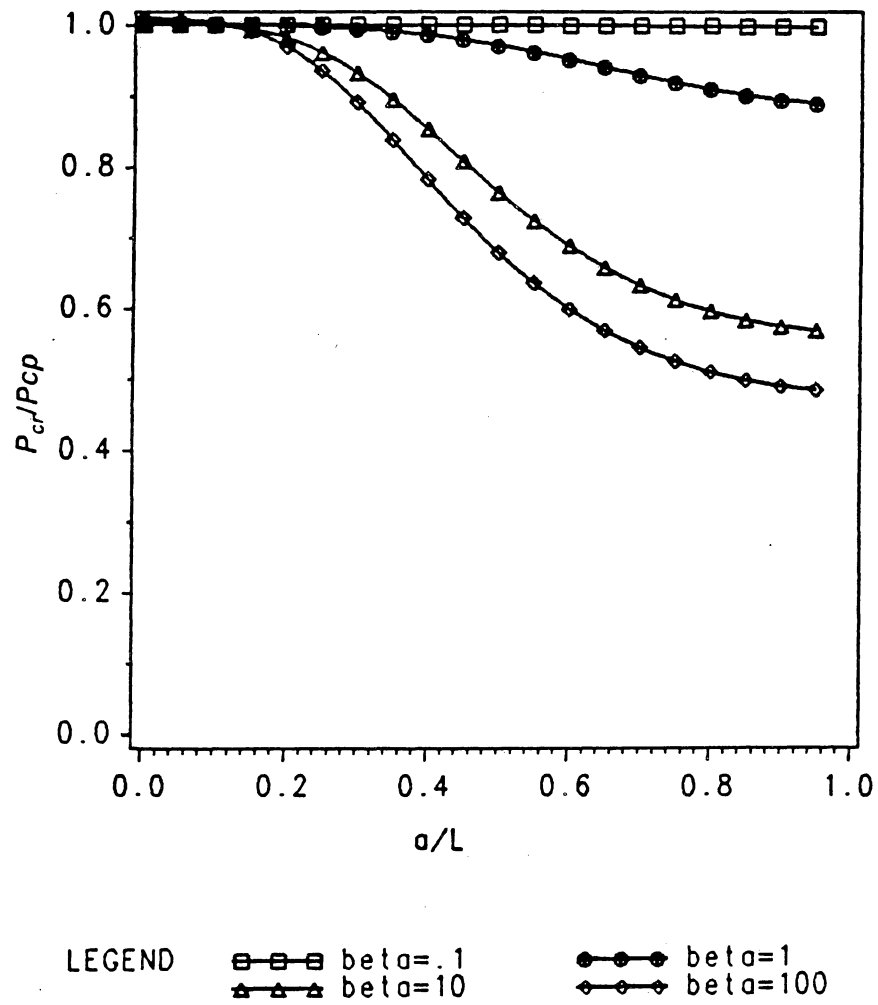


Figure 14: Dimensionless critical load vs. dimensionless delamination length for elastically-supported beams with $\frac{h}{t} = .3$ and $\alpha = 10$

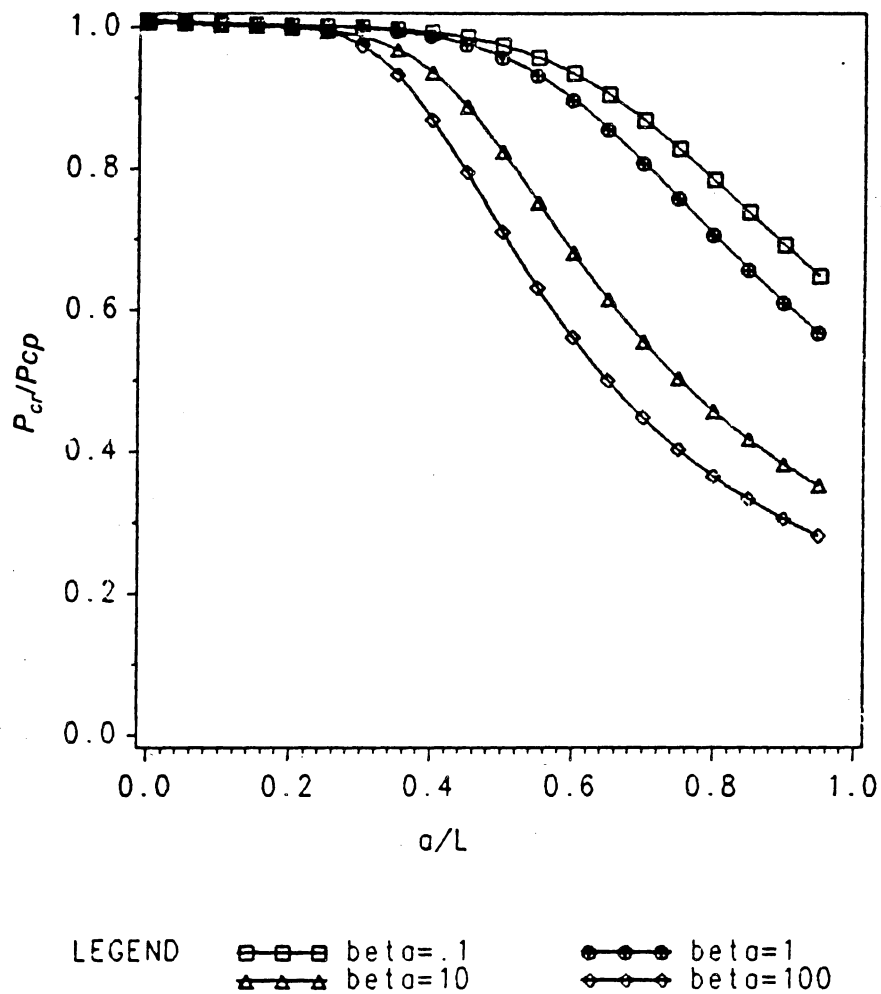


Figure 15: Dimensionless critical load vs. dimensionless delamination length for elastically-supported beams with $\frac{h}{t} = .3$ and $\alpha = 100$

Table 1: Buckling Loads ($P_{cr}/\frac{EI}{L^2}$) for Elastically-supported Beams without Delaminations

| $\alpha \backslash \beta$ | .1 | 1 | 10 | 100 |
|---------------------------|-------|-------|-------|--------|
| .1 | 0.247 | 0.697 | 5.196 | 10.268 |
| 1 | 1.757 | 2.205 | 6.682 | 13.496 |
| 10 | 6.551 | 7.361 | 11.44 | 28.207 |
| 100 | 9.530 | 9.901 | 13.59 | 38.055 |

It is observed from the figures that in general the buckling loads for the elastically-supported beams are less affected by the presence of delaminations than the beams with the fixed supports, especially when α and β are small. The reason is that for small values of α and β , the buckling loads for the beams with no delamination are small and global buckling occurs first before local buckling of the delaminated regions occurs. In fact, except for Figure 15 in which $\alpha = 100 \frac{EI}{L^3}$, the critical loads are virtually unaffected for small values of β . As β increases, the buckling loads begin to drop off more and more especially for the larger delamination lengths.

4.4 NONSYMMETRIC DELAMINATIONS

The effect of off-center delaminations (with respect to length) was also studied. In this case region 1 is modeled by 1 element, regions 2 and 3 by 2 elements each, and region 4 by 3 elements (it is much longer in certain cases). Hence, a total of 8 elements is used to analyze a given beam.

The variation of dimensionless critical load for various delamination locations and heights is shown in Table 2 for clamped-clamped beams and in Table 3 for pinned-pinned beams. The normalized delamination length in all cases is $\frac{a}{L} = 0.2$. Results obtained by Simites et al. [5] are also presented in the table for comparison. The most important observation from these two tables is that the buckling loads do not vary significantly with respect to delamination location along the length of the beams. The buckling loads obtained in the

Table 2: $\frac{P_{cr}}{P_{cp}}$ for Clamped-Clamped Beams with Nonsymmetric Delaminations, $\frac{a}{L} = .2$

| | $\frac{l}{L} = 0.0$ | | $\frac{l}{L} = 0.1$ | | $\frac{l}{L} = 0.2$ | | $\frac{l}{L} = 0.3$ | | $\frac{l}{L} = 0.4$ | |
|---------------|---------------------|-------|---------------------|-------|---------------------|-------|---------------------|-------|---------------------|-------|
| $\frac{h}{t}$ | S | T | S | T | S | T | S | T | S | T |
| 0.05 | .0625 | .0633 | .0625 | .0633 | .0625 | .0633 | .0625 | .0633 | .0625 | .0633 |
| 0.10 | .2497 | .2530 | .2497 | .2530 | .2496 | .2529 | .2496 | .2528 | .2494 | .2528 |
| 0.20 | .9328 | .9406 | .9480 | .9530 | .9455 | .9500 | .9309 | .9377 | .9264 | .9339 |
| 0.30 | .9557 | .9618 | .9142 | .9176 | .9195 | .9219 | .9613 | .9684 | .9924 | .9972 |
| 0.40 | .9248 | .9301 | .8652 | .8680 | .8768 | .8789 | .9402 | .9433 | .9950 | .9998 |
| 0.50 | .9051 | .9100 | .8405 | .8431 | .8555 | .8574 | .9277 | .9307 | .9955 | .9999 |

S: Simitises, Sallam, and Yin

T: This study

Table 3: $\frac{P_{cr}}{P_{cp}}$ for Pinned-Pinned Beams with Nonsymmetric Delaminations, $\frac{a}{L} = .2$

| | $\frac{l}{L} = 0.0$ | | $\frac{l}{L} = 0.1$ | | $\frac{l}{L} = 0.2$ | | $\frac{l}{L} = 0.3$ | | $\frac{l}{L} = 0.4$ | |
|---------------|---------------------|-------|---------------------|-------|---------------------|-------|---------------------|-------|---------------------|-------|
| $\frac{h}{t}$ | S | T | S | T | S | T | S | T | S | T |
| 0.05 | .2499 | .2532 | .2699 | .2532 | .2699 | .2532 | .2499 | .2532 | .2499 | .2532 |
| 0.10 | .9882 | .9923 | .9814 | .9864 | .9764 | .9817 | .9733 | .9788 | .9723 | .9782 |
| 0.20 | .9890 | .9899 | .9919 | .9922 | .9954 | .9956 | .9983 | .9985 | .9994 | .9999 |
| 0.30 | .9797 | .9830 | .9851 | .9854 | .9918 | .9920 | .9975 | .9977 | .9996 | .9999 |
| 0.40 | .9690 | .9696 | .9772 | .9775 | .9875 | .9877 | .9962 | .9964 | .9997 | .9999 |
| 0.50 | .9637 | .9642 | .9732 | .9736 | .9853 | .9655 | .9956 | .9958 | .9997 | .9999 |

S: Simiteses, Sallam, and Yin
T: This study

unsymmetric cases are very close to the buckling loads obtained in the symmetric case ($\frac{I}{L} = 0.4$). A comparison with results given by Simites et al. [5] shows that the finite element results are in excellent agreement with the analytical results.

4.5 MULTIPLE DELAMINATIONS

Beams with more than one delamination are now considered. The problem in this section involves beams with two delaminations of the same length, one located directly above the other. The geometry of this problem is shown in Figure 16: the dimensions H and h are the same as before and m is the height of the center delaminated region, so the third dimension depends on the first two. The beams with two delaminations are compared to the same beams with only one delamination: the one that gives the thinnest delamination region (the most critical case).

For beams with two delaminations it is found that the stability of the beam in compression depends greatly on the thinnest delaminated region, especially when one delaminated region is much thinner than the other two. In this case, the critical load versus delamination length curve is very similar to the curve for a beam having just the one thin delamination. For example, if a beam with two delaminations has dimensions of $\frac{h}{t} = 0.2$ and $\frac{H}{t} = 0.4$, then the delaminated regions have dimensionless thicknesses of 0.2, 0.4, and 0.4. The critical loads are then almost identical to those of a beam with one delamination at $\frac{h}{t} = 0.2$. On the other hand, when the delaminated regions have approximately the same heights, the buckling loads drop below those of the corresponding beams having only the thinner delamination.

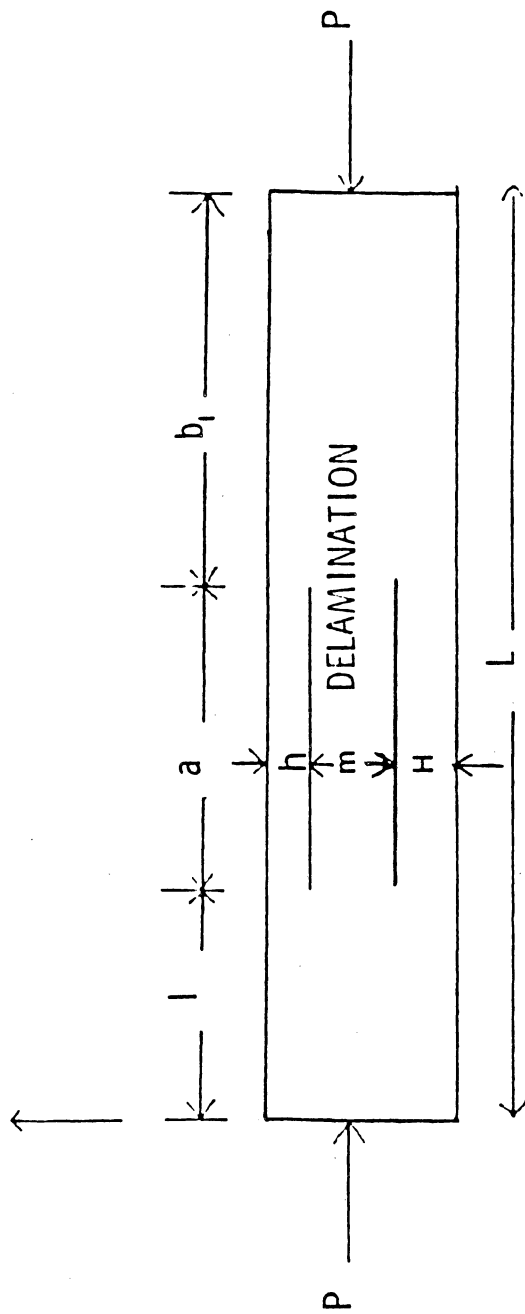
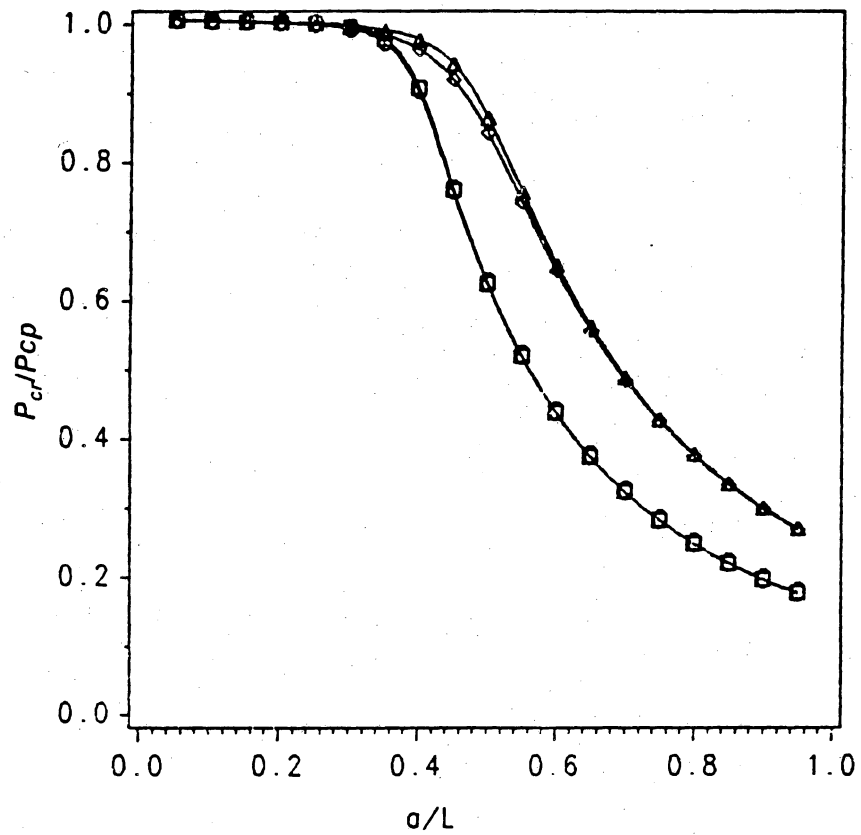


Figure 16: Schematic diagram of beam-plate with two delaminations

Graphs comparing the critical buckling load versus delamination length for beams with one and two delaminations are given in Figures 17-20, and they demonstrate all of the effects previously discussed. Four different curves for pinned-pinned beams are shown in Figure 17. The first case considered is a beam with two delaminations with $\frac{h}{t} = 0.2$ and $\frac{H}{t} = 0.4$ (therefore $\frac{m}{t} = 0.4$) which is compared to a beam with one delamination at $\frac{h}{t} = 0.2$. The top delaminated region is very thin compared to the other regions so buckling depends strongly on the buckling of this region. Therefore, as expected, the buckling loads are almost the same as those for the beam with one delamination at $\frac{h}{t} = 0.2$. The next case in the same figure shows results similar to those of the first case; however, two of the delaminated regions of the beam with two delaminations are closer together (0.25 and 0.3). For this reason the buckling loads do not depend strictly on the failure of the thinnest region. Between $\frac{a}{L} = 0.3$ and $\frac{a}{L} = 0.6$, the beam with two delaminations is slightly less stable than the corresponding beam with one delamination at $\frac{h}{t} = 0.25$. Still the second delamination has a very small affect on the buckling load.

All the same curves as in Figure 17 are shown in Figure 18 for clamped-clamped boundary conditions. The results are similar: the first case of the beam with two delaminations having one delaminated region much thinner (0.2, 0.4, 0.4) is the same as the corresponding beam having just the thinner delamination. In the second case the buckling loads are similar except

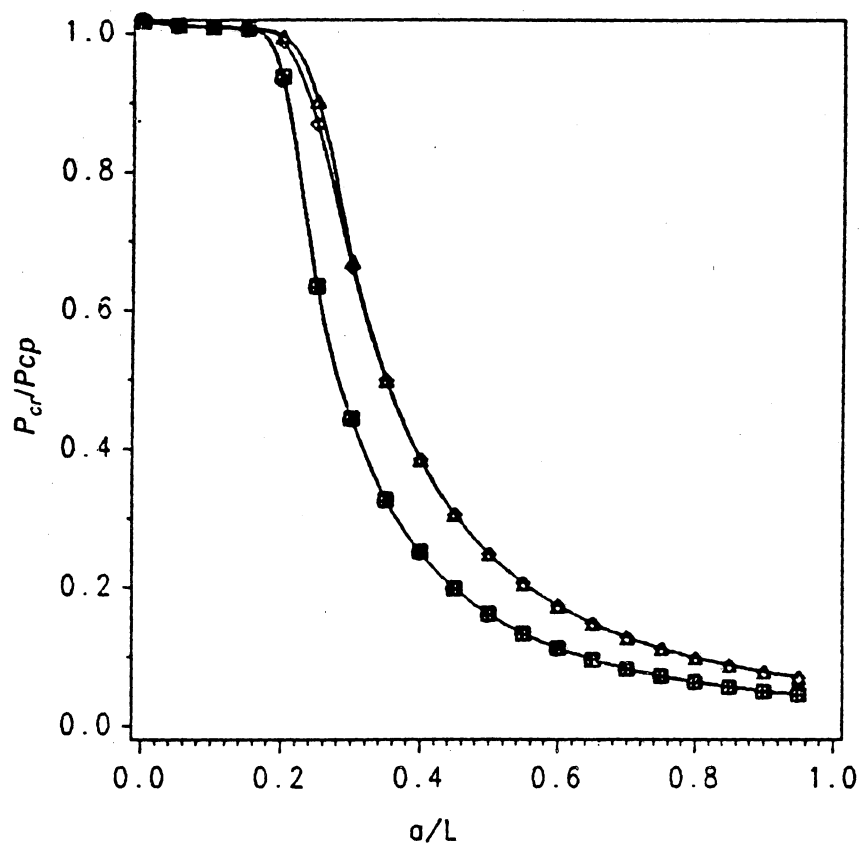


LEGEND

□-□-□ 1, $h/t=.2$
 ▲-▲-▲ 1, $h/t=.25$

○-○-○ 2, $h/t=.2, H/t=.4$
 ◇-◇-◇ 2, $h/t=.25, H/t=.3$

Figure 17: Dimensionless critical load vs. dimensionless delamination length for pinned-pinned beams with one and two delaminations and $\frac{a}{L} = .5$

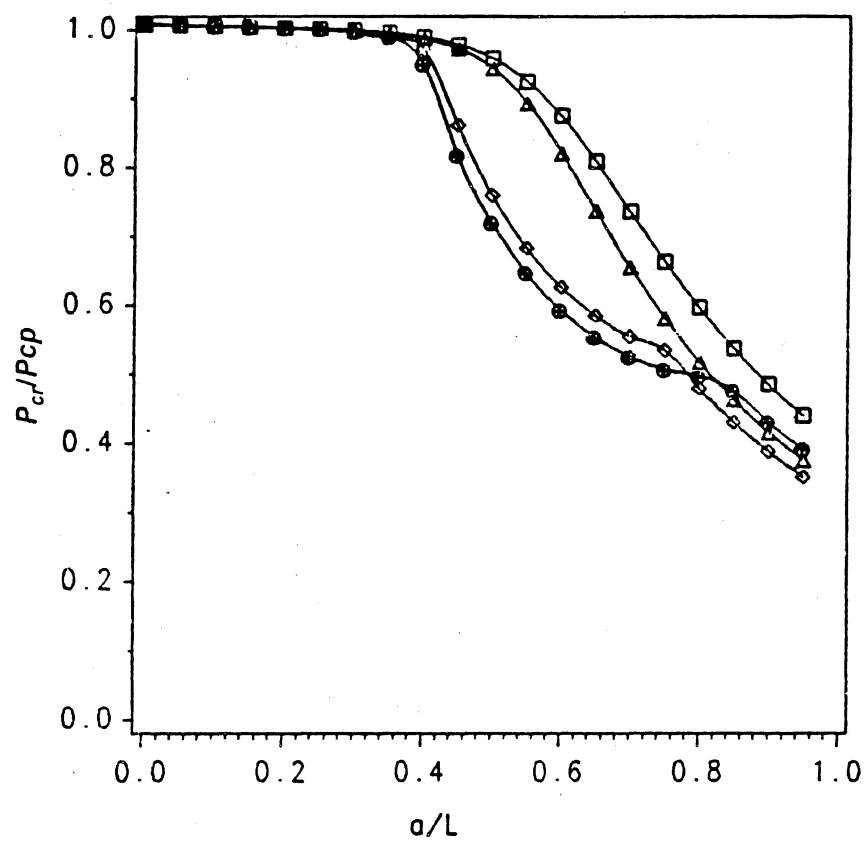


LEGEND

□-□-□ 1, $h/t = .2$
 ▲-▲-▲ 1, $h/t = .25$

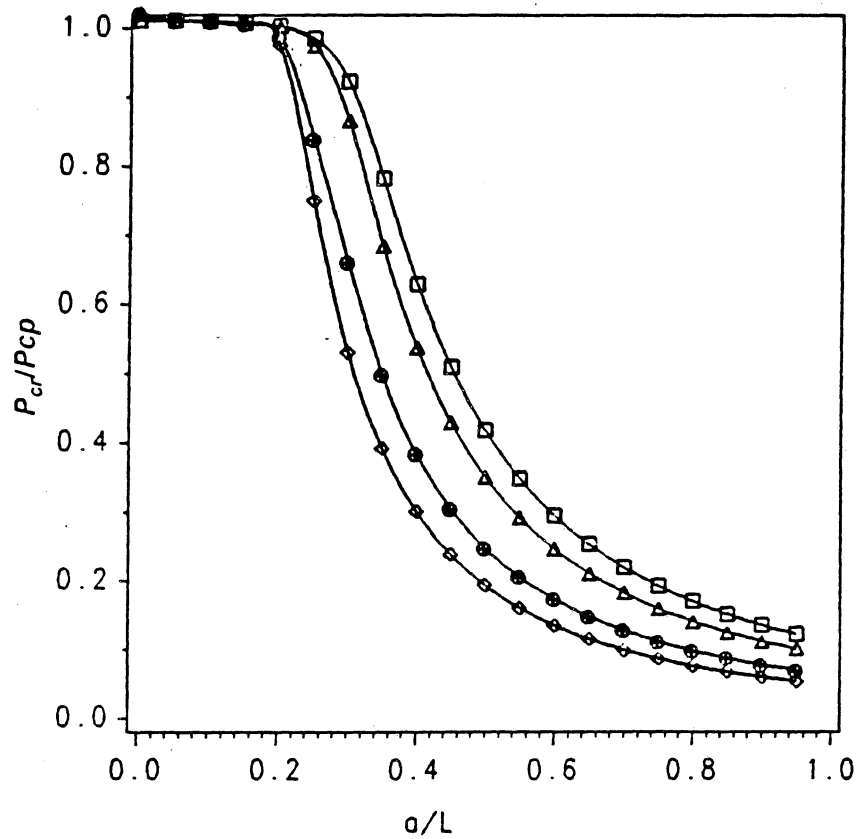
●-●-● 2, $h/t = .2, H/t = .4$
 ◆-◆-◆ 2, $h/t = .25, H/t = .3$

Figure 18: Dimensionless critical load vs. dimensionless delamination length for clamped-clamped beams with one and two delaminations and $\frac{a}{L} = .5$



LEGEND $\square-\square-\square$ 1, $h/t = .33$ $\bullet-\bullet-\bullet$ 2, $h/t = H/t = .33$
 $\triangle-\triangle-\triangle$ 1, $h/t = .3$ $\diamond-\diamond-\diamond$ 2, $h/t = .3, H/t = .4$

Figure 19: Dimensionless critical load vs. dimensionless delamination length for pinned-pinned beams with one and two delaminations and $\frac{a}{L} = .5$



LEGEND

| | | | |
|-------|----------------|-------|-------------------------|
| □—□—□ | 1, $h/t = .33$ | ●—●—● | 2, $h/t = H/t = .33$ |
| △—△—△ | 1, $h/t = .3$ | ◇—◇—◇ | 2, $h/t = .3, H/t = .4$ |

Figure 20: Dimensionless critical load vs. dimensionless delamination length for clamped-clamped beams with one and two delaminations and $\frac{a}{L} = .5$

for the region between $\frac{a}{L} = 0.2$ and $\frac{a}{L} = 0.3$ where the beam with two delaminations is slightly weaker.

Figures 19 and 20 are provided to show what happens when all the delaminated regions have approximately equal heights. In these cases the second delamination has a significant effect. Dimensionless buckling loads are shown in Figure 20 for pinned-pinned beams with regions of 0.33, 0.33, and 0.34 in the first case, and 0.30, 0.30, and 0.40 in the second case. These beams are compared with a beam with one delamination at 0.33 and a beam with one delamination at 0.30. The beams with two delaminations are obviously much weaker with differences of as much as 35 percent near $\frac{a}{L} = 0.55$. The curves begin to come together as $\frac{a}{L}$ approaches 1.

Results for beams with the same dimensions but with clamped-clamped boundary conditions are provided in Figure 20. Here, the beams with two delaminations are much weaker in all cases from $\frac{a}{L} = 0.2$ all the way to $\frac{a}{L} = 1.0$, especially between $\frac{a}{L} = 0.3$ and $\frac{a}{L} = 0.5$.

4.6 CONCLUSIONS ON LINEAR BUCKLING RESULTS

In obtaining the results for the simple cases of the pinned-pinned and clamped-clamped beams, the linear approximation for the axial displacement and the cubic approximation for the transverse displacement were used, and the minimum number of elements was used. These approximations were

found to be sufficient as the results agreed almost exactly with the analytical results of Simites et al. [5] (analytical results were done only for these simple cases). The finite element method can easily handle various boundary conditions as was shown in Section 4.3.

For the nonsymmetric problem in Section 4.4, more elements were needed for cases when element length differences were large. The number of elements used to model the four different regions was chosen such that all the element lengths were approximately equal. However, it is obvious from Tables 1 and 2 that the buckling loads are only slightly affected by the location with respect to length of the delamination. In fact, unless a very high degree of accuracy is required, centering the delamination and performing a symmetric analysis (fewer elements required) provides a very accurate solution.

The solution of problems with two delaminations (Section 4.5) can also be made simpler and more efficient in most cases. As discussed previously, the buckling load is hardly affected by the second delamination unless all the delamination heights are very close together (see Figures 17-20). If one delamination height is small (smallest height of approximately $\frac{h}{t} = 0.25$ or less), an accurate buckling load may be obtained by doing the problem as if only the thinner delamination existed. Hence, the problem is greatly simplified and requires fewer elements. Analogous results are obtained for beams having more than two delaminations.

Chapter 5. Postbuckling and Energy Release Rate Results

5.1 OVERVIEW

In this chapter the nonlinear postbuckling and energy release rate results are presented using the methods previously discussed. In Section 5.2 a convergence study is performed for the incremental solution and results for several cases are compared to the analytical results of Yin, Sallam, and Simites [6]. In the next section the effects of the delamination are studied by comparing the response of beams with and without delaminations on load-end shortening and load-deflection plots. In Section 5.4 the more economical constant mode shape analysis is used to find energy release rates, and the results are compared to the results obtained using the incremental method. Next, results on energy release rates for beams with various boundary conditions are given in Section 5.5. In Section 5.6 the effects of nonsymmetric

delaminations on the energy release rate are considered. Finally, conclusions on the different types of methods are given in Section 5.7.

5.2 INCREMENTAL METHOD

In this section a convergence study is performed for the incremental method to determine the number of elements which is best for accuracy and efficiency. These results are compared to the analytical results of Yin et al [6]. Next, incremental results are obtained for some additional clamped-clamped cases and compared to the analytical results. The representative beams having delamination heights of $\frac{h}{t} = 0.3$ (thick delamination) and $\frac{h}{t} = 0.1$ (thin delamination) are chosen. The analytical results are given only for clamped-clamped beam-plates.

A diagram showing the applied loads is given in Figure 21: the load applied to the region above the delamination is Q_T and the load applied to the region below the delamination is Q_B . The purpose of these two loads is only to initiate bending, and it was found that as long as these loads are very small, changing their magnitudes slightly does not effect the solution. Therefore, for consistency, the values of the transverse loads applied in all cases in this chapter are $Q_B = -0.0001Pcp$ and $Q_T = 0.0001Pcp$. Q_B is negative and Q_T is positive because in all cases considered in this chapter, the bottom region deflects downwards and the top region deflects upwards in the postbuckling region.

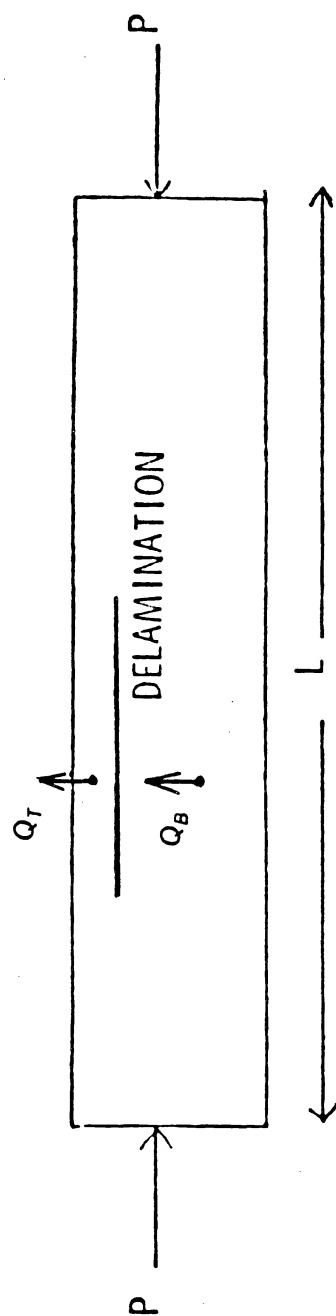


Figure 21: Diagram of applied loads used to find nonlinear postbuckling solution

The convergence study for the incremental method for $\frac{h}{t} = 0.3$ and $\frac{a}{L} = 0.5$ is shown in Figure 22. Dimensionless axial load, \bar{P} , is plotted versus dimensionless energy release rate, \bar{G} , for the incremental solution with three different numbers of elements, and these curves are compared with the analytical solution of Yin et al [6]. The axial load is nondimensionalized by

$$\bar{P} = \frac{P}{EI} \left(\frac{L}{2\pi} \right)^2 \quad (5.1)$$

which is again the critical load for the same beam with no delaminations. The dimensionless buckling load for the case of $\frac{h}{t} = 0.3$ and $\frac{a}{L} = 0.5$ found in Chapter 4 is 0.35. The equation for the dimensionless energy release rate which is used in all cases is

$$\bar{G} = \frac{G}{Et^5} \left(\frac{L}{2} \right)^4 \quad (5.2)$$

\bar{G} is extremely small before the critical \bar{P} is reached and \bar{G} increases monotonically at the critical \bar{P} . The \bar{P} versus \bar{G} curves start at the respective buckling loads in all plots of \bar{P} versus \bar{G} . All of the curves in Figure 22 are nearly coincident near the buckling load and begin to diverge for larger values of \bar{P} . As more elements are added, the finite element solution begins to converge towards the analytical solution. It can be seen from Figure 22 that

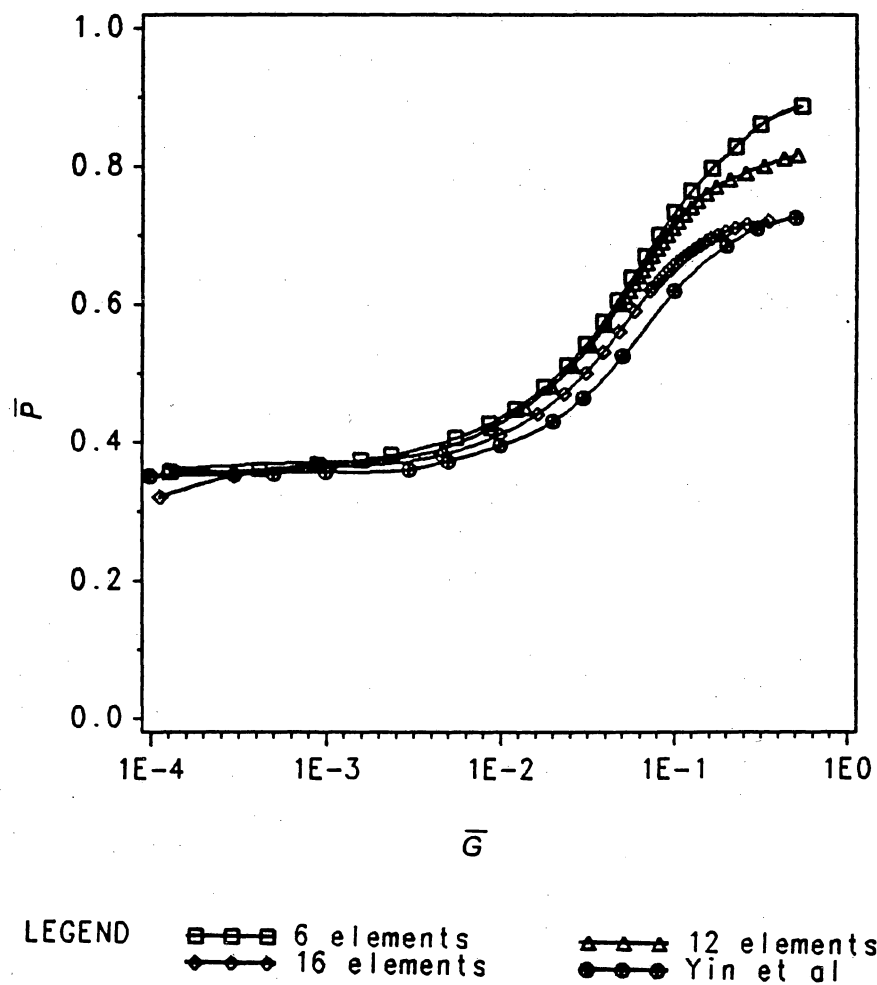


Figure 22: Dimensionless axial load vs. dimensionless energy release rate using incremental method for clamped-clamped beams with $\frac{h}{t} = .3$ and $\frac{a}{L} = .5$

the 16-element solution is very close to the analytical solution. Hereafter, this 16-element solution is used for all cases of $\frac{h}{t} = 0.3$.

Next, a convergence test for $\frac{h}{t} = 0.1$ is performed and the results are shown in Figure 23. The dimensionless buckling load is 0.04 for the case of $\frac{h}{t} = 0.1$ and $\frac{a}{L} = 0.5$. As in Figure 22, all the solutions are nearly identical near the buckling load. The finite element solutions approach the analytical solution as the number of elements is increased from 6 to 10. However, the finite element solutions begin to diverge when the number of elements is increased beyond 10. Apparently, numerical difficulties exist for very thin delaminations. Since the 10-element solution is the most accurate compared to the analytical solution, it is used for all cases of $\frac{h}{t} = 0.1$ in the remainder of the thesis.

Next, additional finite element energy release rate results for more cases of clamped-clamped delaminated beam-plates are compared to the analytical results. Note, this simple boundary condition case is the only one which can be compared since the analytical results were only provided for this case. Finite element results for other various boundary conditions are also given in this chapter. Dimensionless axial load versus dimensionless energy release rate is plotted in Figure 24 for clamped-clamped delaminated beams with $\frac{h}{t} = 0.3$ with dimensionless delamination lengths of 0.4 and 0.6. The finite element solution agrees very well with the analytical results for loads near buckling. The finite element curves gradually rise above the analytical curves, but in each of the two cases the two different solutions remain close together.

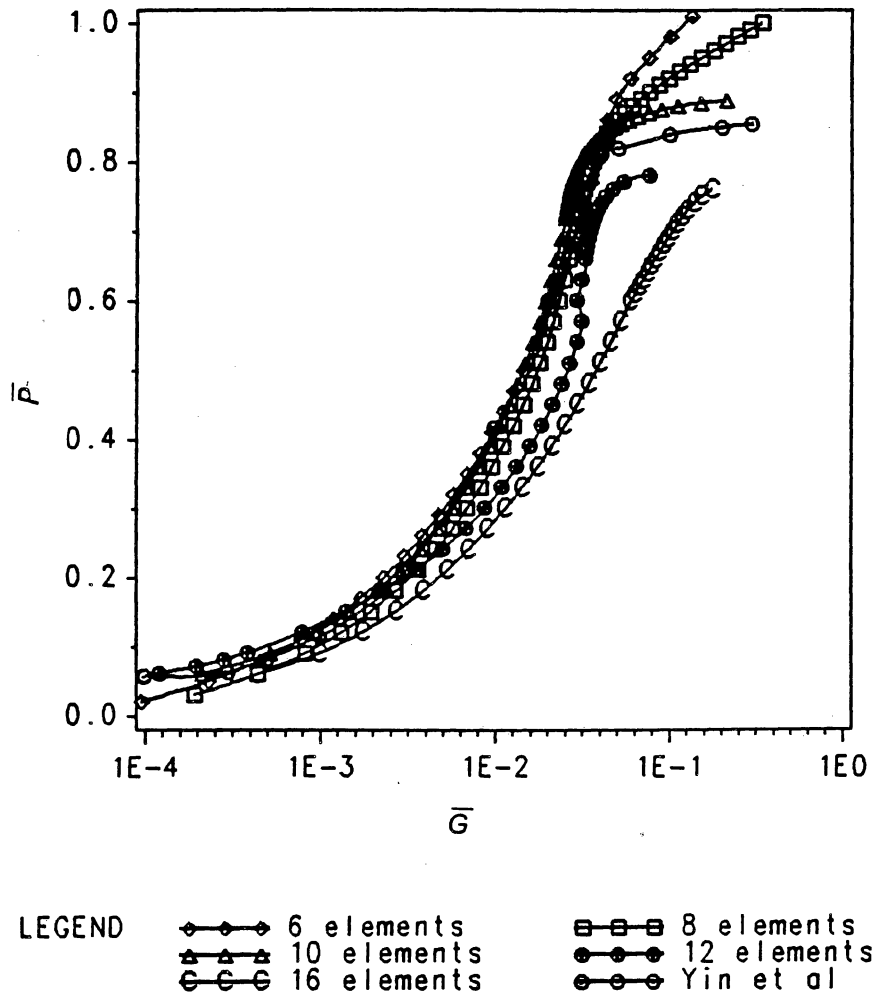
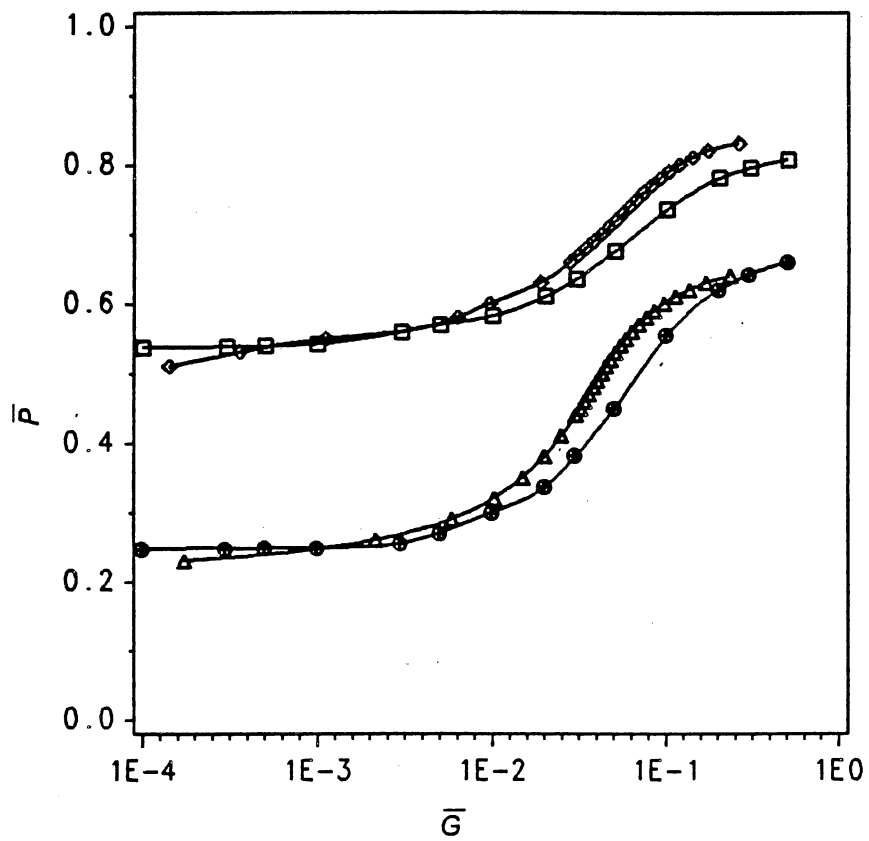


Figure 23: Dimensionless axial load vs. dimensionless energy release rate using incremental method for clamped-clamped beams with $\frac{h}{t} = .1$ and $\frac{a}{L} = .5$



LEGEND $\diamond-\diamond-\diamond$ FEM, $a/L=.40$ $\square-\square-\square$ Yin, $a/L=.40$
 $\triangle-\triangle-\triangle$ FEM, $a/L=.60$ $\bullet-\bullet-\bullet$ Yin, $a/L=.60$

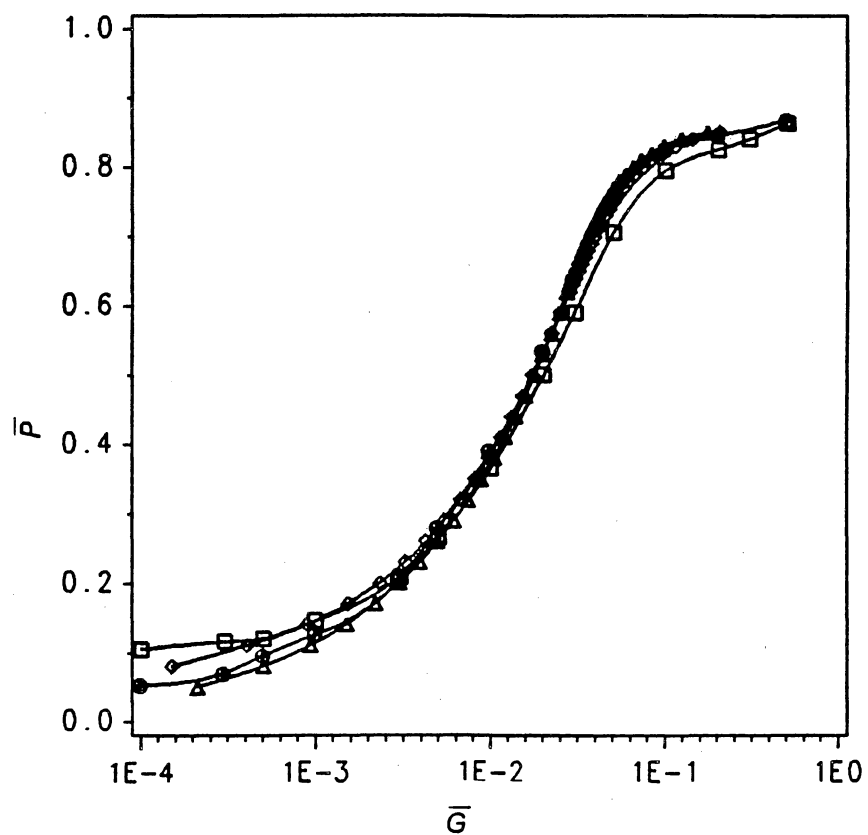
Figure 24: Dimensionless axial load vs. dimensionless energy release rate using incremental method for clamped-clamped beams with $\frac{h}{t} = .3$

the same plots are shown in Figure 25 for the thinner delamination of $\frac{h}{t} = 0.1$ and for dimensionless crack lengths of $\frac{a}{L} = 0.3$ and 0.4 . In the thinner delamination case, the axial load increases rapidly with energy release rate. The finite element curves nearly coincide with the analytical curves throughout the range of axial loads considered. Some load versus displacement diagrams will be given in the next section to show the effects of the delaminations.

5.3 COMPARISON OF DELAMINATED BEAMS WITH AND WITHOUT DELAMINATIONS

In this section the effect of a single delamination with length $\frac{a}{L} = 0.5$ on the postbuckling strength of the beam-plate is discussed. Two delamination thicknesses for the beam-plate are considered, $\frac{h}{t} = 0.1$ and $\frac{h}{t} = 0.3$. The strengths of the delaminated beam-plates are compared to the strengths of an undelaminated beam-plate which was modeled using five elements. The results for the undelaminated beam were obtained using one transverse load with magnitude of $0.0002P_{cp}$ which was applied downwards at the midlength in order to initiate bending of the undelaminated beam. In the graphs the equation for the dimensionless axial displacement, \bar{u} , is

$$\bar{u} = \frac{u}{L} \left(\frac{L}{t} \right)^2 \quad (5.3)$$



LEGEND \diamond - \diamond - \diamond FEM, $a/L=.30$ \square - \square - \square Yin, $a/L=.30$
 \triangle - \triangle - \triangle FEM, $a/L=.40$ \bullet - \bullet - \bullet Yin, $a/L=.40$

Figure 25: Dimensionless axial load vs. dimensionless energy release rate using incremental method for clamped-clamped beams with $\frac{h}{t} = .1$

Also, the boundary conditions are clamped-clamped, and T stands for top (Region 3) and B stands for bottom (Region 2).

The load-deflection plot for an undelaminated beam-plate and a delaminated beam-plate with $\frac{h}{t} = 0.3$ and $\frac{a}{L} = 0.5$ is shown in Figure 26. In the figures *perfect* refers to a beam-plate with no delaminations. The undelaminated beam shows very little displacement until \bar{P} is close to unity where the beam buckles and the displacement increases rapidly. Thus, $\bar{P} = 1$ is the strength of the undelaminated beam-plate. On the other hand, the stability of the delaminated beam-plate is greatly reduced by the delamination as buckling occurs at much lower \bar{P} . The dimensionless linear buckling load calculated in Chapter 4 for this case was 0.35 and this corresponds to local buckling of the thinner (top) region as seen in the figure. After $\bar{P} = 0.35$ the postbuckling response of the thicker (bottom) region is much stiffer than the thin region. When the load reaches approximately $\bar{P} = 0.50$ the bottom region begins to substantially soften such that excessive displacements occur at $\bar{P} = 0.71$. Thus, $\bar{P} = 0.71$ is the strength of the delaminated beam-plate with $\frac{h}{t} = 0.3$.

Next the load-deflection plot is shown in Figure 27 for the case of the thin delamination where $\frac{h}{t} = 0.1$. In this case local buckling occurs in the top region at the very small load of $\bar{P} = 0.04$ (the dimensionless linear buckling load). However, the region below the delamination with dimensionless thickness of $\frac{H}{t} = 0.9$ is sufficiently thick to be buckling resistant at $\bar{P} = 0.04$.

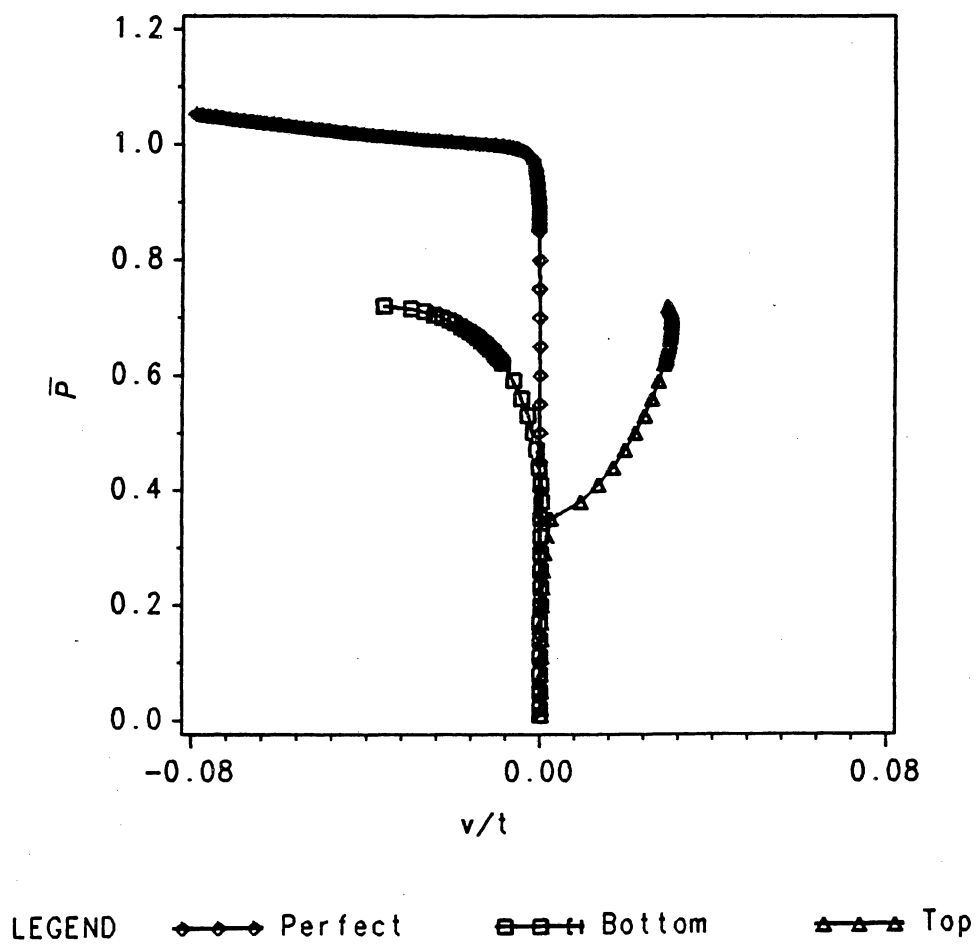


Figure 26: Load-deflection plot for undelaminated beam and beam with delamination at $\frac{h}{t} = .3$

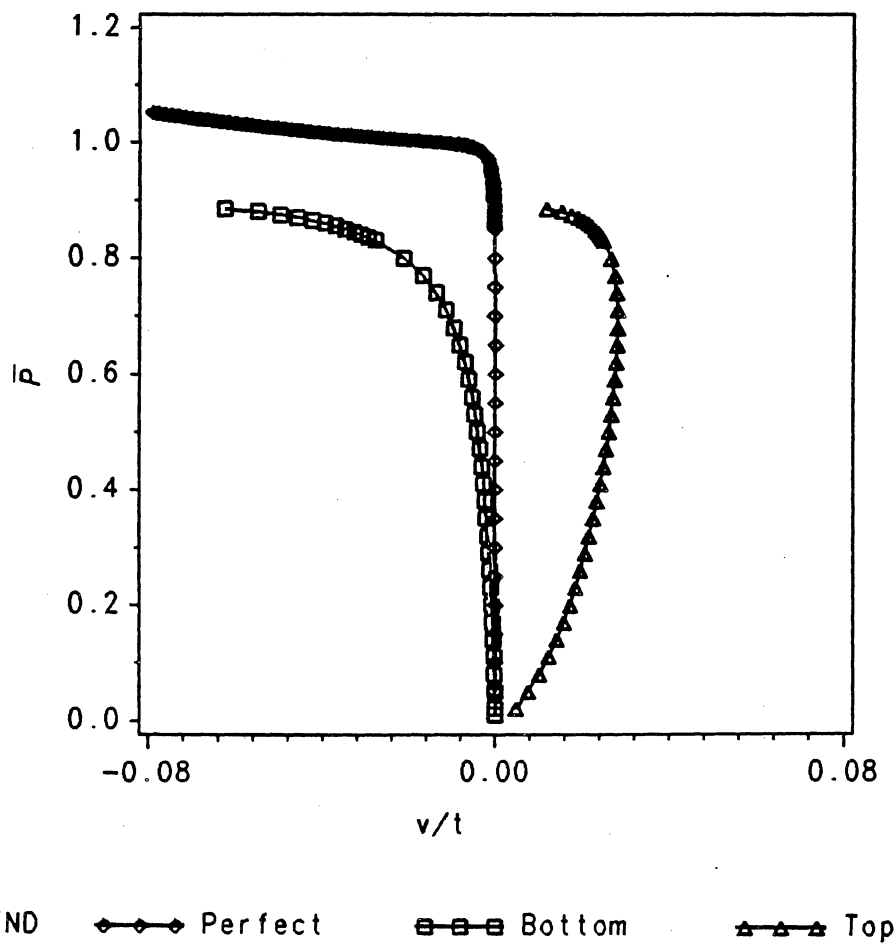


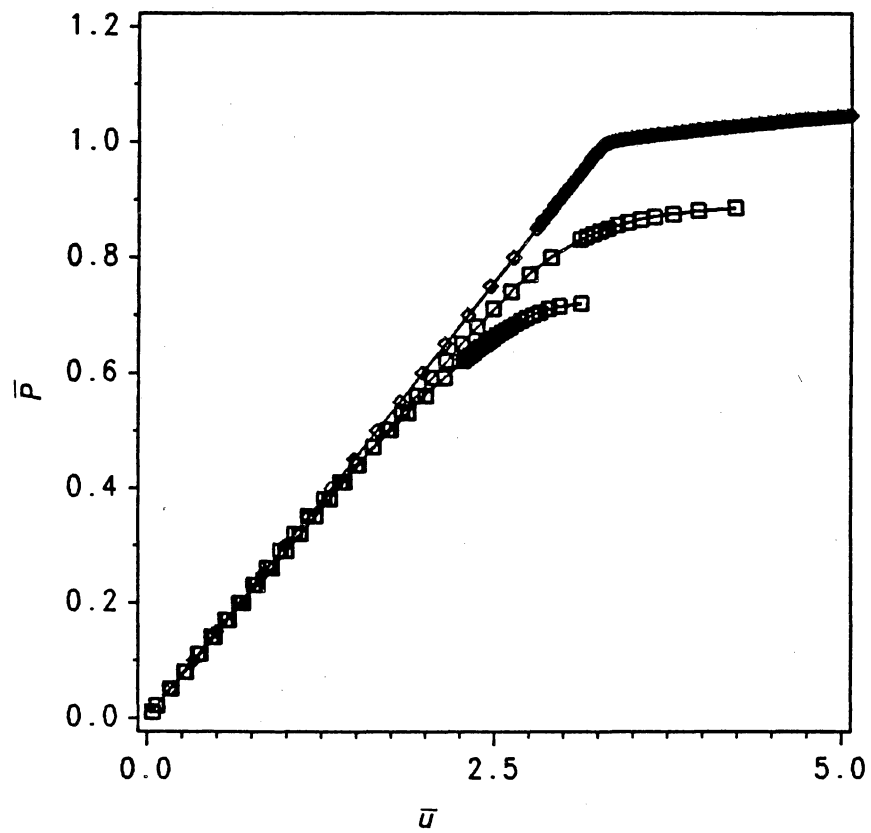
Figure 27: Load-deflection plot for undelaminated beam and beam with delamination at $\frac{h}{t} = .1$

This bottom region begins to buckle near $\bar{P} = 0.40$ and the beam-plate does not exhibit excessive displacements until $\bar{P} = 0.89$ (the postbuckling strength).

The load-end shortening curves for the undelaminated beam, for a beam with a delamination at $\frac{h}{t} = 0.1$, and for a beam with a delamination at $\frac{h}{t} = 0.3$ are shown in Figure 28. The slope of the curve for the undelaminated beam is linear up to about $\bar{P} = 1.0$ where the beam begins to buckle. The slopes of the curves for the two delaminated beam-plates both remain approximately linear up to about $\bar{P} = 0.45$. As was evident in the load-deflection diagrams, the beam-plate with $\frac{h}{t} = 0.3$ has a strength $\bar{P} = 0.71$ whereas the beam-plate with $\frac{h}{t} = 0.1$ delamination has a strength $\bar{P} = 0.89$. The beam-plate with $\frac{h}{t} = 0.1$ is stronger than the beam-plate with $\frac{h}{t} = 0.3$ because the region below the delamination is thicker and it can carry higher loads after the top region buckles. Thus, although the linear buckling load increases as $\frac{h}{t}$ increases from 0.1 to 0.3, the postbuckling strength decreases, and the strength decreases nearly in proportion to $\frac{h}{t}$.

5.4 CONSTANT MODE SHAPE METHOD

As mentioned previously, the incremental method used in the previous two sections is expensive. In this section postbuckling and energy release rate results using the less expensive constant mode shape method are presented. First, a convergence study is performed and then additional cases are compared to the results obtained using the incremental solution. Again, this



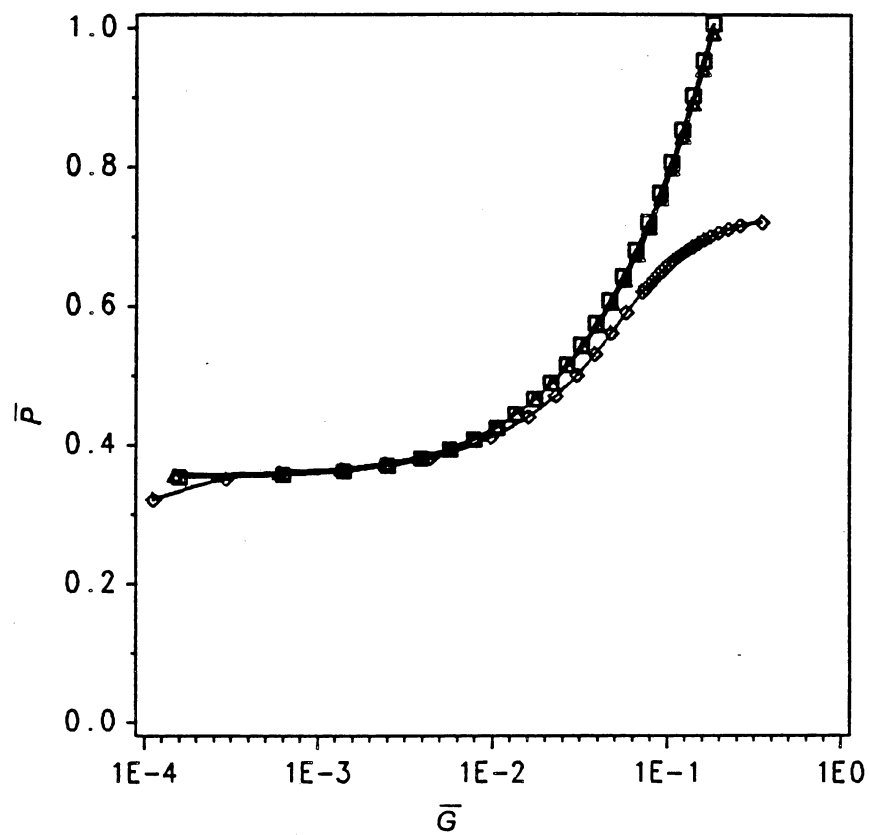
LEGEND \diamond Perfect \square h/t=.3 \square h/t=.1

Figure 28: Load-end shortening plot for undelaminated beam and beams with delaminations

method involves the assumption that the buckling mode shape remains constant; therefore, it is expected to provide accurate results only for small displacements in the postbuckling range. However, this method involves no iterations and hence is much more economical compared to the incremental/iterative approach.

In Figures 29 and 30 nondimensional axial load versus nondimensional energy release rate is plotted for clamped-clamped beams with $\frac{a}{L} = 0.5$ and delaminated regions of $\frac{h}{t} = 0.3$ (Figure 29) and $\frac{h}{t} = 0.1$ (Figure 30). The 6-element and 10-element constant mode shape solutions are plotted along with the incremental solution (using 16 elements in Figure 29 and 10 elements in Figure 30). In Figure 29, upon comparing the 6-element solution with the 10-element solution, it is seen that the two curves are almost coincidental. In Figure 30, the 10-element solution gives slightly higher values for the energy release rate than the 6-element solution, but the curves are very close together. Hence, the 6-element solution is used in all cases for the constant mode shape solution. As expected, the constant mode shape solution agrees well with the incremental solution for values of \bar{P} near buckling and not as well for the higher axial loads. The incremental solution must be used in the higher load region to obtain accurate energy release rates.

Next, \bar{P} versus $\frac{\delta}{t}$ is plotted using the constant mode shape assumption for the two representative cases of thick and thin delaminations. δ is the amplitude of the mode shape; therefore it is also equal to the transverse displacement at



LEGEND $\square-\square-\square$ 6 elements $\triangle-\triangle-\triangle$ 10 elements
 $\diamond-\diamond-\diamond$ incremental

Figure 29: Dimensionless axial load vs. dimensionless energy release rate using incremental and constant mode shape methods for clamped-clamped beams with $\frac{h}{t} = .3$ and $\frac{a}{L} = .5$

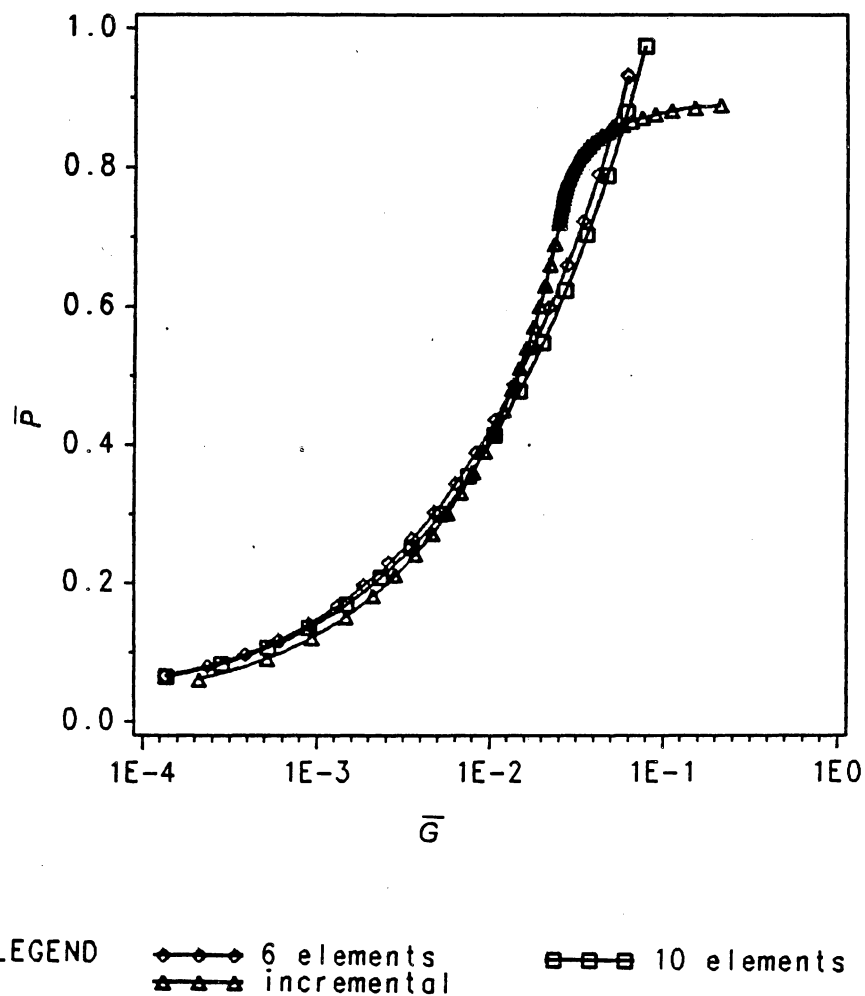


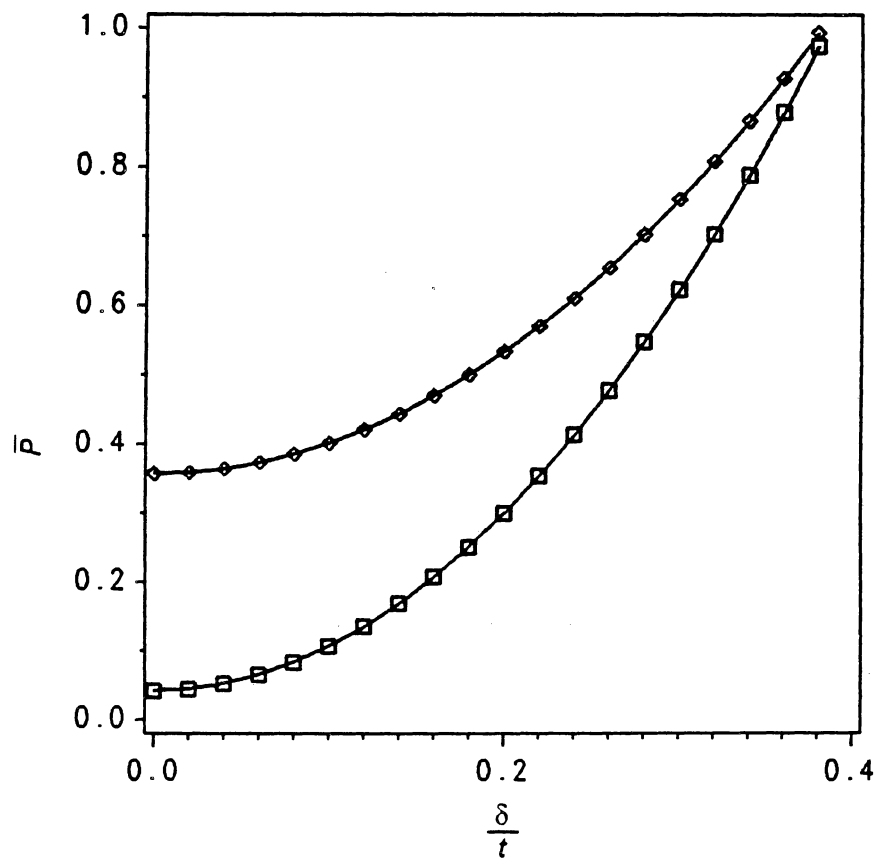
Figure 30: Dimensionless axial load vs. dimensionless energy release rate using incremental and constant mode shape methods for clamped-clamped beams with $\frac{h}{t} = .1$ and $\frac{a}{L} = .5$

the midlength of Region 3 since this is the largest displacement in the buckling mode. In the constant mode shape procedure all displacements increase proportionally to δ . The two curves for the thick and thin delaminations are shown in Figure 31. Both curves start out level at the respective buckling loads and then increase rapidly with \bar{P} . The curve for $\frac{h}{t} = 0.1$ has a larger slope because the delaminated region is thin, so the axial displacement in this region increases very quickly with increasing axial load. Additional results obtained using this method as well as the incremental procedure for beam-plates with various boundary conditions are given in the next section.

5.5 VARIOUS BOUNDARY CONDITIONS

In this section the energy release rates for beam-plates with different types of boundary conditions are calculated. Energy release rate results are provided for pinned-pinned beams using both the incremental method and the constant mode shape method (analytical results were only provided for clamped-clamped beams). Next, beams with pinned-clamped boundary conditions are studied, and this section concludes with energy release rate results for beam-plates with elastic end conditions.

A graph of \bar{P} versus \bar{G} for pinned-pinned beams with a delamination height of $\frac{h}{t} = 0.1$ is shown in Figure 32. Incremental and constant mode shape curves are shown for two different cases of $\frac{a}{L} = 0.40$ and $\frac{a}{L} = 0.60$. For the



LEGEND $\diamond-\diamond-\diamond$ $h/t=.3$ $\square-\square-\square$ $h/t=.1$

Figure 31: Load-deflection plot for clamped-clamped beams with $\frac{a}{L} = .5$

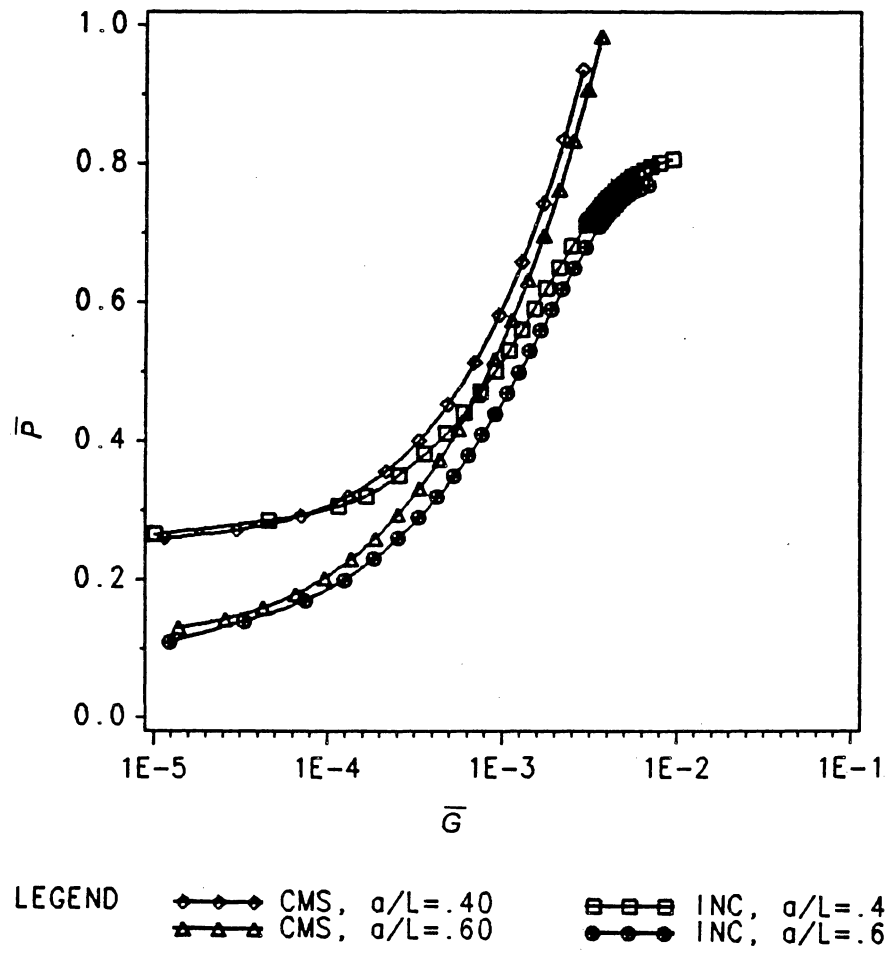


Figure 32: Dimensionless axial load vs. dimensionless energy release rate using incremental and constant mode shape methods for pinned-pinned beams with $\frac{h}{t} = .1$

pinned-pinned cases, P is nondimensionalized by the critical load of a pinned-pinned beam with no delaminations:

$$\bar{P} = \frac{P}{EI} \left(\frac{L}{\pi} \right)^2 \quad (5.4)$$

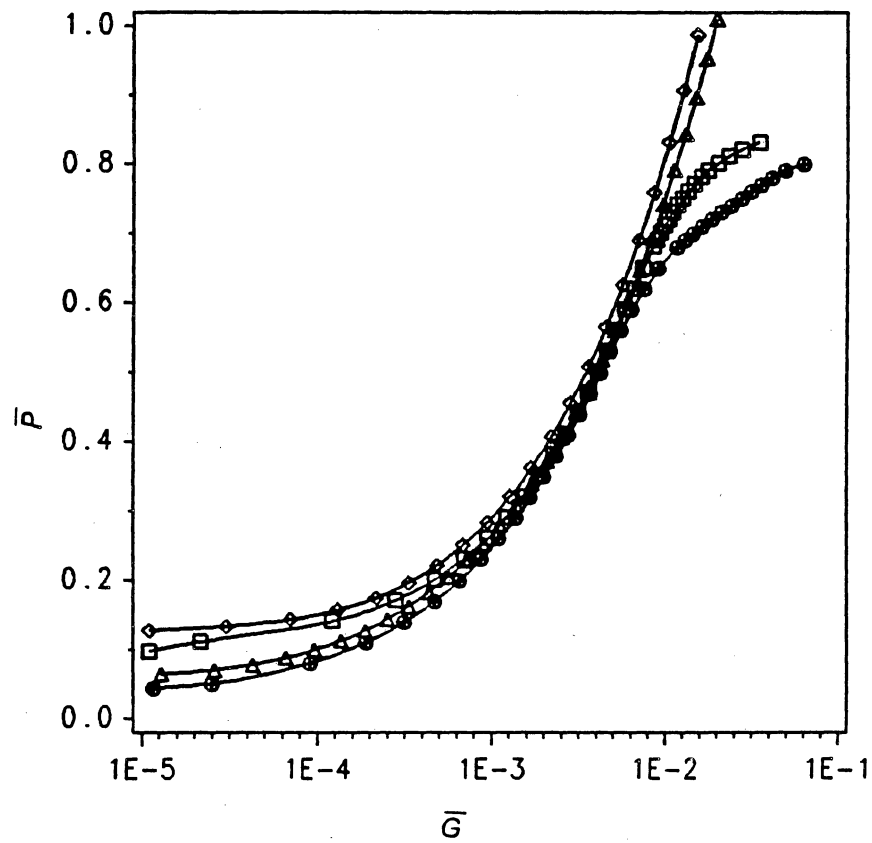
The energy release rate is nondimensionalized as before. Again, the solutions for the two different methods agree only in the small displacement range. The two incremental solutions begin to flatten at about $\bar{P} = 0.7$, whereas the constant mode shape solutions continue to rise rapidly.

The next plot, Figure 33, is for pinned-clamped beams with the the same delamination height of $\frac{h}{t} = 0.1$, and here, nondimensionalization for \bar{P} is

$$\bar{P} = \frac{PL^2}{20.19EI} \quad (5.5)$$

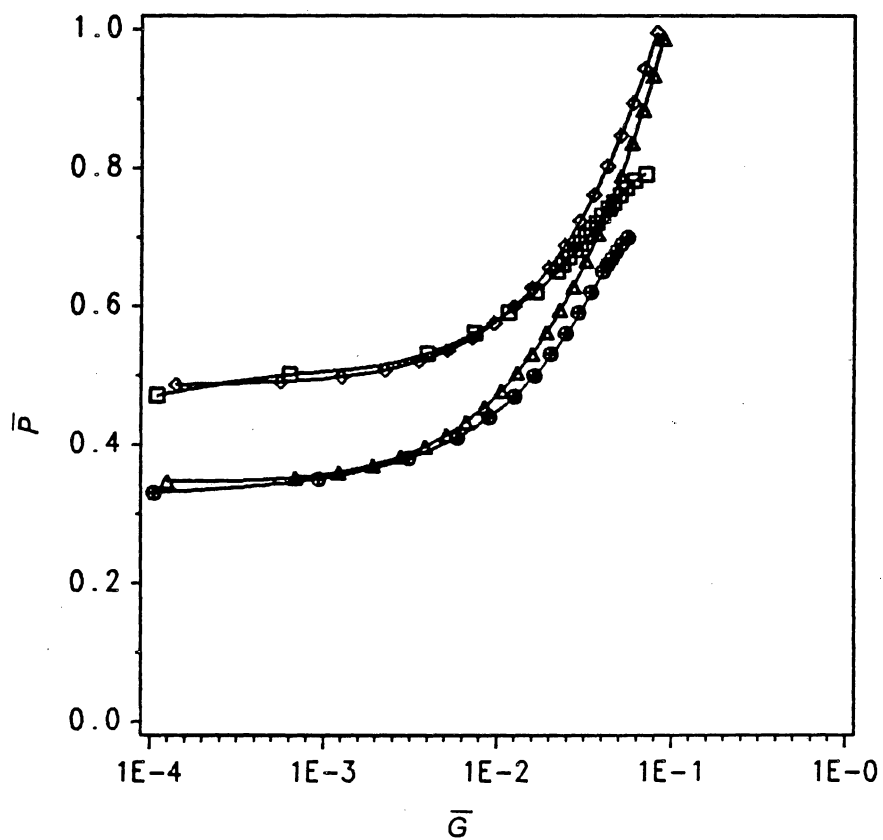
In this case the constant mode shape solutions agree well with the incremental solutions for both dimensionless crack lengths of $\frac{a}{L} = 0.4$ and $\frac{a}{L} = 0.6$ up to a load of approximately $\bar{P} = 0.65$. The incremental energy release rates are lower for $\frac{a}{L} = 0.6$ than for $\frac{a}{L} = 0.4$ for all values of incremental loads.

The next type of boundary conditions to be covered in this section is elastic end conditions. Again, the axial load is nondimensionalized by the buckling load of a perfect beam with the same end conditions (see Table 1). Results are given in Figure 34 for an elastically-supported beam with spring constants of $\alpha = 100 \frac{EI}{L^3}$ and $\beta = 10 \frac{EI}{L}$ and the dimensionless delamination height is



LEGEND ◇-◇-◇ CMS, $a/L = .40$ □-□-□ INC, $a/L = .40$
 ▲-▲-▲ CMS, $a/L = .60$ ●-●-● INC, $a/L = .60$

Figure 33: Dimensionless axial load vs. dimensionless energy release rate using incremental and constant mode shape methods for pinned-clamped beams with $\frac{h}{t} = .1$



LEGEND ◇-◇-◇ CMS, $a/L=.50$ □-□-□ INC, $a/L=.50$
 ▲-▲-▲ CMS, $a/L=.60$ ●-●-● INC, $a/L=.60$

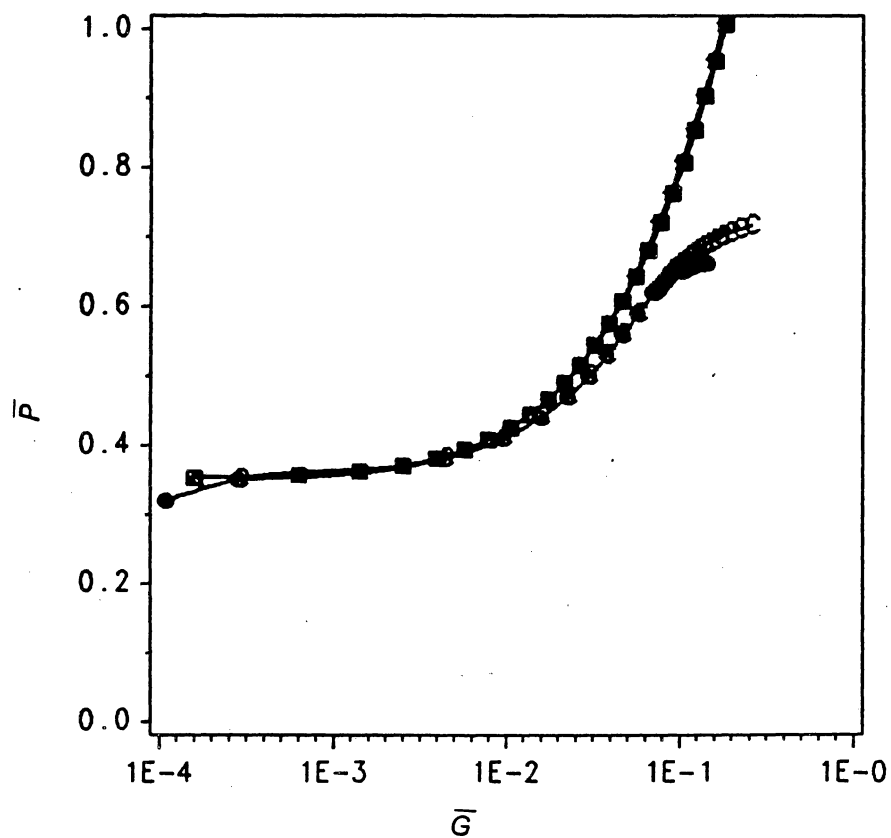
Figure 34: Dimensionless axial load vs. dimensionless energy release rate using incremental and constant mode shape methods for elastically-supported beams with $\frac{h}{t} = .3$, $\alpha = 100$, $\beta = 10$

$\frac{h}{t} = 0.3$. Both solutions are given for \bar{P} versus \bar{G} for two different delamination lengths. The differences between the constant mode shape solutions and the incremental solutions are very small until $\bar{P} = 0.6$. The energy release rates obtained from the incremental solution are greater than those obtained from the constant mode shape solution for axial loads far into the postbuckling range.

5.6 NONSYMMETRIC DELAMINATIONS

Beams with delaminations which are not centered with respect to the length of the beam will now be considered. In order to study the effect of off-center delaminations on the energy release rate, \bar{P} versus \bar{G} is plotted for clamped-clamped beams with $\frac{a}{L} = 0.5$ for two different delamination locations (see Figure 2 for geometry). Figure 35 is for a delamination height of $\frac{h}{t} = 0.3$, and Figure 36 for $\frac{h}{t} = 0.1$. In all cases curves are given for the constant mode shape solution and the incremental/iterative solution. The three different dimensionless delamination locations are $\frac{l}{L} = 0.15, 0.20$, and 0.25 . Since the dimensionless crack length is 0.50 , $\frac{l}{L} = 0.25$ represents a symmetric delamination.

In Figure 35 the constant mode shape solutions indicate that delamination location has no effect since these solutions are the same for all three delamination locations. The three incremental solutions are the same near buckling, but there are small differences at the higher axial loads: the energy



LEGEND ◇-◇-◇ CMS, $I/L = .15$ ●-●-● INC, $I/L = .15$
 ▲-▲-▲ CMS, $I/L = .20$ ○-○-○ INC, $I/L = .20$
 ■-■-■ CMS, $I/L = .25$ □-□-□ INC, $I/L = .25$

Figure 35: Dimensionless axial load vs. dimensionless energy release rate using incremental and constant mode shape methods for clamped-clamped beams with nonsymmetric delaminations and $\frac{h}{t} = .3$ and $\frac{a}{L} = .5$

release rates become slightly lower as the delamination is moved from the center of the beam. Also, the global buckling loads become slightly lower.

In Figure 36, where $\frac{h}{t} = 0.1$, the three constant mode shape curves are again almost identical. On the other hand, the incremental solutions for the two nonsymmetrically delaminated beam-plates are drastically different from the incremental solution for the symmetric delamination. After \bar{P} reaches 0.7 the energy release rates are much lower in the nonsymmetric cases. These energy release rates drop off because as the delamination is moved further and further to one side of the beam-plate, the undelaminated region on the opposite side becomes longer and longer and buckling occurs in this region for the unsymmetric cases with $\frac{h}{t} = 0.1$. The stress field at the crack tip then changes and hence the energy release rate changes. Note that crack growth would occur in the unsymmetric cases before it would occur in the symmetric cases because the energy release rates are higher for the same axial load; therefore, the critical energy release rate would be reached sooner than in the symmetric delamination case. These effects of nonsymmetric delaminations cannot be predicted by the constant mode shape method since the mode shape (except for changing in amplitude) remains constant after buckling.

5.7 CONCLUSIONS

For the constant mode shape procedure the simple 6-element model is recommended since adding more elements did not change the energy release

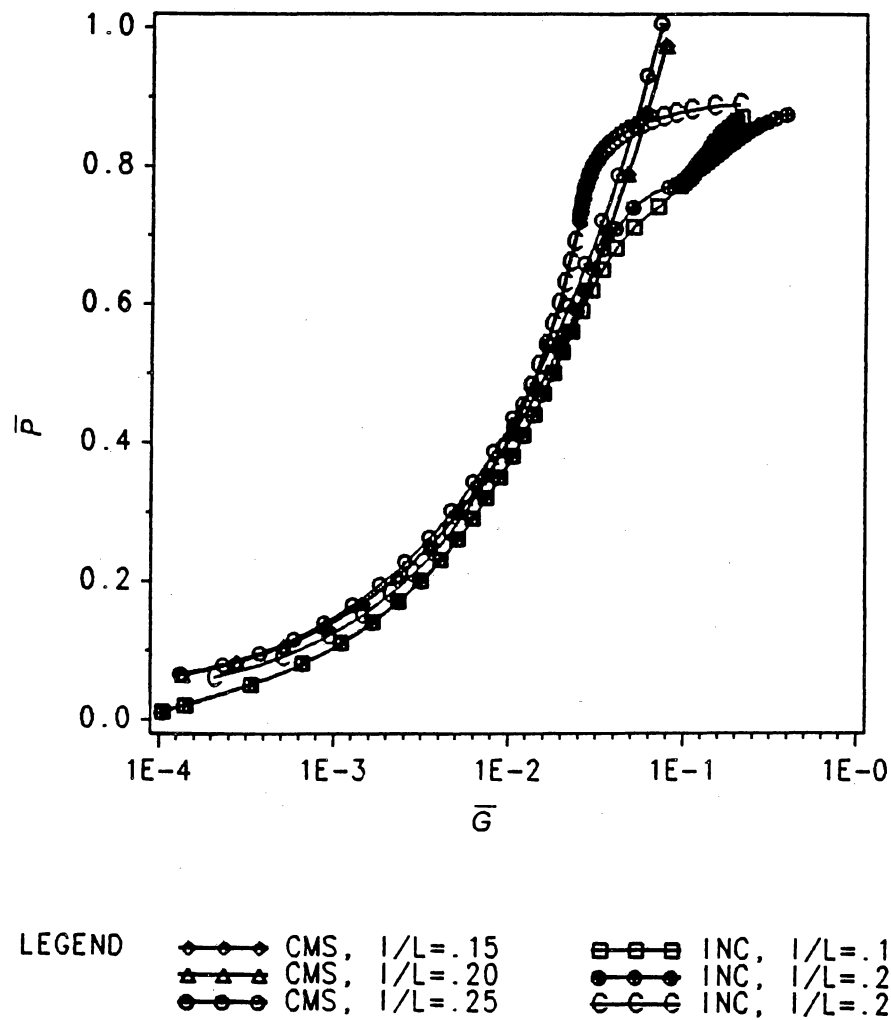


Figure 36: Dimensionless axial load vs. dimensionless energy release rate using incremental and constant mode shape methods for clamped-clamped beams with nonsymmetric delaminations and $\frac{h}{t} = .1$ and $\frac{a}{L} = .5$

rates calculated by this method. For the incremental solution the 16-element solution is recommended for the thicker delamination, $\frac{h}{t} = 0.3$, and the 10-element solution is recommended for the thinner delamination, $\frac{h}{t} = 0.1$. There were some convergence problems for the thin delamination cases; however, the 10-element element solution provided results which compared very well to the analytical results of Yin et al [6] for several different values of delamination length.

The load versus displacement diagrams given in Section 5.3 show that the strengths of beam-plates are significantly affected by the presence of a delamination. Local buckling occurs in the delaminated beam-plates at small loads especially for thin delaminations. It was found that the postbuckling strength of the delaminated beam-plate relative to the strength of the undelaminated beam-plate decreased almost in proportion to $\frac{h}{t}$. Besides failure by excessive displacements during postbuckling, delaminated beam-plates can fail if the critical energy release rate is reached and crack growth occurs.

Each of the two different solution procedures has its own advantages for finding the postbuckling solution and then the energy release rate. The incremental procedure allows for changing mode shape and it provides accurate results for \bar{P} versus \bar{G} at all values of axial load. The results agree very well with the previous analytical solutions which were done only for simple cases. Also, the incremental procedure can predict differences in

energy release rates caused by moving the delamination away from the center (nonsymmetric delaminations) as was shown in Section 5.5. However, using the incremental load method along with the Newton-Raphson technique is iterative and requires a great deal of operations and computer time; hence, the constant mode shape method was formulated. This procedure is a much more economical technique which takes a small fraction of the computer time of the incremental procedure. It provides a good first approximation for the energy release rates and is also accurate at loads just beyond the buckling load. It is not as effective at the higher loads because of the inherent assumption that the buckling mode shape remains constant, and the mode shape does in fact change in this region. Another significant disadvantage of the constant mode shape method is that it cannot be used to predict global buckling loads of delaminated beam-plates. In the final chapter the incremental procedure is used in conjunction with a numerical differentiation technique in order to obtain results for beams with multiple delaminations.

Chapter 6. Multiple Delaminations

6.1 OVERVIEW

In this chapter a numerical differentiation technique is provided for finding the energy release rates of beams with more than one delamination. It is assumed that all the delaminations grow the same amount and that the total energy release rate is being calculated. The algebraic expression used before is invalid for this problem. Consequently, a numerical differentiation method is employed which is described in Section 6.2. First, results obtained using the numerical method are tested with incremental results for beam-plates with one delamination in Section 6.3. The numerical differentiation method is then employed to find energy release rates for beam-plates with two delaminations. The final section contains conclusions on the numerical differentiation method.

6.2 NUMERICAL DIFFERENTIATION

In this section a simple numerical differentiation technique is provided to find energy release rates for beams with multiple delaminations. The numerical formula for the energy release rate is

$$G = \frac{\Delta U}{\Delta a} \quad (6.1)$$

where U is the strain energy and a is the delamination length. The contributions of the transverse forces to the strain energy are negligible compared to the contribution of the axial load; hence, the strain energy is easily calculated from

$$U = \int_0^{u_1} P du \quad (6.2)$$

where u_1 is the end deflection at the point where the load is applied. In other words U equals the area under the load-end shortening diagram.

Therefore, the steps used to obtain the energy release rate from numerical differentiation are as follows:

1. Obtain the postbuckling solution curve P versus u for two different crack lengths.
2. Compute the strain energies by finding the areas under the curves up to certain values of u using Simpson's Rule.

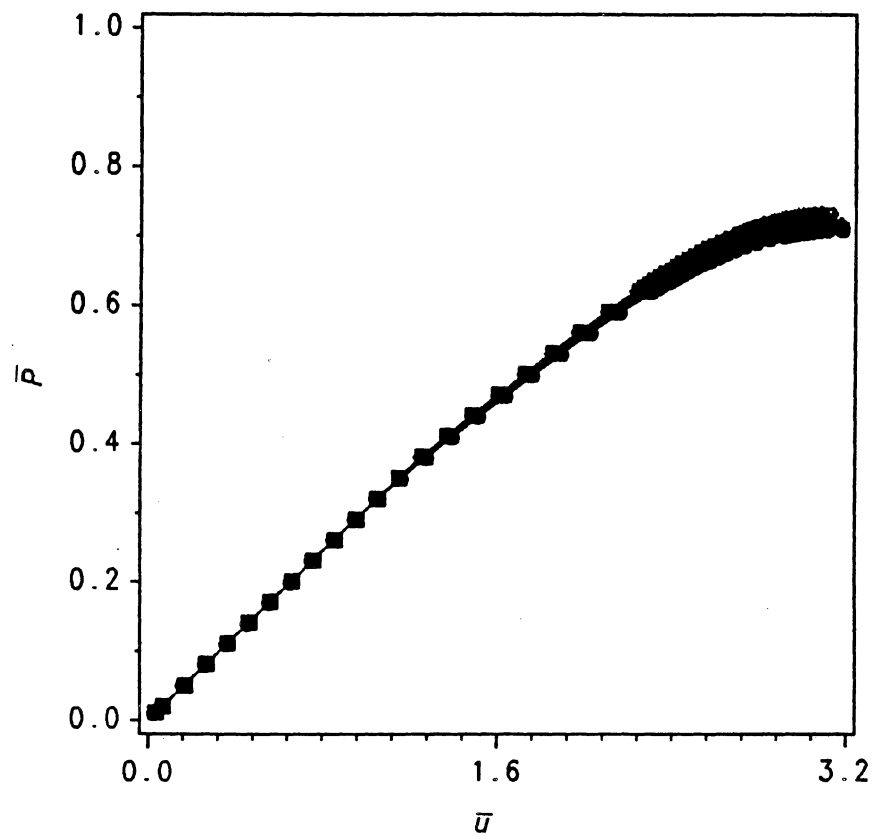
3. Subtract the areas under one curve from the areas under the second curve to get ΔU and divide by the difference in crack length (Δa).

Hence G is found using Equation 6.1.

6.3 RESULTS USING NUMERICAL DIFFERENTIATION

Before numerical differentiation is employed to find results for multiple delaminations, the technique is tested using a beam-plate with one delamination. The effect of using different Δa 's is also considered in this test case. For a beam-plate with one delamination energy release rate results may be obtained using numerical differentiation and then compared to the incremental results (where the expression given by Yin and Wang [7] may also be used to calculate the energy release rate). The incremental solution must be used to find the load versus displacement diagram because assuming a constant mode shape will not provide accurate results for the axial displacement.

The test case to be compared is a clamped-clamped beam with $\frac{h}{t} = 0.3$ and $\frac{a}{L} = 0.5$. The incremental solution \bar{P} versus \bar{u} for six different dimensionless crack lengths is shown in Figure 37. Using these curves the energy release rate is obtained for three different Δa 's using central differences. It is observed from the figure that in the postbuckling range (local buckling occurs at approximately $\bar{P} = 0.35$), the larger the crack length, the larger the axial



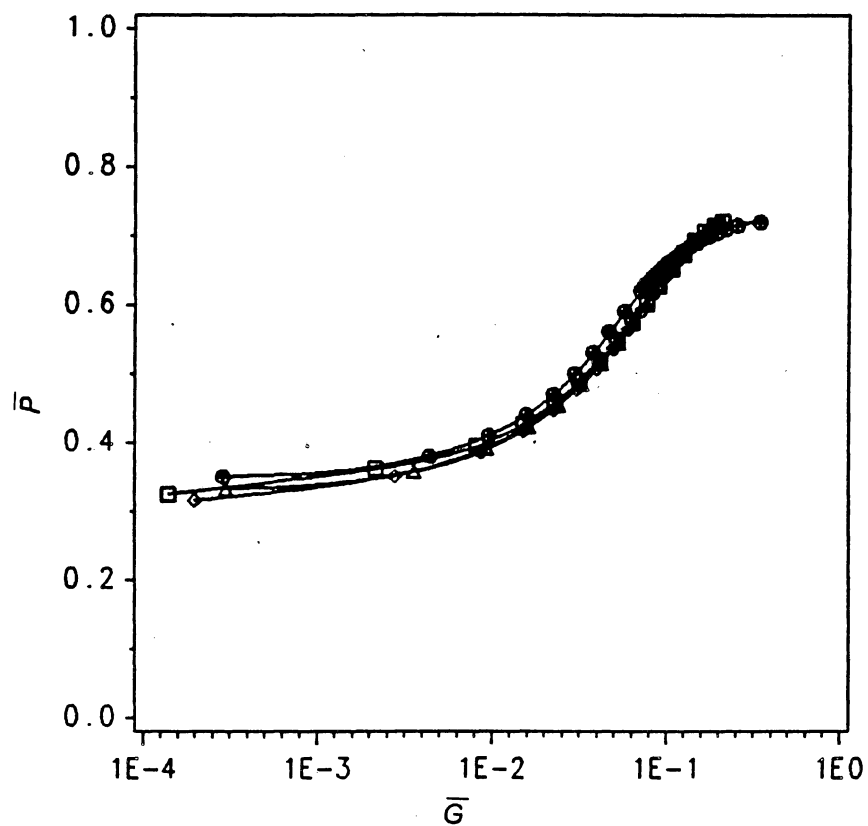
LEGEND $\diamond-\diamond-\diamond$ $a/L = .485$ $\square-\square-\square$ $a/L = .490$ $*-*-*$ $a/L = .495$
 $\triangle-\triangle-\triangle$ $a/L = .505$ $\bullet-\bullet-\bullet$ $a/L = .510$ $\circ-\circ-\circ$ $a/L = .515$

Figure 37: Load-end shortening plot for clamped-clamped beams with $\frac{h}{t} = .3$

deformation for the same load because of the loss of stiffness associated with longer cracks.

ΔU is now calculated by integrating up certain values of u and finding the difference in the areas under the two curves. Then G may be calculated by dividing ΔU by Δa . The energy release rates are compared in Figure 38 with the incremental solution for $\frac{a}{L} = 0.5$ and $\frac{h}{t} = 0.3$. The three curves obtained using numerical differentiation are all almost identical to each other and are also very close to the incremental solution. The middle value of $\frac{\Delta a}{L} = 0.02$ is chosen for use in all of the following cases of beam-plates with two delaminations.

The numerical differentiation technique has provided results which match the incremental solution very closely and do not depend on Δa near the chosen value of 0.02. Now the method is extended to beam-plates with two delaminations. The geometry for the beams with two delaminations is the same as in Chapter 4 (see Figure 16). The loading is the same as for the beam-plates with one delamination: $Q_T = 0.0001Pcp$ is applied to the top delaminated region, and $Q_B = -0.0001Pcp$ is applied to the bottom delaminated region (no transverse load is applied to the center delaminated region). For each of the examples, the postbuckling solution using the incremental method is shown on the end shortening plot, followed by the load versus energy release rate curve calculated using the numerical differentiation formula.



LEGEND $\square-\square$ Num dif, $da/L=.01$ $\triangle-\triangle$ Num dif, $da/L=.02$
 $\diamond-\diamond$ Num dif, $da/L=.03$ $\bullet-\bullet$ Incremental

Figure 38: Dimensionless axial load vs. dimensionless energy release rate using numerical differentiation for clamped-clamped beams with $\frac{h}{t} = .3$

The dimensionless load-end shortening curve is plotted in Figure 39 for a clamped-clamped beam with $\frac{h}{t} = 0.1$ and $\frac{H}{t} = 0.6$ (hence $\frac{m}{t} = 0.3$). The four different curves are for four different values of dimensionless delamination length. For beams with two delaminations the end displacement increases much more rapidly in the postbuckling range compared to the beams with one delamination because the beam-plate is significantly weakened in postbuckling by the second delamination.

The energy release rates are calculated using central differences for $\frac{a}{L} = 0.4$ using $\frac{a}{L} = 0.39$ and 0.41 and for $\frac{a}{L} = 0.5$ using $\frac{a}{L} = 0.49$ and 0.51 . The results are shown in Figure 40: the two curves start out close together, separate, then converge again as the axial load is increased. The energy release rates are greater for the longer crack length than for the shorter crack length at a given load.

The next case to be examined is a pinned-pinned beam with two delaminations at the same height locations of $\frac{h}{t} = 0.1$ and $\frac{H}{t} = 0.6$ (Figures 41 and 42). The displacements are much smaller than they were in the clamped-clamped case (compare Figures 39 and 41). This is because \bar{P} reaches 1 at a load four times smaller than in the clamped-clamped case (the axial load is nondimensionalized by the critical load of an undelaminated beam which is four times smaller for a pinned-pinned beam). In Figure 41 the \bar{P} versus \bar{u} solutions for four different delamination lengths are shown. The results of the numerical differentiation for these cases are plotted in Figure 42. The energy

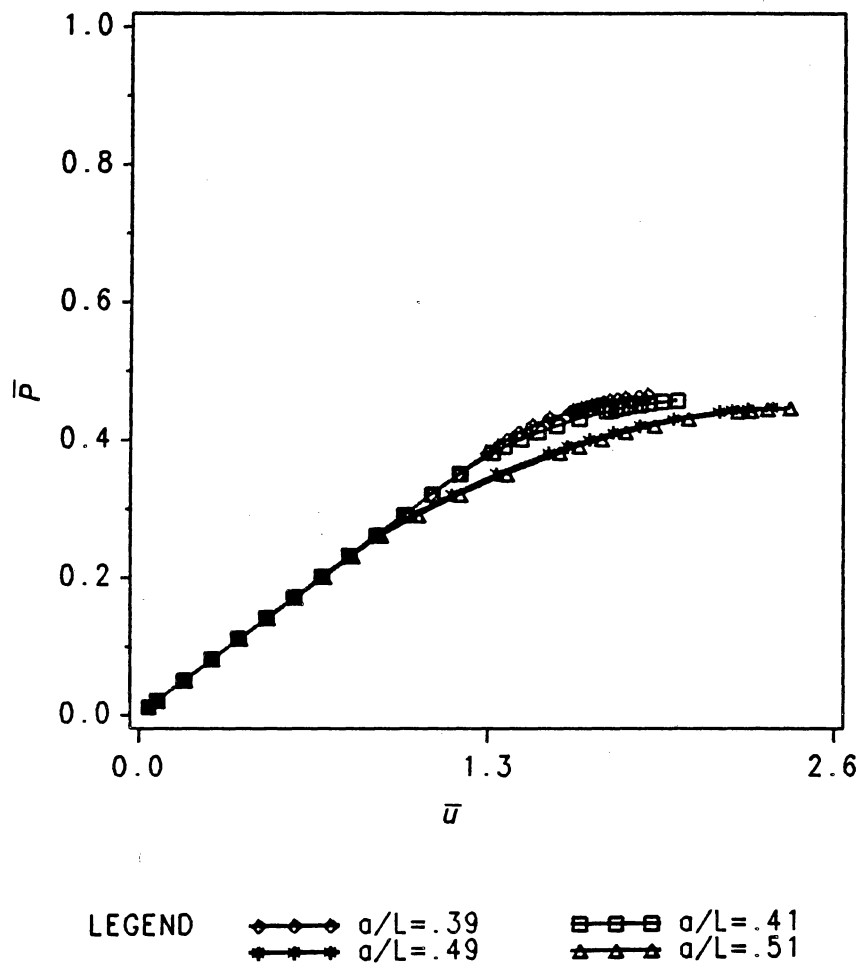


Figure 39: Load-end shortening plot for clamped-clamped beams with two delaminations at $\frac{h}{t} = .3$ and $\frac{H}{t} = .6$

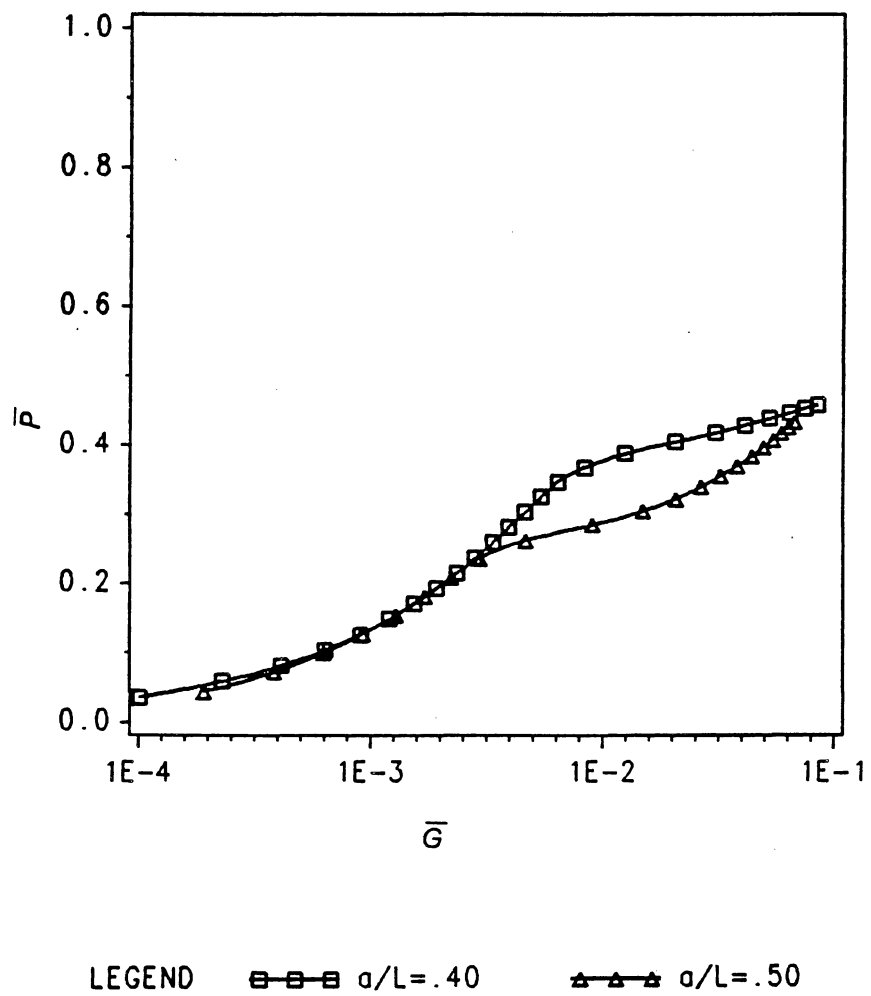
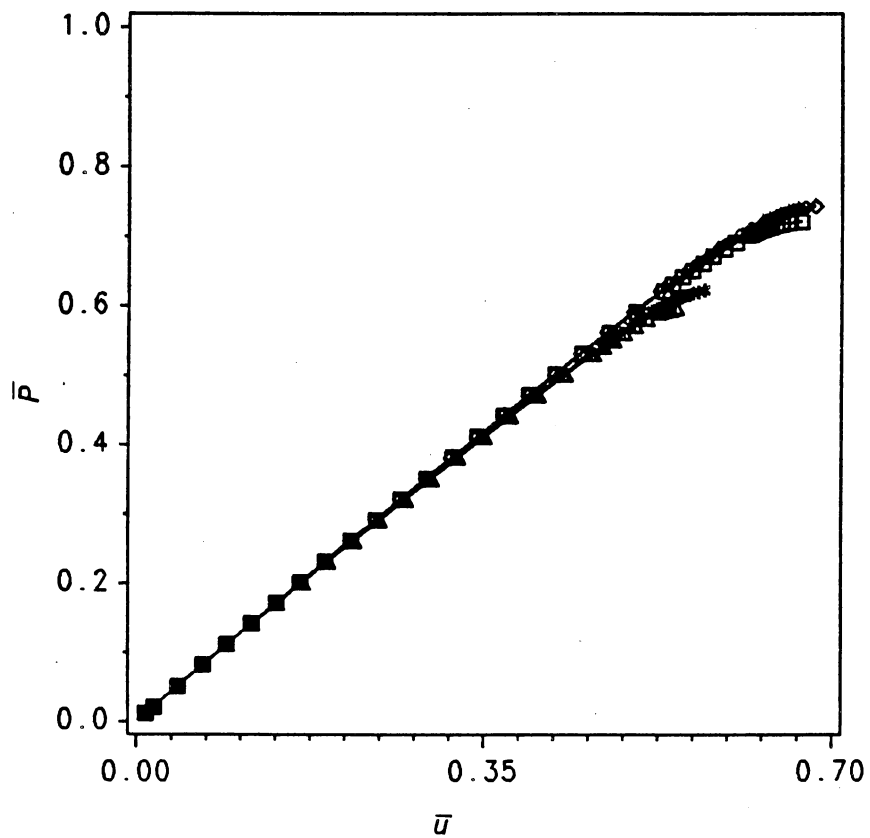


Figure 40: Dimensionless axial load vs. dimensionless energy release rate using numerical differentiation for clamped-clamped beams with $\frac{h}{t} = .3$ and $\frac{H}{t} = .6$



LEGEND $\diamond-\diamond-\diamond$ $a/L=.39$ $\square-\square-\square$ $a/L=.41$
 $\ast-\ast-\ast$ $a/L=.49$ $\triangle-\triangle-\triangle$ $a/L=.51$

Figure 41: Load-end shortening plot for pinned-pinned beams with two delaminations at $\frac{h}{t} = .3$ and $\frac{H}{t} = .6$

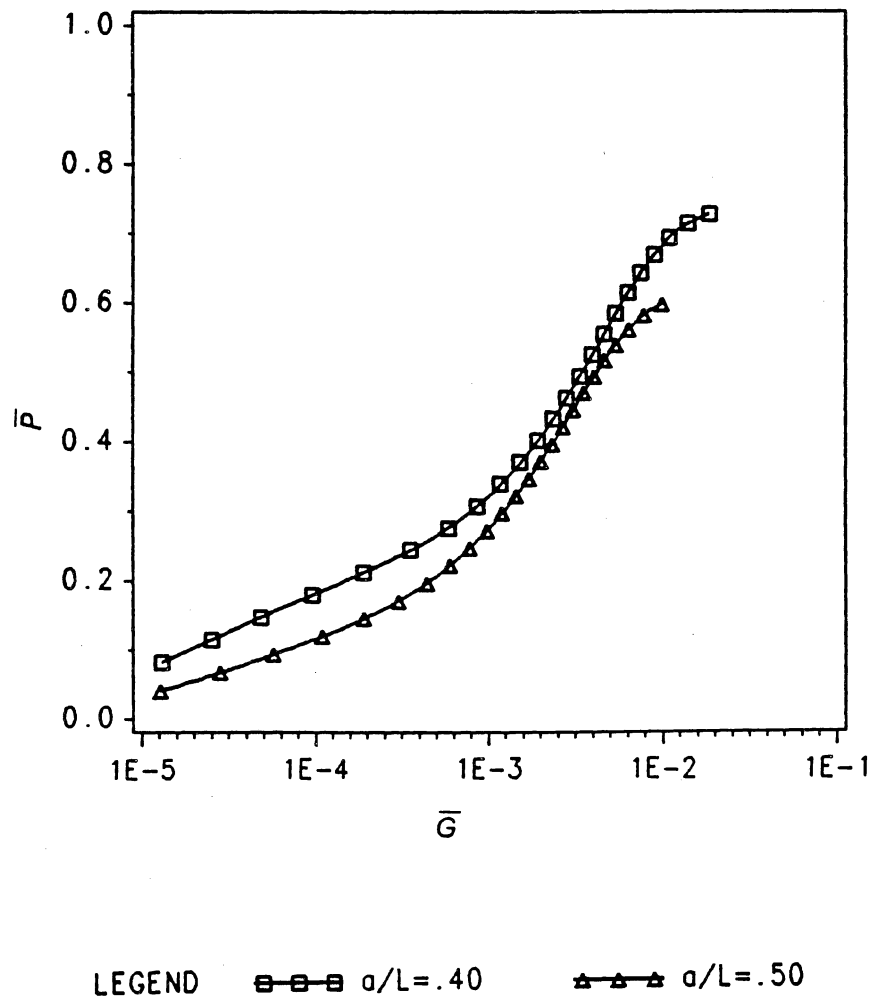


Figure 42: Dimensionless axial load vs. dimensionless energy release rate using numerical differentiation for pinned-pinned beams with $\frac{h}{t} = .3$ and $\frac{H}{t} = .6$

release rate curves for this case start out lower and rise more rapidly compared to the curves for the previous case of clamped-clamped beam-plates.

Next, a clamped-clamped beam-plate with delamination heights of $\frac{h}{t} = 0.2$ and $\frac{H}{t} = 0.5$ is considered. The postbuckling solution for axial load versus axial displacement at the point of the applied load is plotted in Figure 43. All four curves are approximately linear up to about $\bar{P} = 0.32$ after which they become highly nonlinear. The energy release rates for this case, shown in Figure 44, increase very rapidly with increasing axial load; hence, the possibility of delamination growth is high even at small axial loads.

The final case which is studied is a clamped-clamped beam-plate with delamination heights of $\frac{h}{t} = 0.1$, $\frac{m}{t} = 0.5$, and $\frac{H}{t} = 0.4$. Here, the load versus displacement curves remain approximately linear and then become slightly nonlinear just before failure due to excessive displacement in postbuckling. Although it is not evident in Figure 45, numerical solutions for small load increments beyond the last points on the curves could not be found. This implies very large displacements or failure of the beam. The global buckling load is reached very suddenly possibly because the thickest delaminated region is in the center in this case: this thick region stabilizes the beam-plate and when this region buckles the postbuckling strength is immediately lost. The results for the energy release rates are shown in Figure

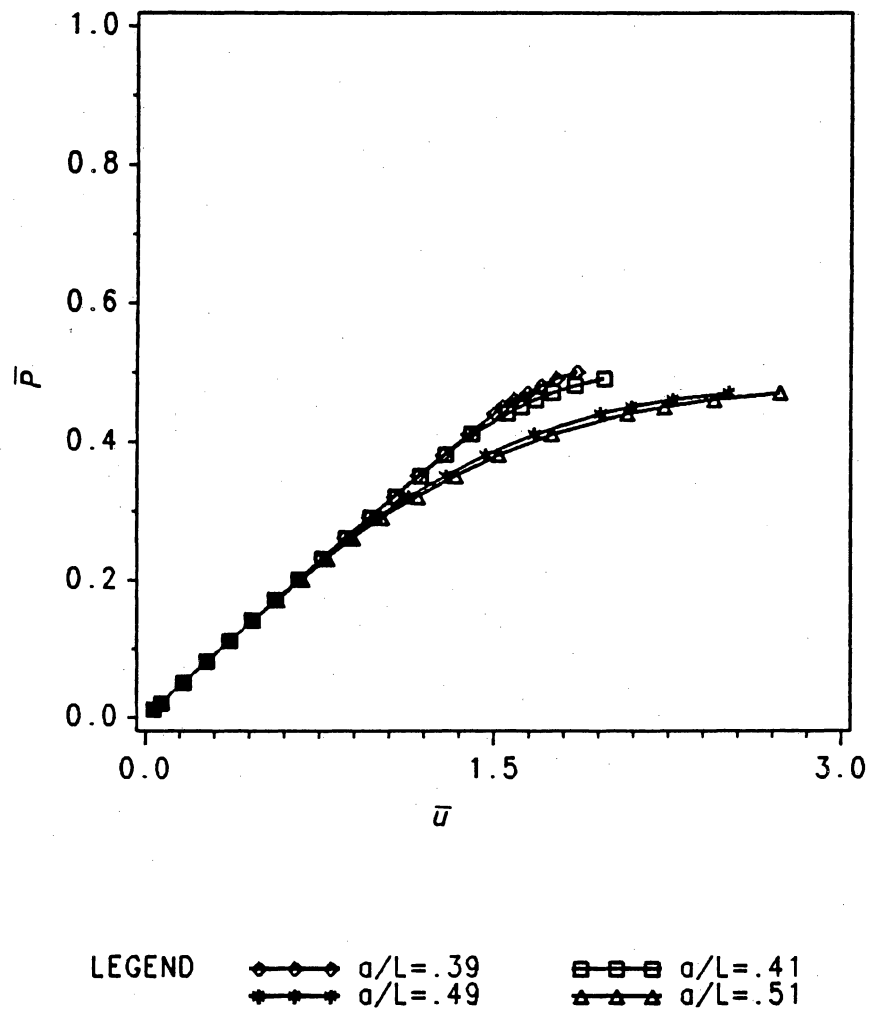


Figure 43: Load-end shortening plot for clamped-clamped beams with two delaminations at $\frac{h}{t} = .2$ and $\frac{H}{t} = .5$

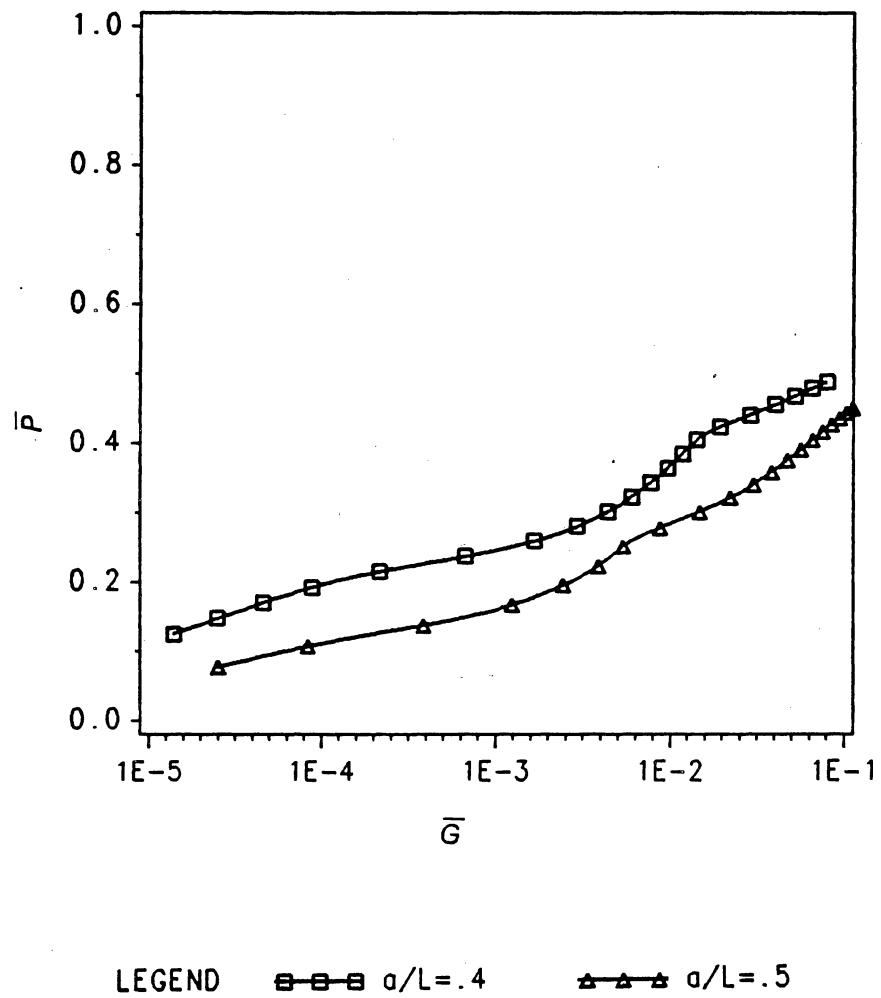


Figure 44: Dimensionless axial load vs. dimensionless energy release rate using numerical differentiation for clamped-clamped beams with $\frac{h}{t} = .2$ and $\frac{H}{t} = .5$

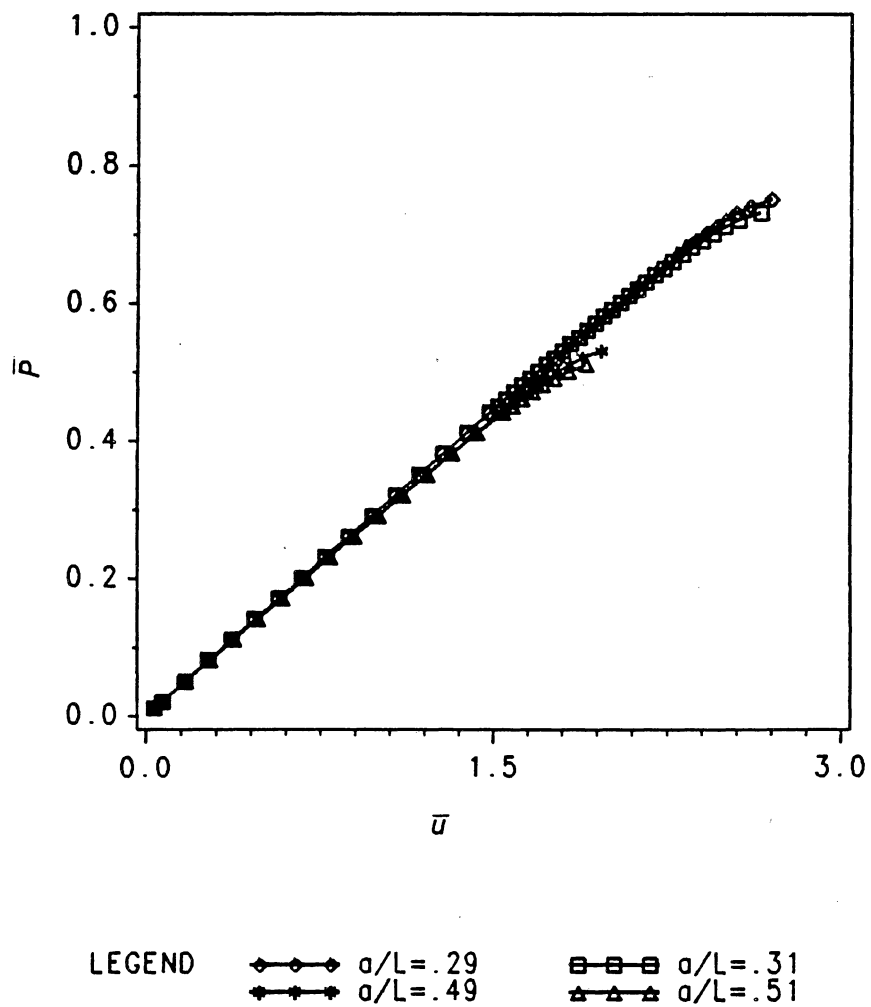


Figure 45: Load-end shortening plot for clamped-clamped beams with two delaminations at $\frac{h}{t} = .1$ and $\frac{H}{t} = .4$

46. Again, the longer crack exhibits greater energy release rates than the shorter crack at a given load.

6.4 CONCLUSIONS

The numerical differentiation technique is an excellent method for finding energy release rates in delaminated beam-plates. The postbuckling solution of the applied load versus the end displacement is all that is needed to find the energy release rate. The same results were obtained using three different Δa 's in the range of 0.01 to 0.03 for the test case, and these results agreed well with the incremental solutions; therefore, any Δa in this range may be chosen. In this chapter finite element numerical differentiation results were provided for beam-plates with one and two delaminations. The numerical differentiation method may also be extended to handle beams with three or more delaminations.

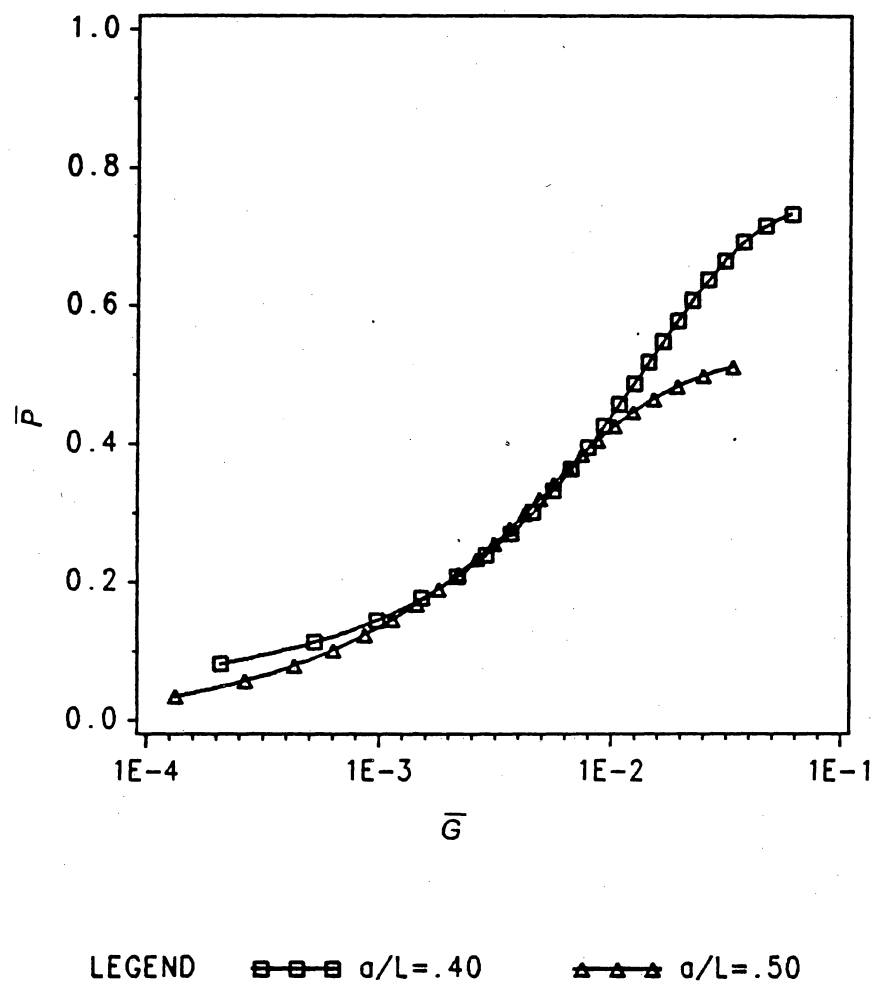


Figure 46: Dimensionless axial load vs. dimensionless energy release rate using numerical differentiation for clamped-clamped beams with $\frac{h}{t} = .1$ and $\frac{H}{t} = .4$

Chapter 7. Final Remarks and Recommendations

7.1 FINAL REMARKS

For the linear bifurcation buckling analysis, an extremely simple, efficient, and versatile finite element model to determine the critical buckling load of a delaminated beam-plate has been demonstrated. This method can easily handle symmetric, unsymmetric, and multiple delaminations and also various boundary conditions.

For the postbuckling analysis, two methods of solution were used: the incremental method and the constant mode shape method. The constant mode shape method is very inexpensive compared to the incremental method and is recommended for use in the small displacement range of the postbuckling solution. For greater accuracy in the larger displacement range, and for finding global buckling loads, the incremental/iterative finite element

procedure (although expensive) provides a very accurate postbuckling solution.

The energy release rates for beams with one delamination were calculated using the algebraic expression provided by Yin and Wang [7]. However, for beams with more than one delamination, this expression cannot be used; hence, the numerical differentiation method was introduced. This method is also simple and versatile and can handle beams with any number of delaminations.

7.2 RECOMMENDATIONS FOR FUTURE WORK

This study was done for isotropic materials with geometric nonlinearities only, neglecting shear effects. This work may be extended to include laminated composite materials, shear effects, material nonlinearities, and dynamic loadings. The laminated composites may be analyzed by employing the 20 degree-of-freedom beam element of Kapania and Raciti [26] which is also capable of including shear effects. Material nonlinearities may also be significant for certain loadings, and, finally, transient loads which can change the crack geometry may also be considered.

It would be informative to investigate the failure load of the beam-plate as a function of $\frac{h}{t}$ and $\frac{a}{L}$. Assuming a linear elastic material, two modes of failure are likely: either a failure by excessive displacement in postbuckling, or a

failure due to crack propagation because the critical strain energy release rate is exceeded.

Also, the energy release rate for beams with two delaminations was calculated assuming the growth of both cracks were equal. However, the stresses at different crack tips are unlikely to be the same in most cases, causing only one of the delaminations to grow. The numerical differentiation technique in Chapter 6 may be extended to handle this problem.

References.

1. Rhodes, M.D., Williams, J.G. and Starnes, J.H., Jr., "Effect of Impact Damage on the Compression Strength of Filamentary-Composite Hat-Stiffened Panels," Presented at the *23rd SAMPE National Symposium and Exhibition*, Anaheim, CA, May 2-4, 1978, SAMPE Vol. 23, Selected Applications of Materials for Products and Energy, pp. 310-319, May 1978.
2. Rhodes, M.D., Williams, J.G. and Starnes, J.H., Jr., "Effect of Low-Velocity Impact Damage on the Compressive Strength of Graphite- Epoxy Hot Stiffened Panels," *NASA Tech. Note D-8411*, April 1977.
3. Wilkins, D.J., Eiserman, J.R., Camin, R.A., Margolis, W.S., and Benson, R.A., "Characterizing Delamination Growth in Graphite-Epoxy," Damage in Composite Materials, *ASTM STP 775*, Edited by K.L. Reifsnider, 1982, pp. 168-183.
4. Chai, H., Babcock, C.D., and Knauss, G., "One Dimensional Modeling of Failure in Laminated Plates by Delamination Buckling," *International Journal of Solids and Structures*, Vol. 17, No. 11, 1981, pp. 1069-1083.
5. Simitises, G.J., Sallam, S., and Yin, W.L., "Effect of Delamination of Axially Loaded Homogeneous Laminated Plates," *AIAA Journal*, Vol. 23, No. 9, September 1985, pp. 1437-1444.
6. Yin, W.L., Sallam, S.N., and Simitises, G.J., "Ultimate Axial Load Capacity of a Delaminated Beam-Plate," *AIAA Journal*, Vol. 24, No. 1, January 1986, pp. 123-128.

7. Yin, W.L. and Wang, J.T.S., "The Energy-Release Rate in the Growth of a One-Dimensional Delamination," *Journal of Applied Mechanics*, Vol. 51, 1984, pp. 939-941.
8. Kardomateas, G.A. and Schmueser, D.W., "Effect of Transverse Shearing Forces on Buckling and Postbuckling of Delaminated Composites under Compressive Loads," *Proceedings, AIAA/ASME/AMS/ASCE 28th Structures, Structural Dynamics, and Materials Conference*, Monterey, California, Part 1, pp. 757-765, April 1987.
9. Yin, W.L., "Cylindrical Buckling of Laminated and Delaminated Plates," *Proceedings, AIAA/ASME/AMS/ASCE 27th Structures, Structural Dynamics, and Materials Conference*, San Antonio, Texas, Part 1, pp. 159-164, May 1986.
10. Yin, W.L., "Axisymmetric Buckling and Growth of a Circular Delamination in a Compressed Laminate," *International Journal of Solids and Structures*, Vol. 21, No. 5, 1985, pp. 503-514.
11. Yin, W.L. and Fei, Z., "Buckling Load of a Circular Plate with a Concentric Delamination," *Mechanics Research Communications*, Vol. 11(5), 1984, pp. 337-344.
12. Yin, W.L. and Fei, Z., "Delamination Buckling and Growth in a Clamped Circular Plate," *Proceedings, AIAA/ASME/AMS/ASCE 26th Structures, Structural Dynamics, and Materials Conference*, Orlando, Florida, Part 1, pp. 274-282, April 1985.
13. Yin, W.L., "Energy Balance and the Speed of Crack Growth in a Buckled Strip Delamination," *Proceedings, AIAA/ASME/AMS/ASCE 28th Structures, Structural Dynamics, and Materials Conference*, Monterey, California, Part 1, pp. 748-756, April 1987.
14. Bottega, W.J. and Maewal, A., "Delamination Buckling and Growth in Laminates," *Journal of Applied Mechanics*, Vol. 50, March 1983, pp. 185-189.
15. Whitney, J.M., "Stress Analysis of the End Notch Flexure Specimen for Mode II Delamination of Composite Materials," *Proceedings, AIAA/ASME/AMS/ASCE 28th Structures, Structural Dynamics, and Materials Conference*, Monterey, California, Part 1, pp. 676-681, April 1987.
16. Whitcomb, J.D., "Instability Related Delamination Growth," *Journal of Composite Materials*, Vol. 15, September 1981, pp. 403-419.

17. Horban, B. and Palazotto, A., "The Experimental Cylindrical Composite Panels with Eccentrically Located Circular Delaminations," *Proceedings, AIAA/ASME/AMS/ASCE 27th Structures, Structural Dynamics, and Materials Conference*, San Antonio, Texas, Part 1, pp. 165-179, May 1986.
18. Seifert, G. and Palazotto, A., "The Effect of Centrally Located Midplane Delamination on the Instability of Composite Panels," *Experimental Mechanics*, Vol. 26, No. 4, December 1986, pp. 330-336.
19. Williams, J.F., Stouffer, D.C., Ilic, S., and Jones, R., "An Analysis of Delamination Behaviour," *Composite Structures*, Vol. 5, 1986, pp. 203-216.
20. Vizzini, A.J. and Lagace, P.A., "An Elastic Foundation Model to Predict the Growth of Delaminations," *Proceedings, AIAA/ASME/AMS/ASCE 28th Structures, Structural Dynamics, and Materials Conference*, Monterey, California, Part 1, pp. 776-782, April 1987.
21. Yang, T.Y. and Saigal, S., "A Simple Element For Static and Dynamic Response of Beams with Material and Geometric Nonlinearities," *International Journal for Numerical Methods in Engineering*, Vol. 20, 1984, pp. 851-867.
22. Kapania, R.K. and Yang, T.Y., "Buckling, Postbuckling and Nonlinear Vibrations of Laminated Imperfect Plates," Presented at 1986 Pressure Vessel and Piping Conference and Exhibition, Chicago, Il., July 20-24. Nonlinear Analysis and NDE of Composite Material Vessels and Components, PVP-Vol. 115, ASME, Edited by D. Hui, J.C. Duke Jr. and H. Chung, pp. 13-22. To appear in the *AIAA Journal*.
23. Koiter, W.T., *On the Stability of Elastic Equilibrium*, (in Dutch with English summary), thesis, Delft, H.J. Paris, Amsterdam, 1945. English translation, *Air Force Flight Dyn. Lab. Tech. Rep.*, AFFDL-TR-70-25, February 1970.
24. Broek, D., *Elementary Engineering Fracture Mechanics*, Sijthoff and Noordhoff International Publishers, The Netherlands, 1978, pp. 8-16.
25. Yang, T.Y., *Finite Element Structural Analysis*, Prentice Hall, Englewood Cliffs, New Jersey, 1985, pp. 113-114.
26. Raciti, S., *Nonlinear Vibrations of Unsymmetrically Laminated Beams*, M.Sc. Thesis, Virginia Polytechnic Institute and State University, 1987.

27. Zienciewicz, O.C., *The Finite Element Method*, 3rd Edition, McGraw Hill, London, 1977, pp.501-504.
28. Kondoh, K. and Atluri, S.N., "A Simplified Finite Element Method for Large Deformation, Post-Buckling Analysis of Large Frame Structures, Using Explicitly Derived Tangent Stiffness Matrices," *International Journal for Numerical Methods in Engineering*, Vol, 23, No. 1, January 1981, pp. 69-90.
29. Riks, E., "The Application of Newton's Method to the Problem of Elastic Stability," *Journal of Applied Mechanics*, pp. 1060-1066.
30. Wempner, G.A., "Discrete Approximations Related to Nonlinear Theories of Solids," *International Journal of Solids and Structures*, Vol. 7, 1971, pp. 1581-1599.
31. Crisfield, M.A., "An Arc-Length Method Including Line Searches and Acceleration," *International Journal for Numerical Methods in Engineering*, Vol. 19, 1983, pp. 1269-1289.
32. Kapania, R.K. and Yang, T.Y., "Formulations of an Imperfect Quadrilateral Doubly Curved Shell Element for Postbuckling Analysis," *AIAA Journal*, Vol. 24, No. 2, pp. 310-311, 1986.

Appendix 1: Constant Mode Shape Program

This appendix will contain the constant mode shape finite element program. Input and output files are given for the example of a delaminated clamped-clamped beam-plate with $\frac{a}{L} = 0.5$ and $\frac{h}{t} = 0.1$. Six elements are used. First the linear buckling load and the axial load versus energy release rate curve is found using the constant mode shape program. The input file, the constant mode shape program, and the output are shown below.

INPUT FOR CONSTANT MODE SHAPE PROGRAM

| | |
|--------------|---|
| 0.1 | - HEIGHT OF DELAMINATION |
| 1,2,1 | - NUMBER OF ELEMENTS OF DIFFERENT REGIONS |
| 50.,100.,50. | - LENGTH OF DIFFERENT REGIONS |
| 0.,0.,0. | - ALPHA, BETA, GAMMA |
| 5 | - NUMBER OF BOUNDARY CONDITIONS |
| 2 | - RESTRAINED DEGREE OF FREEDOM |
| 3 | - RESTRAINED DEGREE OF FREEDOM |
| 28 | - RESTRAINED DEGREE OF FREEDOM |
| 29 | - RESTRAINED DEGREE OF FREEDOM |
| 30 | - RESTRAINED DEGREE OF FREEDOM |

```

C*****
C  THIS IS A FINITE ELEMENT PROGRAM FOR THE NONLINEAR
C  ANALYSIS OF DELAMINATED BEAM-PLATES.
C  THIS PROGRAM CALCULATES THE BUCKLING LOAD AND THE ENERGY
C  RELEASE RATES ASSUMING THE BUCKLING MODE SHAPE REMAINS
C  CONSTANT.
C  IT HANDLES BEAMS WITH VARIOUS BOUNDARY CONDITIONS
C  INCLUDING BEAMS WITH ELASTIC SUPPORTS, BEAMS ON ELASTIC
C  FOUNDATIONS, AND BEAMS WITH NONSYMMETRIC DELAMINATIONS.
C      BY: DAVID R. WOLFE
C*****
      IMPLICIT REAL*8 (A-H,O-Z)
      REAL*8 LL(4),IN(4)
      REAL*8 H(4),K(6,6),G(6,6),KU(50,50),GU(50,50),T(50,50),
      1TT(50,50),K1T(50,50),G1T(50,50),KT(50,50),GT(50,50),KR1(1500),
      2GR1(1500),KR(50,50),GR(50,50),FREQ(50),RMODE(50,50),WKAREA(50),
      3A(4),B(4),RM(50),RM1(50),NN1(6,6),NN2(6,6),NU1(50,50),NU2(50,50),
      4NUR1(50,50),NUR2(50,50),NU1T(50,50),NU2T(50,50),N1T(50,50),
      5N2T(50,50),KTOT(50,50),F(50),MS,KUU1(500),KUU(25,25),UU(30),
      6KWW1(1000),NWW(1000),KWW(50,50),NWW2(50,50),NUW(750),NUW1(25,50),
      7QU(25),QW(50),KINV(25,25),NWU1(50,25),QW1(50,1),A1(50,1),B8(25),
      8AA(1,1),B2(25,1),B3(25,1),B4(50,1),BB(1,1),CL(50,1),CC(1,1),
      9FO(50,1),D1(25,1),D2(50,1),DD(1,1),QWT(1,50),QL(25),QB(50),
      1K11(6,6),K33(37,37),N111(6,6),N211(6,6),N133(41,41),N233(37,37),
      2C(6,6)
      DIMENSION NBC(10),IL(4),MUBC(5),MWBC(5)

C
C  HB - HEIGHT OF DELAMINATION
C  N1 - NUMBER OF ELEMENTS OF REGION BEFORE DELAMINATION
C  N2 - NUMBER OF ELEMENTS OF REGION IN DELAMINATION REGION
C  N3 - NUMBER OF ELEMENTS OF REGION AFTER DELAMINATION
C  RL1 - LENGTH OF REGION BEFORE DELAMINATION
C  RL2 - LENGTH OF DELAMINATION REGION
C  RL3 - LENGTH OF REGION AFTER DELAMINATION
C  NNBC - TOTAL NUMBER OF ZERO DEGREES OF FREEDOM
C  NBC - VECTOR OF ZERO DEGREES OF FREEDOM
C  RL - TOTAL LENGTH
C  ALPHA - EXTENSIONAL SPRING CONSTANT
C  BETA - BENDING SPRING CONSTANT
C  GAMMA - ELASTIC FOUNDATION SPRING CONSTANT
C  TH - THICKNESS
C  NUDOF - DEGREES OF FREEDOM
C  PCP - CRITICAL LOAD OF PERFECT BEAM (DEFINE BELOW ON LINE 81)
C
      READ(51,*)HB
      READ(51,*)N1,N2,N3
      READ(51,*)RL1,RL2,RL3
      READ(51,*)ALPHA,BETA,GAMMA
      READ(51,*)NNBC
      DO 10 I=1,NNBC
         READ(51,*)NBC(I)
         IF(NBC(I).GT.17) NBC(I)=NBC(I)-12
10  CONTINUE
      NUDOF=3*(N1+2*N2+N3)+12
      NA=(N1+N2)*3+6
      NA1=NA+1

```

```

NA6=NA+6
TH=10.
RL=200.
E=30.D6
IA=NUDOF-1
IB=NUDOF
LL(1)=RL1/FLOAT(N1)
LL(2)=RL2/FLOAT(N2)
LL(3)=LL(2)
LL(4)=RL3/FLOAT(N3)
H(1)=TH
H(2)=(1.-HB)*TH
H(3)=HB*TH
H(4)=TH
DO 20 I=1,4
    IN(I)=H(I)**3/12.
    A(I)=H(I)*E/LL(I)
    B(I)=E*IN(I)/LL(I)**3
20 CONTINUE
    GAM=GAMMA*E*IN(1)/RL**4
C
C*****MAKE SURE PCP IS CORRECT
C
    PCP=DARCOS(-1.D0)**2*E*IN(1)/RL**2+GAM*RL**2/3.14159**2
C
C*****FORM UNRESTRAINED MATRICES
C
    DO 50 I=1,NUDOF
    DO 50 J=1,NUDOF
        KU(I,J)=0.
        GU(I,J)=0.
50 CONTINUE
    CALL MATR(1,K,G,C,A,B,LL,HB)
    DO 55 I=1,6
    DO 55 J=1,6
        K11(I,J)=K(I,J)
55 CONTINUE
    N=0
    DO 70 M=1,N1
    DO 60 I=1,6
    DO 60 J=1,6
        KU(I+N,J+N)=KU(I+N,J+N)+K(I,J)+GAM*C(I,J)
        GU(I+N,J+N)=GU(I+N,J+N)+G(I,J)
60    CONTINUE
        N=N+3
70 CONTINUE
    CALL MATR(2,K,G,C,A,B,LL,HB)
    DO 100 IC=1,2
        N=N+3
    DO 90 M=1,N2
    DO 80 I=1,6
    DO 80 J=1,6
        KU(I+N,J+N)=KU(I+N,J+N)+K(I,J)+GAM*C(I,J)
        GU(I+N,J+N)=GU(I+N,J+N)+G(I,J)
80    CONTINUE
        N=N+3

```

```

90    CONTINUE
      CALL MATR(3,K,G,C,A,B,LL,HB)
      DO 95 I = 1,6
        DO 95 J = 1,6
          K33(I+NA,J+NA) = K(I,J)
95    CONTINUE
100   CONTINUE
      CALL MATR(4,K,G,C,A,B,LL,HB)
      N = N + 3
      DO 120 M = 1,N3
        DO 110 I = 1,6
          DO 110 J = 1,6
            KU(I+N,J+N) = KU(I+N,J+N) + K(I,J) + GAM*C(I,J)
            GU(I+N,J+N) = GU(I+N,J+N) + G(I,J)
110    CONTINUE
          N = N + 3
120   CONTINUE
C
C*****ADD EXTRA TERMS FROM ELASTIC SUPPORTS TO STIFFNESS MATRIX
C
      KU(2,2) = KU(2,2) + ALPHA*E*IN(1)/RL**3
      KU(3,3) = KU(3,3) + BETA*E*IN(1)/RL
      KU(IA,IA) = KU(IA,IA) + ALPHA*E*IN(1)/RL**3
      KU(IB,IB) = KU(IB,IB) + BETA*E*IN(1)/RL
C
C*****FORM TRANSFORMATION MATRIX
C
      NM12 = NUDOF-12
      DO 130 I = 1,NUDOF
        DO 130 J = 1,NM12
          T(I,J) = 0.
130   CONTINUE
        IEND1 = 3*N1 + 3
        DO 140 I = 1,IEND1
          T(I,I) = 1.
140   CONTINUE
        IEND2 = 3*(N1 + 2*N2) + 9
        IB3 = IEND2 + 1
        DO 150 I = IB3,NUDOF
          T(I,I-12) = 1.
150   CONTINUE
        II = N2*3-1
        IB2 = IEND1 + 1
        ID = IB2 + II
        DO 160 I = IB2,ID
          T(I,I-3) = 1.
160   CONTINUE
        T(IB2,IB2-1) = H(3)/2.
        INE = N2*3-6
        DO 170 J = 1,3
          T(ID+J,INE+J+ID) = 1.
170   CONTINUE
        T(ID+1,ID+3+INE) = H(3)/2.
        I3 = ID + 3
        INF = 3*N2 + 6
        DO 180 J = 1,3

```



```

      T(I3 + J,I3 + J-INF) = 1.
180 CONTINUE
      T(I3 + 1,I3-INF + 3) = -H(2)/2.
      I7 = ID + 7
      ID = I7 + II
      DO 190 J = I7, ID
        T(J,J-9) = 1.
190 CONTINUE
      T(IB3-3,IB3-10) = -H(2)/2.
      DO 200 I = 1, NUDOF
        DO 200 J = 1, NM12
          TT(J,I) = T(I,J)
200 CONTINUE
C
C*****FORM TRANSFORMED STIFFNESS MATRICES
C
      CALL VMULFF(TT,KU,NM12,NUDOF,NUDOF,50,50,K1T,50,IER)
      CALL VMULFF(TT,GU,NM12,NUDOF,NUDOF,50,50,G1T,50,IER)
      CALL VMULFF(K1T,T,NM12,NUDOF,NM12,50,50,KT,50,IER)
      CALL VMULFF(G1T,T,NM12,NUDOF,NM12,50,50,GT,50,IER)
C
C*****FORM RESTRAINED MATRICES
C
      M = 1
      DO 270 I = 1, NM12
        DO 270 J = 1, NM12
          DO 280 L = 1, NNBC
            IF (I.EQ.NBC(L).OR.J.EQ.NBC(L))GO TO 270
280      CONTINUE
            KR1(M) = KT(I,J)
            GR1(M) = GT(I,J)
            M = M + 1
270 CONTINUE
      NR = NM12 - NNBC
      M = 1
      DO 290 I = 1, NR
        DO 290 J = 1, NR
          KR(I,J) = KR1(M)
          GR(I,J) = GR1(M)
          M = M + 1
290 CONTINUE
C
C*****FIND NON-DIMENSIONALIZED CRITICAL LOAD
C
      CALL EIGENR(50,NR,GR,KR,FREQ,RMODE)
      PCR = 1./FREQ(NR)/PCP
      WRITE(52,*)'THE NON-D CRITICAL BUCKLING LOAD IS', PCR
C
C*****ADD ZERO DOF'S TO MODAL VECTOR
C
      I2 = 1
      DO 301 I1 = 1, NM12
        DO 302 I3 = 1, NNBC
          IF (I1.EQ.NBC(I3)) THEN
            RM(I1) = 0
            GO TO 301

```

```

        ENDIF
302    CONTINUE
        RM(I1) = RMODE(I2,NR)
        I2 = I2 + 1
301 CONTINUE
C
C*****NORMALIZE MODAL VECTOR
C
        C1 = 0.
        DO 307 I = 1, NM12
307 IF (DABS(RM(I)).GT.DABS(C1)) C1 = RM(I)
        DO 308 I = 1, NM12
            RM(I) = RM(I)/C1
308 CONTINUE
C
C*****EXPAND MODAL VECTOR
C
        IL(1) = IB2
        IL(2) = IB2 + N2*3
        IL(3) = IL(2) + 3
        IL(4) = IL(3) + N2*3
        I2 = 1
        DO 311 I = 1, NM12
            DO 312 I1 = 1, 4
                IF (I2.EQ.IL(I1)) I2 = I2 + 3
312    CONTINUE
                RM1(I2) = RM(I)
                I2 = I2 + 1
311 CONTINUE
            RM1(IB2) = RM1(IB2-3) + H(3)/2.*RM1(IB2-1)
            RM1(IB2 + 1) = RM1(IB2-2)
            RM1(IB2 + 2) = RM1(IB2-1)
            RM1(IB3-3) = RM1(IB3)-H(2)/2.*RM1(IB3 + 2)
            RM1(IB3-2) = RM1(IB3 + 1)
            RM1(IB3-1) = RM1(IB3 + 2)
            NDD = IL(2)
            RM1(NDD) = RM1(IB3) + H(3)/2.*RM1(IB3 + 2)
            RM1(NDD + 1) = RM1(IB3 + 1)
            RM1(NDD + 2) = RM1(IB3 + 2)
            RM1(NDD + 3) = RM1(IB2-3)-H(2)/2.*RM1(IB2-1)
            RM1(NDD + 4) = RM1(IB2-2)
            RM1(NDD + 5) = RM1(IB2-1)
C
C*****FORM UNRESTRAINED NONLINEAR MATRICES
C
        DO 450 I = 1, NUDOF
        DO 450 J = 1, NUDOF
            NU1(I,J) = 0.
            NU2(I,J) = 0.
450 CONTINUE
        N = 0
        DO 470 M = 1, N1
            X1 = RM1(N + 2)
            Y1 = RM1(N + 3)
            X2 = RM1(N + 5)
            Y2 = RM1(N + 6)

```

```

      CALL MM(X1,Y1,X2,Y2,LL(1),A(1),NN1,NN2)
      DO 475 I=1,6
      DO 475 J=1,6
        N111(I,J)=NN1(I,J)
        N211(I,J)=NN2(I,J)
475    CONTINUE
      DO 460 I=1,6
      DO 460 J=1,6
        NU1(I+N,J+N)=NU1(I+N,J+N)+NN1(I,J)
        NU2(I+N,J+N)=NU2(I+N,J+N)+NN2(I,J)
460    CONTINUE
      N=N+3
470 CONTINUE
      DO 500 IC=1,2
      N=N+3
      DO 490 M=1,N2
        X1=RM1(N+2)
        Y1=RM1(N+3)
        X2=RM1(N+5)
        Y2=RM1(N+6)
        CALL MM(X1,Y1,X2,Y2,LL(2),A(2),NN1,NN2)
        IF(IC.EQ.2.AND.M.EQ.1)THEN
          DO 495 I=1,6
          DO 495 J=1,6
            N133(I+NA,J+NA)=NN1(I,J)
            N233(I+NA,J+NA)=NN2(I,J)
495        CONTINUE
          ENDIF
          DO 480 I=1,6
          DO 480 J=1,6
            NU1(I+N,J+N)=NU1(I+N,J+N)+NN1(I,J)
            NU2(I+N,J+N)=NU2(I+N,J+N)+NN2(I,J)
480        CONTINUE
          N=N+3
490        CONTINUE
          A(2)=A(3)
500 CONTINUE
      N=N+3
      DO 520 M=1,N3
        X1=RM1(N+2)
        Y1=RM1(N+3)
        X2=RM1(N+5)
        Y2=RM1(N+6)
        CALL MM(X1,Y1,X2,Y2,LL(4),A(4),NN1,NN2)
        DO 510 I=1,6
        DO 510 J=1,6
          NU1(I+N,J+N)=NU1(I+N,J+N)+NN1(I,J)
          NU2(I+N,J+N)=NU2(I+N,J+N)+NN2(I,J)
510        CONTINUE
        N=N+3
520 CONTINUE
C
C*****FORM TRANSFORMED NONLINEAR STIFFNESS MATRICES
C
      CALL VMULFF(TT,NU1,NM12,NUDOF,NUDOF,50,50,NU1T,50,IER)
      CALL VMULFF(TT,NU2,NM12,NUDOF,NUDOF,50,50,NU2T,50,IER)

```

```

      CALL VMULFF(NU1T,T,NM12,NUDOF,NM12,50,50,N1T,50,IER)
      CALL VMULFF(NU2T,T,NM12,NUDOF,NM12,50,50,N2T,50,IER)
C
C*****FORM RESTRAINED NONLINEAR MATRICES
C
      M=1
      DO 570 I=1,NM12
      DO 570 J=1,NM12
        DO 580 L2=1,NNBC
          IF (I.EQ.NBC(L2).OR.J.EQ.NBC(L2)) GO TO 570
        580  CONTINUE
          KR1(M)=N1T(I,J)
          GR1(M)=N2T(I,J)
          M=M+1
        570 CONTINUE
      M=1
      NRE=NM12-NNBC
      DO 590 I=1,NRE
      DO 590 J=1,NRE
        NUR1(I,J)=KR1(M)
        NUR2(I,J)=GR1(M)
        M=M+1
      590 CONTINUE
C
C*****SEPARATE BOUNDARY CONDITIONS
C
      MWR=0
      MUR=0
      DO 663 I=1,NNBC
        IF ((NBC(I)+2)/3*3.EQ.NBC(I)+2) GO TO 662
        MWR=MWR+1
        MWBC(MWR)=NBC(I)*2/3
        GO TO 663
      662  MUR=MUR+1
          MUBC(MUR)=(NBC(I)+2)/3
      663 CONTINUE
C
C*****FORM KUU
C
      ND3=NM12/3
      N2U=ND3-MUR
      N2W=2*ND3-MWR
      M=1
      DO 605 I=1,NM12
      DO 605 J=1,NM12
        IF((I+2)/3*3.NE.I+2.OR.(J+2)/3*3.NE.J+2) GO TO 605
        DO 607 I1=1,NNBC
          IF(I.EQ.NBC(I1).OR.J.EQ.NBC(I1))GO TO 605
        607  CONTINUE
          KUU1(M)=KT(I,J)
          M=M+1
        605 CONTINUE
      M=1
      DO 610 I=1,N2U
      DO 610 J=1,N2U
        KUU(I,J)=KUU1(M)

```

```

      M=M+1
610 CONTINUE
C
C*****FORM INVERSE OF KUU (=KINV)
C
      CALL LINV1F(KUU,N2U,25,KINV,0,WKAREA,IER)
C
C*****FORM KWW AND NWW2
C
      N2D3=NM12/3*2
      M=1
      DO 615 I=1,NM12
      DO 615 J=1,NM12
        IF((I+2)/3*3.EQ.I+2.OR.(J+2)/3*3.EQ.J+2) GO TO 615
        DO 617 I1=1,NNBC
          IF(I.EQ.NBC(I1).OR.J.EQ.NBC(I1))GO TO 615
617    CONTINUE
        KWW1(M)=KT(I,J)
        NWW(M)=N2T(I,J)
        M=M+1
615 CONTINUE
      M=1
      DO 620 I=1,N2W
      DO 620 J=1,N2W
        KWW(I,J)=KWW1(M)
        NWW2(I,J)=NWW(M)
        M=M+1
620 CONTINUE
C
C*****FORM NUW1
C
      M=1
      DO 625 I=1,NM12
      DO 625 J=1,NM12
        IF((I+2)/3*3.EQ.I+2.OR.(J+2)/3*3.EQ.J+2) GO TO 625
        DO 627 I1=1,NNBC
          IF(I.EQ.NBC(I1).OR.J.EQ.NBC(I1))GO TO 625
627    CONTINUE
        NUW(M)=N1T(I,J)
        M=M+1
625 CONTINUE
      M=1
      DO 630 I=1,N2W
      DO 630 J=1,N2U
        NWU1(I,J)=NUW(M)
        M=M+1
630 CONTINUE
C
C*****FORM QW
C
      M1=1
      DO 635 I=1,NM12
      DO 637 I1=1,NNBC
        IF(I.EQ.NBC(I1))GO TO 635
637    CONTINUE
        IF((I+2)/3*3.EQ.I+2)GO TO 635

```

```

        QW(M1) = RM(I)
        QW1(M1,1) = RM(I)
        QWT(1,M1) = RM(I)
        M1 = M1 + 1
635 CONTINUE
C
C*****FIND NUW1
C
        DO 645 I = 1, N2W
        DO 645 J = 1, N2U
            NUW1(J,I) = .5*NWU1(I,J)
645 CONTINUE
C
C*****MULTIPLY MATRICES TO FIND CONSTANTS
C
        CALL VMULFF(KWW,QW1,N2W,N2W,1,50,50,A1,50,IER)
        CALL VMULFF(QWT,A1,1,N2W,1,1,50,AA,1,IER)
        AAA = AA(1,1)
        CALL VMULFF(NUW1,QW1,N2U,N2W,1,25,50,B2,25,IER)
        CALL VMULFF(KINV,B2,N2U,N2U,1,25,25,B3,25,IER)
        CALL VMULFF(NWU1,B3,N2W,N2U,1,50,25,B4,50,IER)
        CALL VMULFF(QWT,B4,1,N2W,1,1,50,BB,1,IER)
        BBB = BB(1,1)
        CALL VMULFF(NWW2,QW1,N2W,N2W,1,50,50,CL,50,IER)
        CALL VMULFF(QWT,CL,1,N2W,1,1,50,CC,1,IER)
        CCC = CC(1,1)
        DO 650 I = 1, N2U
            FO(I,1) = 0.0
650 CONTINUE
        FO(1,1) = 1.
        CALL VMULFF(KINV,FO,N2U,N2U,1,25,25,D1,25,IER)
        CALL VMULFF(NWU1,D1,N2W,N2U,1,50,25,D2,50,IER)
        CALL VMULFF(QWT,D2,1,N2W,1,1,50,DD,1,IER)
        DDD = DD(1,1)
        DEL = 0.0000
        DO 701 I22 = 1, 31
            PP = -AAA/DDD + (BBB-CCC)/DDD*DEL**2
C
C*****FIND QU
C
        DO 660 I = 1, N2U
            QU(I) = PP*D1(I,1)-B3(I,1)*DEL**2
660 CONTINUE
C
C*****FORM DISPLACEMENT VECTOR
C
        I2 = 1
        DO 665 I1 = 1, ND3
            DO 667 I3 = 1, MUR
                IF (I1.EQ.MUBC(I3)) THEN
                    QL(I1) = 0
                    GO TO 665
                ENDIF
            667 CONTINUE
            QL(I1) = QU(I2)
            I2 = I2 + 1

```

```

665 CONTINUE
  I2=1
  DO 670 I1=1,N2D3
    IF (MWR.EQ.0) GO TO 673
    DO 672 I3=1,MWR
      IF (I1.EQ.MWBC(I3)) THEN
        QB(I1)=0
        GO TO 670
      ENDIF
    CONTINUE
  QB(I1)=QW(I2)
  I2=I2+1
670 CONTINUE
  M=1
  M1=1
  DO 675 I=1,NM12
    IF((I+2)/3*.3.EQ.I+2)GO TO 677
    RM(I)=QB(M)*DEL
    M=M+1
    GO TO 675
  677  RM(I)=QL(M1)
    M1=M1+1
675 CONTINUE
C
C*****EXPAND MODAL VECTOR
C
  I2=1
  DO 680 I=1,NM12
    DO 682 I1=1,4
      IF (I2.EQ.IL(I1)) I2=I2+3
    682  CONTINUE
    RM1(I2)=RM(I)
    I2=I2+1
680 CONTINUE
  RM1(IB2)=RM1(IB2-3)+H(3)/2.*RM1(IB2-1)
  RM1(IB2+1)=RM1(IB2-2)
  RM1(IB2+2)=RM1(IB2-1)
  RM1(IB3-3)=RM1(IB3)-H(2)/2.*RM1(IB3+2)
  RM1(IB3-2)=RM1(IB3+1)
  RM1(IB3-1)=RM1(IB3+2)
  NDD=IL(2)
  RM1(NDD)=RM1(IB3)+H(3)/2.*RM1(IB3+2)
  RM1(NDD+1)=RM1(IB3+1)
  RM1(NDD+2)=RM1(IB3+2)
  RM1(NDD+3)=RM1(IB2-3)-H(2)/2.*RM1(IB2-1)
  RM1(NDD+4)=RM1(IB2-2)
  RM1(NDD+5)=RM1(IB2-1)
C
C*****FIND INTERNAL FORCES
C
  DO 702 J=1,6
    DO 702 K1=1,6
      KTOT(J,K1)=K11(J,K1)+DEL*N111(J,K1)+DEL**2*N211(J,K1)
    702  CONTINUE
    DO 703 J=1,6
      F(J)=0.

```

```

        DO 704 K1=1,6
          F(J)=F(J)+KTOT(J,K1)*RM1(K1)
704    CONTINUE
703    CONTINUE
        DO 712 J=NA1,NA6
          DO 712 K1=NA1,NA6
            KTOT(J,K1)=K33(J,K1)+DEL*N133(J,K1)+DEL**2*N233(J,K1)
712    CONTINUE
          DO 713 J=NA1,NA6
            F(J)=0.
            DO 714 K1=NA1,NA6
              F(J)=F(J)+KTOT(J,K1)*RM1(K1)
714    CONTINUE
713    CONTINUE
C
C*****FIND ENERGY-RELEASE RATE
C
        HHB=1.-HB
        PS=HB*(-F(4)+6.*HHB*F(3)/TH)-F(NA+1)
        MS=-F(NA+3)-F(6)*HB**3
        AB=(TH*PS)**2/(HB*HHB)
        BC=12.*MS**2/HB**3
        CD=12.*(TH*PS/2.-MS)**2/HHB**3
        RRG=1./(24.*E*IN(1))*(AB+BC+CD)
        PB=F(1)/PCP
        GB=(RL/2.):**4*RRG/(E*TH**5)
        WRITE(3,19)GB,PB
19    FORMAT(3X,E15.8,5X,E15.8)
        IF (PB.GT.1.) GO TO 800
        DEL=DEL+.20
701 CONTINUE
800 STOP
        END
        SUBROUTINE EIGENR(NDIM,N,A,B,LAMBDA,X)                                EIGR
C
C*****THIS SUBROUTINE CALCULATES EIGENVALUES AND EIGENVECTORS
C
C*****
        REAL*8 A(NDIM,NDIM),B(NDIM,NDIM),X(NDIM,NDIM),LAMBDA(NDIM)
        REAL*8 E(256),S,T,TOL,EPS,DSQRT
        DO 4 I=1,N
          DO 4 J=1,N
            S=B(I,J)
            IF(I.EQ.1) GO TO 2
            I1=I-1
            DO 1 K=1,I1
              1  S=S-B(I,K)*B(J,K)
              2  IF(J.NE.I) GO TO 3
              IF(S.LE.0.D0) PRINT 13
              T=DSQRT(DABS(S))
              B(I,I)=T
              GO TO 4
              3  B(J,I)=S/T
              4  CONTINUE
            DO 6 I=1,N
              DO 6 J=1,N

```



```

      S=A(I,J)
      IF(I.EQ.1) GO TO 6
      I1=I-1
      DO 5 K=1,I1
5     S=S-B(I,K)*A(J,K)
6   A(J,I)=S/B(I,I)
      DO 10 J=1,N
      DO 10 I=J,N
        S=A(I,J)
        IF(I.EQ.J) GO TO 8
        I1=I-1
        DO 7 K=J,I1
7       S=S-A(K,J)*B(I,K)
8     IF(J.EQ.1) GO TO 10
        J1=J-1
        DO 9 K=1,J1
9       S=S-A(J,K)*B(I,K)
10    A(I,J)=S/B(I,I)
      TOL = 2.44D-63
      CALL TRED2(NDIM,N,TOL,A,LAMBDA,E,X)
      EPS = 2.22D-16
      CALL TQL2(NDIM,N,EPS,LAMBDA,E,X,IERR)
      IF(IERR.NE.0) PRINT 14
      DO 12 J=1,N
      DO 12 IBACK=1,N
      I=N+1-IBACK
      S=X(I,J)
      IF(I.EQ.N) GO TO 12
      I1=I+1
      DO 11 K=I1,N
11     S=S-B(K,I)*X(K,J)
12    X(I,J)=S/B(I,I)
      RETURN
13  FORMAT(' ***B IS NOT POSITIVE DEFINITE****')
14  FORMAT(' ***TQL2 DID NOT CONVERGE****')
      END
      SUBROUTINE TRED2 (NM,N,TOL,A,D,E,Z)
C*****
      IMPLICIT REAL*8 (A-H,O-Z)
      REAL*8 A(NM,N),D(N),E(N),Z(NM,N)
      DO 100 I = 1, N
        DO 100 J = 1, I
          Z(I,J) = A(I,J)
100  CONTINUE
      IF (N .EQ. 1) GO TO 320
      DO 300 II = 2, N
        I = N + 2 - II
        L = I - 2
        F = Z(I,I-1)
        G = 0.0D0
        IF (L .LT. 1) GO TO 140
        DO 120 K = 1, L
120     G = G + Z(I,K) * Z(I,K)
        IF(DABS(F).LT.DABS(1.D-8)) F=0.
140     H = G + F * F
        IF (G .GT. TOL) GO TO 160

```

TRED

```

      E(I) = F
      H = 0.0D0
      GO TO 280
160   L = L + 1
      G = -DSIGN(DSQRT(H),F)
      E(I) = G
      H = H - F * G
      Z(I,I-1) = F - G
      F = 0.0D0
      DO 240 J = 1, L
        Z(J,I) = Z(I,J) / H
        G = 0.0D0
        DO 180 K = 1, J
180     G = G + Z(J,K) * Z(I,K)
        JP1 = J + 1
        IF (L .LT. JP1) GO TO 220
        DO 200 K = JP1, L
200     G = G + Z(K,J) * Z(I,K)
220     E(J) = G / H
        F = F + G * Z(J,I)
240   CONTINUE
      HH = F / (H + H)
      DO 260 J = 1, L
        F = Z(I,J)
        G = E(J) - HH * F
        E(J) = G
        DO 260 K = 1, J
          Z(J,K) = Z(J,K) - F * E(K) - G * Z(I,K)
260   CONTINUE
280   D(I) = H
300   CONTINUE
320   D(1) = 0.0D0
      E(1) = 0.0D0
      DO 500 I = 1, N
        L = I - 1
        IF (D(I) .EQ. 0.0D0) GO TO 380
        DO 360 J = 1, L
          G = 0.0D0
          DO 340 K = 1, L
340     G = G + Z(I,K) * Z(K,J)
          DO 360 K = 1, L
            Z(K,J) = Z(K,J) - G * Z(K,I)
360   CONTINUE
380   D(I) = Z(I,I)
      Z(I,I) = 1.0D0
      IF (L .LT. 1) GO TO 500
      DO 400 J = 1, L
        Z(I,J) = 0.0D0
        Z(J,I) = 0.0D0
400   CONTINUE
500   CONTINUE
      RETURN
      END
      SUBROUTINE TQL2 (NM,N,MACHEP,D,E,Z,ERROR)
C*****
      IMPLICIT REAL*8 (A-H,O-Z)

```

TQL2

```

REAL*8 MACHEP,D(N),E(N),Z(NM,N)
INTEGER ERROR
ERROR = 0
IF (N.EQ. 1) GO TO 1001
DO 100 I = 2, N
100 E(I-1) = E(I)
F = 0.0D0
B = 0.0D0
E(N) = 0.0D0
DO 240 L = 1, N
J = 0
H = MACHEP * (DABS(D(L)) + DABS(E(L)))
IF (B.LT. H) B = H
DO 110 M = L, N
IF (DABS(E(M)) .LE. B) GO TO 120
110 CONTINUE
120 IF (M.EQ. L) GO TO 220
130 IF (J.EQ. 30) GO TO 1000
J = J + 1
P = (D(L+1) - D(L)) / (2.0D0 * E(L))
R = DSQRT(P * P + 1.0D0)
H = D(L) - E(L) / (P + DSIGN(R,P))
DO 140 I = L, N
140 D(I) = D(I) - H
F = F + H
P = D(M)
C = 1.0D0
S = 0.0D0
MML = M - L
DO 200 II = 1, MML
I = M - II
G = C * E(I)
H = C * P
IF (DABS(P) .LT. DABS(E(I))) GO TO 150
C = E(I) / P
IF(DABS(C).LT.DABS(1.0D-9)) C=0.
R = DSQRT(C * C + 1.0D0)
E(I+1) = S * P * R
S = C / R
C = 1.0D0 / R
GO TO 160
150 C = P / E(I)
R = DSQRT(C * C + 1.0D0)
E(I+1) = S * E(I) * R
S = 1.0D0 / R
C = C / R
160 P = C * D(I) - S * G
D(I+1) = H + S * (C * G + S * D(I))
DO 180 K = 1, N
H = Z(K,I+1)
Z(K,I+1) = S * Z(K,I) + C * H
Z(K,I) = C * Z(K,I) - S * H
180 CONTINUE
200 CONTINUE
E(L) = S * P
D(L) = C * P

```

```
IF (DABS(E(L)) .GT. B) GO TO 130
```

```
220 D(L) = D(L) + F
```

```
240 CONTINUE
```

```
    NM1 = N - 1
```

```
    DO 300 I = 1, NM1
```

```
        K = I
```

```
        P = D(I)
```

```
        IP1 = I + 1
```

```
        DO 260 J = IP1, N
```

```
            IF (D(J) .GE. P) GO TO 260
```

```
            K = J
```

```
            P = D(J)
```

```
260 CONTINUE
```

```
    IF (K .EQ. I) GO TO 300
```

```
    D(K) = D(I)
```

```
    D(I) = P
```

```
    DO 280 J = 1, N
```

```
        P = Z(J,I)
```

```
        Z(J,I) = Z(J,K)
```

```
        Z(J,K) = P
```

```
280 CONTINUE
```

```
300 CONTINUE
```

```
    GO TO 1001
```

```
1000 ERROR = L
```

```
1001 RETURN
```

```
END
```

```
    SUBROUTINE MM(V1,T1,V2,T2,L,A,N1,N2)
```

```
C
```

```
C*****THIS SUBROUTINE CALCULATES COMPONENTS OF NONLINEAR MATRICES
```

```
C
```

```
    REAL*8 M1(6,6),M2(6,6),L,V1,T1,V2,T2,A,N1(6,6),N2(6,6)
```

```
    DO 20 M = 1,6
```

```
    DO 20 J = 1,6
```

```
        M1(M,J) = 0.
```

```
        M2(M,J) = 0.
```

```
20 CONTINUE
```

```
    M1(2,4) = 6./5./L*V1 + .1*T1-6./5./L*V2 + .1*T2
```

```
    M1(2,1) = -M1(2,4)
```

```
    M1(3,4) = .1*V1 + 2./15.*L*T1-.1*V2-1./30.*L*T2
```

```
    M1(3,1) = -M1(3,4)
```

```
    M1(5,4) = M1(2,1)
```

```
    M1(5,1) = -M1(5,4)
```

```
    M1(6,4) = .1*V1-1./30.*L*T1-.1*V2 + 2./15.*L*T2
```

```
    M1(6,1) = -M1(6,4)
```

```
    M2(2,2) = (72./L**3*V1**2 + 18./L**2*V1*T1 + 3./L*T1**2
```

```
1-144./L**3*V1*V2-18./L**2*V2*T1 + 18./L**2*V1*T2
```

```
2 + 72./L**3*V2**2-18./L**2*V2*T2 + 3./L*T2**2)/35.
```

```
    M2(3,3) = (3.*(-V1*T1 + V2*T1 + V1*T2-L*T1*T2-V2*T2) + 18./L*V1**2
```

```
1 + 12.*L*T1**2-36./L*V1*V2 + 18./L*V2**2 + 1.*L*T2**2)/210.
```

```
    M2(5,5) = M2(2,2)
```

```
    M2(6,6) = (1.*(V1*T1-V2*T1-V1*T2-T1*T2*L + V2*T2) + 6./L*V1**2
```

```
1 + 1./3.*L*T1**2-12./L*V1*V2 + 6./L*V2**2 + 4.*L*T2**2)/70.
```

```
    M2(3,2) = (18./L**2*(V1**2 + V2**2) + 12./L*(V1*T1-V2*T1) +
```

```
11./2.*(T2**2-T1**2)-32./L**2*V1*V2 + 1.*T1*T2)/70.
```

```
    M2(5,2) = -M2(2,2)
```

```
    M2(5,3) = -M2(3,2)
```

```

      M2(6,2)=(18./L**2*(V1**2-2*V1*V2+V2**2)+1./2.*(T1**2+
      12*T1*T2-T2**2)+12./L*(V1*T2-V2*T2))/70.
      M2(6,3)=(1.*(V1*T1-T1*V2+V1*T2-V2*T2)-1./2.*L*(T1**2
      1+T2**2)+2./3.*L*T1*T2)/70.
      M2(6,5)=-M2(6,2)
      DO 30 M=1,6
      DO 30 J=1,6
          M2(M,J)=M2(J,M)
30 CONTINUE
      DO 40 M=1,6
      DO 40 J=1,6
          N1(M,J)=(M1(M,J)+.5*M1(J,M))*A
          N2(M,J)=.5*M2(M,J)*A*L
40 CONTINUE
      RETURN
      END
      SUBROUTINE MATR(I,K,G,C,A,B,LL,HB)
C
C*****THIS SUBROUTINE CALCULATES COMPONENTS OF BASIC AND INCREMENTAL
C*****STIFFNESS MATRICES
C
      REAL*8 K(6,6),G(6,6),A(4),B(4),C(6,6)
      REAL*8 LL(4),HB
      DO 27 M=1,6
      DO 27 J=1,6
          K(M,J)=0.
          G(M,J)=0.
          C(M,J)=0.
27 CONTINUE
      K(1,1)=A(I)
      K(2,2)=12.*B(I)
      K(3,3)=4.*B(I)*LL(I)**2
      K(4,4)=A(I)
      K(5,5)=12.*B(I)
      K(6,6)=K(3,3)
      K(4,1)=-A(I)
      K(3,2)=6.*B(I)*LL(I)
      K(5,2)=-12.*B(I)
      K(6,2)=K(3,2)
      K(5,3)=-K(3,2)
      K(6,3)=.5*K(3,3)
      K(6,5)=K(5,3)
      G(2,2)=12./LL(I)
      G(3,3)=4./3.*LL(I)
      G(5,5)=G(2,2)
      G(6,6)=G(3,3)
      G(3,2)=1.
      G(5,2)=-G(2,2)
      G(6,2)=1.
      G(5,3)=-1.
      G(6,3)=-LL(I)/3.
      G(6,5)=-1.
      C(2,2)=156.
      C(3,3)=4.*LL(I)**2
      C(5,5)=156.
      C(6,6)=C(3,3)

```

```

C(3,2)=22.*LL(I)
C(5,2)=54.
C(6,2)=-13.*LL(I)
C(5,3)=13.*LL(I)
C(6,3)=-3.*LL(I)**2
C(6,5)=-22.*LL(I)
DO 40 J=1,6
DO 40 M=1,6
    K(J,M)=K(M,J)
    G(J,M)=G(M,J)
    C(J,M)=C(M,J)
40  CONTINUE
DO 42 M=1,6
DO 42 J=1,6
    G(J,M)=G(J,M)/10.
    C(J,M)=C(J,M)*LL(I)/420.
42  CONTINUE
IF(I.EQ.2)THEN
DO 47 M=1,6
DO 47 J=1,6
    G(M,J)=(1-HB)*G(M,J)
47  CONTINUE
ENDIF
IF(I.EQ.3)THEN
DO 49 M=1,6
DO 49 J=1,6
    G(M,J)=HB*G(M,J)
    C(M,J)=0.
49  CONTINUE
ENDIF
RETURN
END

```

OUTPUT FOR CONSTANT MODE SHAPE PROGRAM

THE NON-D CRITICAL BUCKLING LOAD IS .40484892E-01

| GBAR | PBAR |
|----------------|-----------------|
| 0.62974656E-35 | 0.40484892E-01 |
| 0.67312072E-05 | 0.42030161E-01 |
| 0.28197854E-04 | 0.46665968E-01 |
| 0.68353731E-04 | 0.54392312E-01 |
| 0.13398031E-03 | 0.65209193E-01 |
| 0.23488177E-03 | 0.79116612E-01 |
| 0.38416105E-03 | 0.96114569E-01 |
| 0.59857690E-03 | 0.11620306E +00 |
| 0.89898201E-03 | 0.13938210E +00 |
| 0.13108421E-02 | 0.16565166E +00 |
| 0.18648361E-02 | 0.19501177E +00 |
| 0.25975373E-02 | 0.22746242E +00 |
| 0.35521754E-02 | 0.26300360E +00 |
| 0.47794801E-02 | 0.30163532E +00 |
| 0.63386050E-02 | 0.34335758E +00 |
| 0.82981327E-02 | 0.38817037E +00 |
| 0.10737162E-01 | 0.43607370E +00 |
| 0.13746473E-01 | 0.48706757E +00 |
| 0.17429780E-01 | 0.54115198E +00 |
| 0.21905054E-01 | 0.59832693E +00 |
| 0.27305939E-01 | 0.65859241E +00 |
| 0.33783243E-01 | 0.72194843E +00 |
| 0.41506504E-01 | 0.78839499E +00 |
| 0.50665654E-01 | 0.85793208E +00 |
| 0.61472742E-01 | 0.93055972E +00 |
| 0.74163759E-01 | 0.10062779E +01 |

Appendix 2: Incremental Program

Now the axial load versus energy release rate for the same problem of a clamped-clamped beam with $\frac{h}{t} = .1$ and $\frac{a}{L} = .5$ is calculated using the incremental program with 10 elements. The input, incremental program, and output are given below. The curves for the incremental and constant mode shape solutions are plotted for this case in Figure 30.

INPUT FOR INCREMENTAL PROGRAM

| | |
|--------------|---|
| 9,15 | - RESTRAINED DEGREES OF FREEDOM OF TRANXVERSE LOADS |
| 0.1 | - HEIGHT OF DELAMINATION |
| 2,3,2 | - NUMBER OF ELEMENTS OF DIFFERENT REGIONS |
| 50.,100.,50. | - LENGTH OF DIFFERENT REGIONS |
| 0.,0.,0. | - ALPHA, BETA, GAMMA |
| 5 | - NUMBER OF BOUNDARY CONDITIONS |
| 2 | - ZERO DEGREE OF FREEDOM |
| 3 | - ZERO DEGREE OF FREEDOM |
| 40 | - ZERO DEGREE OF FREEDOM |
| 41 | - ZERO DEGREE OF FREEDOM |
| 42 | - ZERO DEGREE OF FREEDOM |

```

      IMPLICIT REAL*8 (A-H,O-Z)
      REAL*8 LL(4),IN(4)
      REAL*8  H(4),K(6,6),G(6,6),KU(60,60),GU(60,60),T(60,60),
      1TT(60,60),K1T(60,60),G1T(60,60),KT(60,60),GT(60,60),KR1(2500),
      2GR1(2500),KR(60,60),GR(60,60),FREQ(60),RMODE(60,60),WKAREA(60),
      3A(4),B(4),RM(60),RM1(60),KST(60,60),DP(60),DD(60),
      4KTOT(60,60),F(60),MS,RMA(60),KTINV(60,60),P(60),
      6PT(60),PD(60),RMI(60),DS(60),DD1(60),C(6,6)
      DIMENSION NBC(10),IL(4)
C*****
C  THIS IS A FINITE ELEMENT PROGRAM FOR THE NONLINEAR
C  ANALYSIS OF DELAMINATED BEAM-PLATES.
C  IT IS AN INCREMENTAL PROGRAM WHICH TAKES INTO ACCOUNT
C  CHANGING MODE SHAPE.
C  IT CALCULATES AXIAL LOAD VERSUS ENERGY RELEASE RATE
C  FOR BEAMS WITH VARIOUS BOUNDARY CONDITIONS INCLUDING
C  BEAMS WITH ELASTIC SUPPORTS, BEAMS ON ELASTIC
C  FOUNDATIONS, AND BEAMS WITH NONSYMMETRIC DELAMINATIONS.
C  BY: DAVID R. WOLFE
C*****
C
C*****DEFINE CRITICAL LOAD OF PERFECT BEAM BELOW ON LINE BELOW
C  L1,L2 RESTRAINED DEGREES OF FREEDOM OF TRANSVERSE LOADS
C  HB - HEIGHT OF DELAMINATION
C  N1 - NUMBER OF ELEMENTS OF REGION BEFORE DELAMINATION
C  N2 - NUMBER OF ELEMENTS OF REGION IN DELAMINATION REGION
C  N3 - NUMBER OF ELEMENTS OF REGION AFTER DELAMINATION
C  RL1 - LENGTH OF REGION BEFORE DELAMINATION
C  RL2 - LENGTH OF DELAMINATION REGION
C  RL3 - LENGTH OF REGION AFTER DELAMINATION
C  NNBC - TOTAL NUMBER OF ZERO DEGREES OF FREEDOM
C  NBC - VECTOR OF ZERO DEGREES OF FREEDOM
C  RL - TOTAL LENGTH
C  ALPHA - EXTENTIONAL SPRING CONSTANT
C  BETA - BENDING SPRING CONSTANT
C  GAMMA - ELASTIC FOUNDATION SPRING CONSTANT
C  TH - THICKNESS
C  NUDOF - DEGREES OF FREEDOM
C  PCP - CRITICAL LOAD OF PERFECT BEAM (DEFINE BELOW ON LINE 81)
C
      READ(51,*) L1,L2
      READ(51,*) HB
      READ(51,*) N1,N2,N3
      READ(51,*) RL1,RL2,RL3
      READ(51,*) ALPHA,BETA,GAMMA
      READ(51,*) NNBC
      DO 10 I=1,NNBC
         READ(51,*) NBC(I)
         IF(NBC(I).GT.17) NBC(I)=NBC(I)-12
10  CONTINUE
      NUDOF=3*(N1+2*N2+N3)+12
      NA=(N1+N2)*3+6
      NA1=NA+1
      NA6=NA+6
      TH=10.
      RL=200.

```

```

E=30.D6
IA=NUDOF-1
IB=NUDOF
LL(1)=RL1/FLOAT(N1)
LL(2)=RL2/FLOAT(N2)
LL(3)=LL(2)
LL(4)=RL3/FLOAT(N3)
H(1)=TH
H(2)=(1.-HB)*TH
H(3)=HB*TH
H(4)=TH
DO 20 I=1,4
    IN(I)=H(I)**3/12.
    A(I)=H(I)*E/LL(I)
    B(I)=E*IN(I)/LL(I)**3
20 CONTINUE
C
C*****MAKE SURE PCP IS CORRECT
C
    GAM=GAMMA*E*IN(1)/RL**4
C    PCP=20.19*E*IN(1)/RL**2
    PCP=4.0*3.14159**2*E*IN(1)/RL**2
C*****FORM UNRESTRAINED MATRICES
    DO 50 I=1,NUDOF
    DO 50 J=1,NUDOF
        KU(I,J)=0.
        GU(I,J)=0.
50 CONTINUE
    CALL MATR(1,K,G,C,A,B,LL,HB)
C    WRITE(6,57)((G(I,J),J=1,6),I=1,6)
C 57 FORMAT(8E9.2)
    N=0
    DO 70 M=1,N1
        DO 60 I=1,6
        DO 60 J=1,6
            KU(I+N,J+N)=KU(I+N,J+N)+K(I,J)+GAM*C(I,J)
            GU(I+N,J+N)=GU(I+N,J+N)+G(I,J)
60    CONTINUE
        N=N+3
70 CONTINUE
    CALL MATR(2,K,G,C,A,B,LL,HB)
    DO 100 IC=1,2
        N=N+3
        DO 90 M=1,N2
            DO 80 I=1,6
            DO 80 J=1,6
                KU(I+N,J+N)=KU(I+N,J+N)+K(I,J)+GAM*C(I,J)
                GU(I+N,J+N)=GU(I+N,J+N)+G(I,J)
80    CONTINUE
            N=N+3
90    CONTINUE
        CALL MATR(3,K,G,C,A,B,LL,HB)
100 CONTINUE
    CALL MATR(4,K,G,C,A,B,LL,HB)
    N=N+3
    DO 120 M=1,N3

```

```

        DO 110 I=1,6
        DO 110 J=1,6
            KU(I+N,J+N)=KU(I+N,J+N)+K(I,J)+GAM*C(I,J)
            GU(I+N,J+N)=GU(I+N,J+N)+G(I,J)
110     CONTINUE
        N=N+3
120 CONTINUE
C
C*****ADD EXTRA TERMS FROM ELASTIC SUPPORTS TO STIFFNESS MATRIX
C
        KU(2,2)=KU(2,2)+ALPHA*E*IN(1)/RL**3
        KU(3,3)=KU(3,3)+BETA*E*IN(1)/RL
        KU(1A,1A)=KU(1A,1A)+ALPHA*E*IN(1)/RL**3
        KU(1B,1B)=KU(1B,1B)+BETA*E*IN(1)/RL
C*****FORM TRANSFORMATION MATRIX
        NM12=NUDOF-12
        DO 130 I=1,NUDOF
        DO 130 J=1,NM12
            T(I,J)=0.
130 CONTINUE
        IEND1=3*N1+3
        DO 140 I=1,IEND1
            T(I,I)=1.
140 CONTINUE
        IEND2=3*(N1+2*N2)+9
        IB3=IEND2+1
        DO 150 I=IB3,NUDOF
            T(I,I-12)=1.
150 CONTINUE
        II=N2*3-1
        IB2=IEND1+1
        ID=IB2+II
        DO 160 I=IB2,ID
            T(I,I-3)=1.
160 CONTINUE
        T(IB2,IB2-1)=H(3)/2.
        INE=N2*3-6
        DO 170 J=1,3
            T(ID+J,INE+J+ID)=1.
170 CONTINUE
        T(ID+1,ID+3+INE)=H(3)/2.
        I3=ID+3
        INF=3*N2+6
        DO 180 J=1,3
            T(I3+J,I3+J-INF)=1.
180 CONTINUE
        T(I3+1,I3-INF+3)=-H(2)/2.
        I7=ID+7
        ID=I7+II
        DO 190 J=I7,ID
            T(J,J-9)=1.
190 CONTINUE
        T(IB3-3,IB3-10)=-H(2)/2.
        DO 200 I=1,NUDOF
        DO 200 J=1,NM12
            TT(J,I)=T(I,J)

```

```

200 CONTINUE
C*****FORM TRANSFORMED STIFFNESS MATRICES
  CALL VMULFF(TT,KU,NM12,NUDOF,NUDOF,60,60,K1T,60,IER)
  CALL VMULFF(TT,GU,NM12,NUDOF,NUDOF,60,60,G1T,60,IER)
  CALL VMULFF(K1T,T,NM12,NUDOF,NM12,60,60,KT,60,IER)
  CALL VMULFF(G1T,T,NM12,NUDOF,NM12,60,60,GT,60,IER)
C*****FORM RESTRAINED MATRICES
  M=1
  DO 270 I=1,NM12
    DO 270 J=1,NM12
      DO 280 L=1,NNBC
        IF (I.EQ.NBC(L).OR.J.EQ.NBC(L))GO TO 270
280    CONTINUE
        KR1(M)=KT(I,J)
        GR1(M)=GT(I,J)
        M=M+1
270 CONTINUE
      NR=NM12-NNBC
      M=1
      DO 290 I=1,NR
        DO 290 J=1,NR
          KR(I,J)=KR1(M)
          GR(I,J)=GR1(M)
          M=M+1
290 CONTINUE
      NNN=1
C*****FORM DELTA P VECTOR AND TOTAL P VECTOR
      DO 702 J=1,NUDOF
        PT(J)=0.
        DP(J)=0.
702 CONTINUE
        DP(1)=.01*PCP
        PT(L1)=-.0001*PCP
        PT(L2)=.0001*PCP
        DP(L1)=PT(L1)
        DP(L2)=PT(L2)
        DO 293 I=1,NR
          DS(I)=0.0
293 CONTINUE
288 ITER=1
      PL=PT(1)
      CALL FIXMOD(DS,IB2,N2,IB3,RMI,NM12,NNBC,NBC,H,NUDOF)
C*****FORM TANGENT STIFFNESS MATRIX
      CALL KTIN(KR,GR,PL,RMI,LL,A,NUDOF,NM12,T,TT,NBC,NNBC,KTINV,
        1KST,2,N1,N2,N3,KU,KTOT,G,HB,K,B,C)
C*****ADD DELTA P TO TOTAL P
      PT(1)=DP(1)+PT(1)
C*****FIND DELTA DELTA VECTOR
C  PRINT,'DELTA DELTA'
      DO 703 J=1,NR
        DD(J)=0.
        DO 704 K1=1,NR
          DD(J)=DD(J)+KTINV(J,K1)*DP(K1)
704    CONTINUE
C  PRINT,J,DD(J)

```

```

703     CONTINUE
C*****FIND DELTA STAR
      DO 730 I = 1,NR
        DS(I) = DD(I) + DS(I)
730     CONTINUE
777     CALL FIXMOD(DS,IB2,N2,IB3,RM1,NM12,NNBC,NBC,H,NUDOF)
C*****FIND K,N1,N2(DS) THEN INTERNAL FORCES P STAR
C      PRINT,'INTERNAL FORCES PSTAR'
      CALL KTIN(KR,GR,PL,RM1,LL,A,NUDOF,NM12,T,TT,NBC,NNBC,KTINV,
1KST,1,N1,N2,N3,KU,KTOT,G,HB,K,B,C)
      DO 718 J = 1,NR
        P(J) = 0.
        DO 719 K1 = 1,NR
          P(J) = P(J) + KST(J,K1)*DS(K1)
719     CONTINUE
718     CONTINUE
C*****FIND RESIDUAL LOAD
      DO 740 I = 1,NR
        PD(I) = PT(I) - P(I)
740     CONTINUE
C*****FIND DELTA DELTA ONE VECTOR
C      WRITE(52,*) 'DELTA DELTA ONE'
      DO 753 J = 1,NR
        DD1(J) = 0.
        DO 754 K1 = 1,NR
          DD1(J) = DD1(J) + KTINV(J,K1)*PD(K1)
754     CONTINUE
753     CONTINUE
C*****FIND DELTA STAR
      DO 760 I = 1,NR
        DS(I) = DS(I) + DD1(I)
760     CONTINUE
      ITER = ITER + 1
      IF(ITER.GT.30)GO TO 780
      CH = 0.
      DO 756 I = 1,NR
        CH = CH + PD(I)**2
756     CONTINUE
      CH1 = DSQRT(CH/PT(1)**2)
      WRITE(52,*) 'DELTA STAR'
      IF(CH1.GT..001) GO TO 777
      DO 762 I = 1,NR
        DS(I) = DS(I) + DD1(I)
762     CONTINUE
      CALL FIXMOD(DS,IB2,N2,IB3,RM1,NM12,NNBC,NBC,H,NUDOF)
      CALL KTIN(KR,GR,PL,RM1,LL,A,NUDOF,NM12,T,TT,NBC,NNBC,KTINV,
1KST,3,N1,N2,N3,KU,KTOT,G,HB,K,B,C)
      DO 713 J = 1,6
        F(J) = 0.
        DO 714 K1 = 1,6
          F(J) = F(J) + KTOT(J,K1)*RM1(K1)
714     CONTINUE
713     CONTINUE
      DO 723 J = NA1,NA6
        F(J) = 0.
        DO 724 K1 = NA1,NA6

```

```

          F(J) = F(J) + KTOT(J,K1)*RM1(K1)
724      CONTINUE
723      CONTINUE
C*****FIND ENERGY-RELEASE RATE
      HHB = 1.-HB
      PS = HB*(F(1)-6.*HHB*F(3)/TH)-F(NA + 1)
      MS = -F(NA + 3) + F(3)*HB**3
      AB = (TH*PS)**2/(HB*HHB)
      BC = 12.*MS**2/HB**3
      CD = 12.*(TH*PS/2.-MS)**2/HHB**3
      RRG = 1./(24.*E*IN(1))*(AB + BC + CD)
      PB = PT(1)/PCP
      GB = (RL/2.)**4*RRG/(E*TH**5)
      RQ = RM1(20)/TH
      WRITE(4,33)GB,PB
      DL = DS(1)*2.
      VV1 = DS(L1)/10.
      VV2 = DS(L2)/10.
33      FORMAT(3X,E15.8,5X,E15.8)
      NNN = NNN + 1
C*****ADJUST LOAD STEP MANUALLY HERE: YOU NEED SMALL LOAD STEP
C*****NEAR GLOBAL BUCKLING LOAD
      IF(NNN.EQ.3)DP(1) = PCP*.03
      IF(NNN.EQ.23)DP(1) = PCP*.005
C      IF(NNN.EQ.39)DP(1) = PCP*.001
      IF(PB.LT.1.0)GO TO 288
780 WRITE (52,*)'DID NOT CONVERGE THIS STEP'
800 STOP
      END
      SUBROUTINE MM(V1,T1,V2,T2,L,A,N1,N2,IIF)
C
C*****THIS SUBROUTINE CALCULATES COMPONENTS OF NONLINEAR MATRICES
C
      REAL*8 M1(6,6),M2(6,6),L,V1,T1,V2,T2,A,N1(6,6),N2(6,6)
      DO 20 M = 1,6
      DO 20 J = 1,6
          M1(M,J) = 0.
          M2(M,J) = 0.
20      CONTINUE
      M1(2,4) = 6./5./L*V1 + .1*T1-6./5./L*V2 + .1*T2
      M1(2,1) = -M1(2,4)
      M1(3,4) = .1*V1 + 2./15.*L*T1-.1*V2-1./30.*L*T2
      M1(3,1) = -M1(3,4)
      M1(5,4) = M1(2,1)
      M1(5,1) = -M1(5,4)
      M1(6,4) = .1*V1-1./30.*L*T1-.1*V2 + 2./15.*L*T2
      M1(6,1) = -M1(6,4)
      M2(2,2) = (72./L**3*V1**2 + 18./L**2*V1*T1 + 3./L*T1**2
1-144./L**3*V1*V2-18./L**2*V2*T1 + 18./L**2*V1*T2
2 + 72./L**3*V2**2-18./L**2*V2*T2 + 3./L*T2**2)/35.
      M2(3,3) = (3.*(-V1*T1 + V2*T1 + V1*T2-L*T1*T2-V2*T2) + 18./L*V1**2
1 + 12.*L*T1**2-36./L*V1*V2 + 18./L*V2**2 + 1.*L*T2**2)/210.
      M2(5,5) = M2(2,2)
      M2(6,6) = (1.*(V1*T1-V2*T1-V1*T2-T1*T2*L + V2*T2) + 6./L*V1**2
1 + 1./3.*L*T1**2-12./L*V1*V2 + 6./L*V2**2 + 4.*L*T2**2)/70.
      M2(3,2) = (18./L**2*(V1**2 + V2**2) + 12./L*(V1*T1-V2*T1) +

```

```

11./2.*(T2**2-T1**2)-32./L**2*V1*V2+1.*T1*T2)/70.
M2(5,2)=-M2(2,2)
M2(5,3)=-M2(3,2)
M2(6,2)=(18./L**2*(V1**2-2*V1*V2+V2**2)+1./2.*(T1**2+
12*T1*T2-T2**2)+12./L*(V1*T2-V2*T2))/70.
M2(6,3)=(1.*(V1*T1-T1*V2+V1*T2-V2*T2)-1./2.*L*(T1**2
1+T2**2)+2./3.*L*T1*T2)/70.
M2(6,5)=-M2(6,2)
DO 30 M=1,6
DO 30 J=1,6
      M2(M,J)=M2(J,M)
30 CONTINUE
  IF(IIF.EQ.2)THEN
    DO 40 M=1,6
    DO 40 J=1,6
      N1(M,J)=(M1(M,J)+M1(J,M))*A
      N2(M,J)=M2(M,J)*A*L
40   CONTINUE
    ELSE
      DO 50 M=1,6
      DO 50 J=1,6
        N1(M,J)=(M1(M,J)+.5*M1(J,M))*A
        N2(M,J)=.5*M2(M,J)*A*L
50   CONTINUE
    ENDIF
    RETURN
  END
  SUBROUTINE MATR(I,K,G,C,A,B,LL,HB)
C
C*****THIS SUBROUTINE CALCULATES COMPONENTS OF BASIC AND INCREMENTAL
C*****STIFFNESS MATRICES
C
  REAL*8 K(6,6),G(6,6),A(4),B(4),C(6,6)
  REAL*8 LL(4),HB
  DO 27 M=1,6
  DO 27 J=1,6
    K(M,J)=0.
    G(M,J)=0.
    C(M,J)=0.
27   CONTINUE
    K(1,1)=A(I)
    K(2,2)=12.*B(I)
    K(3,3)=4.*B(I)*LL(I)**2
    K(4,4)=A(I)
    K(5,5)=12.*B(I)
    K(6,6)=K(3,3)
    K(4,1)=-A(I)
    K(3,2)=6.*B(I)*LL(I)
    K(5,2)=-12.*B(I)
    K(6,2)=K(3,2)
    K(5,3)=-K(3,2)
    K(6,3)=.5*K(3,3)
    K(6,5)=K(5,3)
    G(2,2)=12./LL(I)
    G(3,3)=4./3.*LL(I)
    G(5,5)=G(2,2)

```



```

      G(6,6) = G(3,3)
      G(3,2) = 1.
      G(5,2) = -G(2,2)
      G(6,2) = 1.
      G(5,3) = -1.
      G(6,3) = -LL(I)/3.
      G(6,5) = -1.
      C(2,2) = 156.
      C(3,3) = 4.*LL(I)**2
      C(5,5) = 156.
      C(6,6) = C(3,3)
      C(3,2) = 22.*LL(I)
      C(5,2) = 54.
      C(6,2) = -13.*LL(I)
      C(5,3) = 13.*LL(I)
      C(6,3) = -3.*LL(I)**2
      C(6,5) = -22.*LL(I)
      DO 40 J = 1,6
      DO 40 M = 1,6
         K(J,M) = K(M,J)
         G(J,M) = G(M,J)
         C(J,M) = C(M,J)
40    CONTINUE
      DO 42 M = 1,6
      DO 42 J = 1,6
         G(J,M) = G(J,M)/10.
         C(J,M) = C(J,M)*LL(I)/420.
42    CONTINUE
      IF(I.EQ.2)THEN
         DO 47 M = 1,6
         DO 47 J = 1,6
            G(M,J) = (1-HB)*G(M,J)
47    CONTINUE
      ENDIF
      IF(I.EQ.3)THEN
         DO 49 M = 1,6
         DO 49 J = 1,6
            G(M,J) = HB*G(M,J)
            C(M,J) = 0.
49    CONTINUE
      ENDIF
      RETURN
      END
      SUBROUTINE FIXMOD(RMA,IB2,N2,IB3,RM1,NM12,NNBC,NBC,H,NUDOF)
C
C*****THIS SUBROUTINE FORMS THE UNRESTRAINED, UNTRANSFORMED
C*****DISPLACEMENT VECTOR FROM THE RESTRAINED, TRANSFORMED
C*****DISPLACEMENT VECTOR
C
      IMPLICIT REAL*8 (A-H,O-Z)
      REAL*8 RMA(60),RM1(60),RM(60),H(4)
      DIMENSION IL(4),NBC(10)
C*****ADD ZERO DOF'S TO MODAL VECTOR
      I2 = 1
      DO 301 I1 = 1,NM12
         DO 302 I4 = 1,NNBC

```

```

        IF (I1.EQ.NBC(I4)) THEN
            RM(I1)=0
            GO TO 301
        ENDIF
302    CONTINUE
        RM(I1)=RMA(I2)
        I2=I2+1
301 CONTINUE
C*****EXPAND MODAL VECTOR
        IL(1)=IB2
        IL(2)=IB2+N2*3
        IL(3)=IL(2)+3
        IL(4)=IL(3)+N2*3
        I2=1
        DO 311 I=1,NM12
            DO 312 I1=1,4
                IF (I2.EQ.IL(I1)) I2=I2+3
312    CONTINUE
                RM1(I2)=RM(I)
                I2=I2+1
311 CONTINUE
                RM1(IB2)=RM1(IB2-3)+H(3)/2.*RM1(IB2-1)
                RM1(IB2+1)=RM1(IB2-2)
                RM1(IB2+2)=RM1(IB2-1)
                RM1(IB3-3)=RM1(IB3)-H(2)/2.*RM1(IB3+2)
                RM1(IB3-2)=RM1(IB3+1)
                RM1(IB3-1)=RM1(IB3+2)
                NDD=IL(2)
                RM1(NDD)=RM1(IB3)+H(3)/2.*RM1(IB3+2)
                RM1(NDD+1)=RM1(IB3+1)
                RM1(NDD+2)=RM1(IB3+2)
                RM1(NDD+3)=RM1(IB2-3)-H(2)/2.*RM1(IB2-1)
                RM1(NDD+4)=RM1(IB2-2)
                RM1(NDD+5)=RM1(IB2-1)
                RETURN
            END
        SUBROUTINE KTIN(KR,GR,PL,RM1,LL,A,NUDOF,NM12,T,TT,NBC,NNBC,
            1KTINV,KST,IIF,N1,N2,N3,KU,KTOT,G,HB,K,B,C)
C
C*****THIS SUBROUTINE ASSEMBLES, TRANSFORMS, AND RESTRAINS THE
C*****NONLINEAR STIFFNESS MATRICES AND FORMS THE TANGENT STIFFNESS
C*****MATRIX    UU IS THE K SIGMA MATRIX
C
        IMPLICIT REAL*8 (A-H,O-Z)
        REAL*8 KR(60,60),GR(60,60),NU1(60,60),NU2(60,60),LL(4),A(4)
        REAL*8 NN1(6,6),NN2(6,6),T(60,60),TT(60,60),G(6,6)
        REAL*8 NU1T(60,60),NU2T(60,60),N1T(60,60),N2T(60,60),KR1(2500)
        REAL*8 GR1(2500),KTAN(60,60),WKAREA(60)
        REAL*8 KTINV(60,60),NUR1(60,60),NUR2(60,60),RM1(60),KST(60,60)
        REAL*8 KTOT(60,60),KU(60,60),K(6,6),B(4),C(6,6)
        REAL*8 UU1(60,60),UUR1(60,60),UU1T(60,60),U1T(60,60),UR1(2500)
        DIMENSION NBC(10)
        NF=60
        NZ=0
C*****FORM UNRESTRAINED NONLINEAR MATRICES
        DO 450 I=1,NUDOF

```

```

DO 450 J=1,NUDOF
  UU1(I,J)=0.
  NU1(I,J)=0.
  NU2(I,J)=0.
450 CONTINUE
  N=N+1
  DO 470 M=1,N1
    U1=RM1(N+1)
    X1=RM1(N+2)
    Y1=RM1(N+3)
    U2=RM1(N+4)
    X2=RM1(N+5)
    Y2=RM1(N+6)
    CALL MM(X1,Y1,X2,Y2,LL(1),A(1),NN1,NN2,IIF)
    CALL MATR(1,K,G,C,A,B,LL,HB)
    DO 460 I=1,6
      DO 460 J=1,6
        NU1(I+N,J+N)=NU1(I+N,J+N)+NN1(I,J)
        NU2(I+N,J+N)=NU2(I+N,J+N)+NN2(I,J)
        UU1(I+N,J+N)=UU1(I+N,J+N)+A(1)*(U2-U1)*G(I,J)
      460 CONTINUE
    N=N+3
  470 CONTINUE
  DO 500 IC=2,3
    N=N+3
    DO 490 M=1,N2
      U1=RM1(N+1)
      X1=RM1(N+2)
      Y1=RM1(N+3)
      U2=RM1(N+4)
      X2=RM1(N+5)
      Y2=RM1(N+6)
      CALL MATR(IC,K,G,C,A,B,LL,HB)
      CALL MM(X1,Y1,X2,Y2,LL(2),A(IC),NN1,NN2,IIF)
      DO 480 I=1,6
        DO 480 J=1,6
          NU1(I+N,J+N)=NU1(I+N,J+N)+NN1(I,J)
          NU2(I+N,J+N)=NU2(I+N,J+N)+NN2(I,J)
          UU1(I+N,J+N)=UU1(I+N,J+N)+A(IC)*(U2-U1)*G(I,J)
        480 CONTINUE
      N=N+3
    490 CONTINUE
  500 CONTINUE
  N=N+3
  DO 520 M=1,N3
    U1=RM1(N+1)
    X1=RM1(N+2)
    Y1=RM1(N+3)
    U2=RM1(N+4)
    X2=RM1(N+5)
    Y2=RM1(N+6)
    CALL MATR(4,K,G,C,A,B,LL,HB)
    CALL MM(X1,Y1,X2,Y2,LL(4),A(4),NN1,NN2,IIF)
    DO 510 I=1,6
      DO 510 J=1,6
        NU1(I+N,J+N)=NU1(I+N,J+N)+NN1(I,J)

```

```

        NU2(I+N,J+N)=NU2(I+N,J+N)+NN2(I,J)
        UU1(I+N,J+N)=UU1(I+N,J+N)+A(4)*(U2-U1)*G(I,J)
510    CONTINUE
        N=N+3
520    CONTINUE
        DO 530 I=1,NUDOF
        DO 530 J=1,NUDOF
            KTOT(I,J)=NU1(I,J)+NU2(I,J)+KU(I,J)
530    CONTINUE
        IF(IIF.EQ.3)GO TO 700
C*****FORM TRANSFORMED NONLINEAR STIFFNESS MATRICES
        CALL VMULFF(TT,UU1,NM12,NUDOF,NUDOF,NF,NF,UU1T,NF,IER)
        CALL VMULFF(TT,NU1,NM12,NUDOF,NUDOF,NF,NF,NU1T,NF,IER)
        CALL VMULFF(TT,NU2,NM12,NUDOF,NUDOF,NF,NF,NU2T,NF,IER)
        CALL VMULFF(UU1T,T,NM12,NUDOF,NM12,NF,NF,U1T,NF,IER)
        CALL VMULFF(NU1T,T,NM12,NUDOF,NM12,NF,NF,N1T,NF,IER)
        CALL VMULFF(NU2T,T,NM12,NUDOF,NM12,NF,NF,N2T,NF,IER)
C*****FORM RESTRAINED NONLINEAR MATRICES
        M=1
        DO 570 I=1,NM12
        DO 570 J=1,NM12
            DO 580 L2=1,NNBC
                IF (I.EQ.NBC(L2).OR.J.EQ.NBC(L2)) GO TO 570
580        CONTINUE
            KR1(M)=N1T(I,J)
            GR1(M)=N2T(I,J)
            UR1(M)=U1T(I,J)
            M=M+1
570    CONTINUE
        M=1
        NRE=NM12-NNBC
        DO 590 I=1,NRE
        DO 590 J=1,NRE
            NUR1(I,J)=KR1(M)
            NUR2(I,J)=GR1(M)
            UUR1(I,J)=UR1(M)
            M=M+1
590    CONTINUE
        IF(IIF.EQ.2)THEN
            DO 600 I=1,NRE
            DO 600 J=1,NRE
                KTAN(I,J)=NUR1(I,J)+1.5*NUR2(I,J)+KR(I,J)+UUR1(I,J)
600    CONTINUE
            ENDIF
            IF(IIF.EQ.1)THEN
                DO 605 I=1,NRE
                DO 605 J=1,NRE
                    KST(I,J)=NUR1(I,J)+NUR2(I,J)+KR(I,J)
605    CONTINUE
            ENDIF
            IF (IIF.EQ.2) THEN
                CALL LINV1F(KTAN,NRE,NF,KTINV,NZ,WKAREA,IER)
            ENDIF
700    RETURN
        END

```

OUTPUT FOR INCREMENTAL PROGRAM

| GBAR | PBAR |
|----------------|------------------|
| 0.10424280E-03 | 0.10000002E-01 |
| 0.14033886E-03 | 0.20000003E-01 |
| 0.33919796E-03 | 0.50000004E-01 |
| 0.67225987E-03 | 0.80000006E-01 |
| 0.11268290E-02 | 0.11000001E + 00 |
| 0.17061085E-02 | 0.14000001E + 00 |
| 0.24042586E-02 | 0.17000001E + 00 |
| 0.32443434E-02 | 0.20000001E + 00 |
| 0.41872530E-02 | 0.23000001E + 00 |
| 0.52397028E-02 | 0.26000001E + 00 |
| 0.63969370E-02 | 0.29000001E + 00 |
| 0.76526362E-02 | 0.32000002E + 00 |
| 0.89993934E-02 | 0.35000002E + 00 |
| 0.10577678E-01 | 0.38000002E + 00 |
| 0.12156659E-01 | 0.41000002E + 00 |
| 0.13795306E-01 | 0.44000002E + 00 |
| 0.15483546E-01 | 0.47000002E + 00 |
| 0.17214533E-01 | 0.50000002E + 00 |
| 0.18978662E-01 | 0.53000002E + 00 |
| 0.20765500E-01 | 0.56000002E + 00 |
| 0.22232170E-01 | 0.59000003E + 00 |
| 0.23845665E-01 | 0.62000003E + 00 |
| 0.24119363E-01 | 0.62500003E + 00 |
| 0.24361650E-01 | 0.63000003E + 00 |
| 0.24689559E-01 | 0.63500002E + 00 |
| 0.24939315E-01 | 0.64000002E + 00 |
| 0.25256515E-01 | 0.64500002E + 00 |
| 0.25516829E-01 | 0.65000002E + 00 |
| 0.25826748E-01 | 0.65500002E + 00 |
| 0.26094186E-01 | 0.66000002E + 00 |
| 0.26400379E-01 | 0.66500002E + 00 |
| 0.26672830E-01 | 0.67000002E + 00 |
| 0.26978080E-01 | 0.67500002E + 00 |
| 0.27254672E-01 | 0.68000001E + 00 |
| 0.27561335E-01 | 0.68500001E + 00 |
| 0.27842211E-01 | 0.69000001E + 00 |
| 0.28152569E-01 | 0.69500001E + 00 |
| 0.28438780E-01 | 0.70000001E + 00 |
| 0.28755349E-01 | 0.70500001E + 00 |
| 0.29048869E-01 | 0.71000001E + 00 |
| 0.29104507E-01 | 0.71500001E + 00 |
| 0.29237166E-01 | 0.72000001E + 00 |
| 0.29421645E-01 | 0.72500001E + 00 |
| 0.29647610E-01 | 0.73000000E + 00 |
| 0.29907018E-01 | 0.73500000E + 00 |
| 0.30194924E-01 | 0.74000000E + 00 |
| 0.30508557E-01 | 0.74500000E + 00 |
| 0.30846846E-01 | 0.75000000E + 00 |
| 0.31210091E-01 | 0.75500000E + 00 |

| | |
|------------------|------------------|
| 0.31599769E-01 | 0.76000000E + 00 |
| 0.32018436E-01 | 0.76500000E + 00 |
| 0.32469700E-01 | 0.77000000E + 00 |
| 0.32958269E-01 | 0.77499999E + 00 |
| 0.33490054E-01 | 0.77999999E + 00 |
| 0.34072337E-01 | 0.78499999E + 00 |
| 0.34714009E-01 | 0.78999999E + 00 |
| 0.35425883E-01 | 0.79499999E + 00 |
| 0.36221121E-01 | 0.79999999E + 00 |
| 0.37115774E-01 | 0.80499999E + 00 |
| 0.38129510E-01 | 0.80999999E + 00 |
| 0.39286567E-01 | 0.81499999E + 00 |
| 0.40617023E-01 | 0.81999999E + 00 |
| 0.42045322E-01 | 0.82499998E + 00 |
| 0.43697771E-01 | 0.82999998E + 00 |
| 0.45696856E-01 | 0.83499998E + 00 |
| 0.48115579E-01 | 0.83999998E + 00 |
| 0.51053927E-01 | 0.84499998E + 00 |
| 0.54582788E-01 | 0.84999998E + 00 |
| 0.58900210E-01 | 0.85499998E + 00 |
| 0.64389966E-01 | 0.85999998E + 00 |
| 0.71478356E-01 | 0.86499998E + 00 |
| 0.80808542E-01 | 0.86999997E + 00 |
| 0.93884525E-01 | 0.87499997E + 00 |
| 0.11394016E + 00 | 0.87999997E + 00 |
| 0.15180795E + 00 | 0.88499997E + 00 |

**The vita has been removed from
the scanned document**